Pathway and surface mechanism studies of 1,3-butadiene selective oxidation over vanadium-molybdenum-oxygen catalysts

by

William David Schroeder

A dissertation submitted to the graduate faculty

in partial fulfillment of the requirements for the degree of

DOCTOR OF PHILOSOPHY

Major: Chemical Engineering

Major Professor: Glenn L. Schrader

Iowa State University

Ames, Iowa

2001

Graduate College

Iowa State University

This is to certify the Doctoral dissertation of

William David Schroeder

has met the dissertation requirements of Iowa State University

Glenn L. Schrader

Major Professor

Charles E. Hall

For the Major Program

For the Graduate College

TABLE OF CONTENTS

Pathway and surface mechanism studies of 1,3-butadiene selective oxidation over vanadium-molybdenum-oxygen catalysts

William David Schroeder

Major Professor: Glenn L. Schrader

Iowa State University

ABSTRACT

The partial oxidation of 1,3-butadiene has been investigated over VMoO catalysts synthesized by sol-gel techniques. Surface areas were 9-14 m^2/g, and compositions were within the solid solution regime, i.e. below 15.0 mol % $MoO_3/(MoO_3 + V_2O_5)$. Laser Raman Spectroscopy and XRD data indicated that solid solutions were formed, and pre- and post-reaction XPS data indicated that catalyst surfaces contained some V^{+4} and were further reduced in 1,3-butadiene oxidation. A reaction pathway for 1,3-butadiene partial oxidation to maleic anhydride was shown to involve intermediates such as 3,4-epoxy-1-butene, crotonaldehyde, furan, and 2-butene-1,4-dial. The addition of water to the reaction stream substantially increased catalyst activity and improved selectivity to crotonaldehyde and furan at specific reaction temperatures. At higher water addition concentrations, furan selectivity increased from 12% to over 25%. The catalytic effects of water addition were related to competitive adsorption with various V_2O_5-based surface sites, including the vanadyl V=O, corner sharing V-O-V and edge sharing V-O oxygen. Higher levels of water addition were proposed to impose acidic character by dissociative

adsorption. In addition, a novel combinatorial synthesis technique for VMoO was used to investigate the phase transitions of V_2O_5, solid solutions of Mo in V_2O_5, $V_9Mo_6O_{40}$, and other reduced VMoO compounds, characterized by laser Raman spectroscopy. The natural composition gradient imposed by the sputter deposition apparatus was used to create VMoO arrays containing 225 samples ranging from 7.0 – 42 mol % $MoO_3/(V_2O_5 + MoO_3)$, determined by EDS analysis.

CHAPTER 1

GENERAL INTRODUCTION

1.1. Introduction

In recent years, several advances have been made in the petrochemical industry for producing building block chemicals. Due to the large availability of lower alkanes from petroleum and natural gas feedstocks, efforts have been made to find catalysts to convert these alkanes directly to valuable intermediates. In addition, the versatility of chemical building blocks such as ethylene oxide provides a high driving force to find other versatile epoxidation products derived from higher olefins.

Both molybdenum and vanadium oxides are contained in a number of materials used for catalytic processes, specifically those processes involving the selective oxidation of hydrocarbons. Separately, molybdenum and vanadium oxides generally have high activity but poor selectivity.[1] As components of multiphase metal oxide catalysts, however, these two metals are contained in several high performance catalysts.

Selective oxidation of n-butane to maleic anhydride was the first commercialized process involving direct alkane oxidation. In 1997, the U.S. market for maleic anhydride was 450 million pounds per year (C&EN May 5, 1997.) The catalyst used in this process is a vanadium-phosphorous-oxygen (denoted VPO) compound. The previous process for maleic anhydride was based on benzene oxidation using promoted vanadium-molybdenum based metal oxide catalysts.

The second large-scale alkane process to be used at the industrial scale was announced by BP in 1996. Currently BP produces 95% of the world's acrylonitrile from

the ammoxidation of propylene. Direct ammoxidation of propane to acrylonitrile using a bismuth-phosphorous-molybdate catalyst is reported to cut costs by 20%, as well as reducing the number of reaction steps. (C&EN Sept. 23, 1996) A key building block chemical in the synthetic fiber industry, acrylonitrile is manufactured at a yearly rate of approximately three billion pounds (C&EN June 29, 1997.)

In addition to lower alkanes, there is a large interest in diolefins as feedstock sources, specifically 1,3-butadiene. This diolefin is a by-product of naphtha cracking in ethylene production. The demand for ethylene is 1.5% larger than 1,3-butadiene, resulting in predictions of a 2 million metric ton per year surplus of 1,3-butadiene by the year 2000. (C&EN, July 18, 1994) Currently several methods are being used to dispose of the excess chemical, all of which provide little profit. Therefore, development of high-activity catalysts to convert 1,3-butadiene to useful products, e.g. maleic anhydride, 3,4-epoxy-1-butene, furan, etc. are of high interest industrially. Eastman Chemical recently commercialized a process for 1,3-butadiene epoxidation to 3,4-epoxy-1-butene using a CsCl or CsF-promoted Ag catalyst. A very diverse chemical intermediate, 3,4-epoxy-1-butene has been reported to be an intermediate for the production of over one hundred different chemicals, several of which are already being commercially produced.[2]

In hydrocarbons with high electron density, like olefins and aromatics, electrophilic oxidation can take place. Activated surface oxygen species attack regions of high electronegativity, i.e. the π-bonds, of an adsorbing molecule. In the epoxidation of ethylene to ethylene oxide, the absorbed oxygen species on a silver surface will attack the C=C bond and form the epoxy ring structure. Electrophilic attack can become quite

aggressive at higher temperatures. Carbon bond cleavage often occurs, sometimes leading to complete oxidation.[3]

Because of the absorption properties of Ag, many catalysts for electrophilic addition are based on Ag or promoted Ag materials. In addition, patent literature reports metal oxides based on Sb have moderate activity for 1,3-butadiene oxidation to furan, as do promoted VMoO compounds.[4,5] The VPO catalyst used in n-butane oxidation to maleic anhydride is proposed to participate in electrophilic addition in 1,3-butadiene oxidation to 2,5-dihydrofuran.[6] The selective oxidation of benzene to maleic anhydride uses promoted V_2O_5-MoO_3 catalysts for electrophilic addition.

Many industrial selective oxidation catalysts are multicomponent metals and metal oxides. Most of these catalytic reactions follow a reduction - reoxidation (redox) process[7] in which absorbed or lattice oxygen react with the activated hydrocarbon species and gas phase oxygen is used to replenish the reduced catalyst surface. Preparation methods for these catalysts normally result in a variety of structural and contact arrangements, making it difficult to understand the fundamental reasons behind catalytic activity. Numerous studies have been done to explain the improvement in catalytic activity that complex metal oxides offer over single-phase catalytic systems. Identifying the participating oxygen species and reactive sites of the hydrocarbon are important in understanding the nature of the reaction mechanism as well as the active sites on the catalyst surface.

The V_2O_5-MoO_3 system has a complex phase structure, including a solid solution of MoO_3 in V_2O_5 and several identified intermediate phases. In the oxidation of benzene,

the most active phase is the saturated solid solution of MoO_3 in V_2O_5. At this composition, several phenomena take place. Chemisorption of oxygen is maximized as more Mo is substituted into the V_2O_5 lattice. It is not clear, however, if the active oxygen species exists in the lattice or on the surface. In the redox process, mobile cations migrate and can alter surface composition. Phase transformations can take place as the Mo/V ratio changes. Cation migration can also cause coherent interfaces to form, which also will affect catalytic properties. Although a great deal of research has been done on the V_2O_5-MoO_3 catalytic system, some basic questions remain.

(1) What are the active phase(s) in V_2O_5-MoO_3 catalysts during selective oxidation of 1,3-butadiene and how does solid solution behavior affect catalytic activity?

(2) Does the 1,2-addition of oxygen to 1,3-butadiene take place over V_2O_5 and VMoO catalysts, and is it possible to isolate 3,4-epoxy-1-butene or 2,5-dihydrofuran before further reaction to produce products such as furan or maleic anhydride?

(3) What are the catalytic effects of water added to the reactant stream, and how are these explained in terms of surface sites and reaction chemistry?

1.2. Research Objectives

The objective of this research was to provide an understanding of the oxidation of 1,3-butadiene using VMoO catalysts to answer the above questions. The low-temperature oxidation of 1,3-butadiene was studied over V_2O_5 and VMoO catalysts. The solid solution of MoO_3 in V_2O_5 was the focus for this research, as it has already exhibited

electrophilic addition in the oxidation of benzene to maleic anhydride. A peroxide-based sol-gel technique was used to synthesize these compounds, aimed at controlling the stoichiometry, phase composition, and homogeneity. Structure, surface area, reaction products, and water addition were investigated for these catalysts in the reaction of air and 1,3-butadiene. The reaction pathway of 1,3-butadiene to maleic anhydride over solid-solution VMoO catalysts was studied by feeding product gases to the reactant stream and relating their products to those of 1,3-butadiene. Water effects on the catalytic system were determined using several characterization techniques, reactor studies, and temperature-programmed desorption. Additionally, combinatorial sputter deposition was used to examine phase structure and composition of mixed vanadium and molybdenum oxides, and correlations to the active phase compositions for selective oxidation of 1,3-butadiene were made.

1.3. Dissertation Organization

The dissertation consists of six chapters and one appendix. Figures and references are located at the end of each chapter. Chapter 1 gives a brief overview of the industrial and scientific benefit of studying 1,3-butadiene selective oxidation over VMoO catalysts and the specific research goals of the author's work. Chapter 2 is an in-depth literature review, focusing on the several key areas related to the main topic, including structural characteristics of VMoO catalysts, mechanistic studies over VMoO catalysts, selective oxidation reaction pathway studies involving C_4 hydrocarbons (emphasizing 1,3-butadiene to maleic anhydride) and main areas still to be investigated. Chapter 3 and Chapter 4 are papers suitable for publication in scientific journals, based on the author's

research on reaction pathway of 1,3-butadiene to maleic anhydride, surface adsorption studies and the effect of water addition to the reactant system. Chapter 5 is a paper suitable for publication in a scientific journal and represents work in the area of combinatorial chemistry, based on a novel preparation method of catalysts using magnetron sputtering. Chapter 6 draws general conclusions and suggests areas of future research activities. The research presented represents original work conducted by the author.

1.4. References

1. Bordes, E., "Structure-Activity and Selectivity Relationships in Heterogeneous Catalysis", R.K. Grasselli and A.W. Sleight eds., Elsevier 797 (1991).
2. Monnier, J. R., 3rd World Congress on Oxidation Catalysis, 135-146, 1997 Elsevier Science B.V., (R.K. Grasselli, St.T. Oyama, A.M. Gaffney and J.E. Lyons, eds.)
3. Bielanski, A. and J. Haber, "Oxygen in Catalysis", New York : M. Dekker, 1991.
4. Bartek, Joseph Peter; Grasselli, Robert Karl; Cepulis, Rimvydas L. *Eur. Pat. Appl.* 1981, 17 pp. CODEN: EPXXDW EP 23382 19810204 CAN 95:80710 AN 1981:480710
5. Farha, Floyd E., Jr.; Johnson, Marvin M.; Tabler, Donald C. *U.S Pat. App.* 1975, 5 pp. CODEN: USXXAM US 3894055 19750708 CAN 83:178797 AN 1975:578797
6. Centi, G. and F. Trifiro, *Journal of Molecular Catalysis* **35** 255-265, (1986).
7. Mars, P. and D.W.v. Krevelen, *Chem. Eng. Sci. Suppl.* **3**, 41 (1954).

Pathway and surface mechanism studies of 1,3-butadiene selective oxidation over vanadium-molybdenum-oxygen catalysts

William David Schroeder

Major Professor: Glenn L. Schrader

Iowa State University

ABSTRACT

The partial oxidation of 1,3-butadiene has been investigated over VMoO catalysts synthesized by sol-gel techniques. Surface areas were 9-14 m^2/g, and compositions were within the solid solution regime, i.e. below 15.0 mol % $MoO_3/(MoO_3 + V_2O_5)$. Laser Raman Spectroscopy and XRD data indicated that solid solutions were formed, and pre- and post-reaction XPS data indicated that catalyst surfaces contained some V^{+4} and were further reduced in 1,3-butadiene oxidation. A reaction pathway for 1,3-butadiene partial oxidation to maleic anhydride was shown to involve intermediates such as 3,4-epoxy-1-butene, crotonaldehyde, furan, and 2-butene-1,4-dial. The addition of water to the reaction stream substantially increased catalyst activity and improved selectivity to crotonaldehyde and furan at specific reaction temperatures. At higher water addition concentrations, furan selectivity increased from 12% to over 25%. The catalytic effects of water addition were related to competitive adsorption with various V_2O_5-based surface sites, including the vanadyl V=O, corner sharing V-O-V and edge sharing V-O oxygen. Higher levels of water addition were proposed to impose acidic character by dissociative

adsorption. In addition, a novel combinatorial synthesis technique for VMoO was used to investigate the phase transitions of V_2O_5, solid solutions of Mo in V_2O_5, $V_9Mo_6O_{40}$, and other reduced VMoO compounds, characterized by laser Raman spectroscopy. The natural composition gradient imposed by the sputter deposition apparatus was used to create VMoO arrays containing 225 samples ranging from 7.0 – 42 mol % $MoO_3/(V_2O_5 + MoO_3)$, determined by EDS analysis.

Pathway and surface mechanism studies of 1,3-butadiene selective oxidation over vanadium-molybdenum-oxygen catalysts

by

William David Schroeder

A dissertation submitted to the graduate faculty

in partial fulfillment of the requirements for the degree of

DOCTOR OF PHILOSOPHY

Major: Chemical Engineering

Major Professor: Glenn L. Schrader

Iowa State University

Ames, Iowa

2001

Graduate College

Iowa State University

This is to certify the Doctoral dissertation of

William David Schroeder

has met the dissertation requirements of Iowa State University

_____

Major Professor

_____

For the Major Program

_____

For the Graduate College

TABLE OF CONTENTS

CHAPTER 1

GENERAL INTRODUCTION

1.1. Introduction

In recent years, several advances have been made in the petrochemical industry for producing building block chemicals. Due to the large availability of lower alkanes from petroleum and natural gas feedstocks, efforts have been made to find catalysts to convert these alkanes directly to valuable intermediates. In addition, the versatility of chemical building blocks such as ethylene oxide provides a high driving force to find other versatile epoxidation products derived from higher olefins.

Both molybdenum and vanadium oxides are contained in a number of materials used for catalytic processes, specifically those processes involving the selective oxidation of hydrocarbons. Separately, molybdenum and vanadium oxides generally have high activity but poor selectivity.[1] As components of multiphase metal oxide catalysts, however, these two metals are contained in several high performance catalysts.

Selective oxidation of n-butane to maleic anhydride was the first commercialized process involving direct alkane oxidation. In 1997, the U.S. market for maleic anhydride was 450 million pounds per year (C&EN May 5, 1997.) The catalyst used in this process is a vanadium-phosphorous-oxygen (denoted VPO) compound. The previous process for maleic anhydride was based on benzene oxidation using promoted vanadium-molybdenum based metal oxide catalysts.

The second large-scale alkane process to be used at the industrial scale was announced by BP in 1996. Currently BP produces 95% of the world's acrylonitrile from

the ammoxidation of propylene. Direct ammoxidation of propane to acrylonitrile using a bismuth-phosphorous-molybdate catalyst is reported to cut costs by 20%, as well as reducing the number of reaction steps. (C&EN Sept. 23, 1996) A key building block chemical in the synthetic fiber industry, acrylonitrile is manufactured at a yearly rate of approximately three billion pounds (C&EN June 29, 1997.)

In addition to lower alkanes, there is a large interest in diolefins as feedstock sources, specifically 1,3-butadiene. This diolefin is a by-product of naphtha cracking in ethylene production. The demand for ethylene is 1.5% larger than 1,3-butadiene, resulting in predictions of a 2 million metric ton per year surplus of 1,3-butadiene by the year 2000. (C&EN, July 18, 1994) Currently several methods are being used to dispose of the excess chemical, all of which provide little profit. Therefore, development of high-activity catalysts to convert 1,3-butadiene to useful products, e.g. maleic anhydride, 3,4-epoxy-1-butene, furan, etc. are of high interest industrially. Eastman Chemical recently commercialized a process for 1,3-butadiene epoxidation to 3,4-epoxy-1-butene using a CsCl or CsF-promoted Ag catalyst. A very diverse chemical intermediate, 3,4-epoxy-1-butene has been reported to be an intermediate for the production of over one hundred different chemicals, several of which are already being commercially produced.[2]

In hydrocarbons with high electron density, like olefins and aromatics, electrophilic oxidation can take place. Activated surface oxygen species attack regions of high electronegativity, i.e. the π-bonds, of an adsorbing molecule. In the epoxidation of ethylene to ethylene oxide, the absorbed oxygen species on a silver surface will attack the C=C bond and form the epoxy ring structure. Electrophilic attack can become quite

aggressive at higher temperatures. Carbon bond cleavage often occurs, sometimes leading to complete oxidation.[3]

Because of the absorption properties of Ag, many catalysts for electrophilic addition are based on Ag or promoted Ag materials. In addition, patent literature reports metal oxides based on Sb have moderate activity for 1,3-butadiene oxidation to furan, as do promoted VMoO compounds.[4,5] The VPO catalyst used in n-butane oxidation to maleic anhydride is proposed to participate in electrophilic addition in 1,3-butadiene oxidation to 2,5-dihydrofuran.[6] The selective oxidation of benzene to maleic anhydride uses promoted V_2O_5-MoO_3 catalysts for electrophilic addition.

Many industrial selective oxidation catalysts are multicomponent metals and metal oxides. Most of these catalytic reactions follow a reduction - reoxidation (redox) process[7] in which absorbed or lattice oxygen react with the activated hydrocarbon species and gas phase oxygen is used to replenish the reduced catalyst surface. Preparation methods for these catalysts normally result in a variety of structural and contact arrangements, making it difficult to understand the fundamental reasons behind catalytic activity. Numerous studies have been done to explain the improvement in catalytic activity that complex metal oxides offer over single-phase catalytic systems. Identifying the participating oxygen species and reactive sites of the hydrocarbon are important in understanding the nature of the reaction mechanism as well as the active sites on the catalyst surface.

The V_2O_5-MoO_3 system has a complex phase structure, including a solid solution of MoO_3 in V_2O_5 and several identified intermediate phases. In the oxidation of benzene,

the most active phase is the saturated solid solution of MoO_3 in V_2O_5. At this composition, several phenomena take place. Chemisorption of oxygen is maximized as more Mo is substituted into the V_2O_5 lattice. It is not clear, however, if the active oxygen species exists in the lattice or on the surface. In the redox process, mobile cations migrate and can alter surface composition. Phase transformations can take place as the Mo/V ratio changes. Cation migration can also cause coherent interfaces to form, which also will affect catalytic properties. Although a great deal of research has been done on the V_2O_5-MoO_3 catalytic system, some basic questions remain.

(1) What are the active phase(s) in V_2O_5-MoO_3 catalysts during selective oxidation of 1,3-butadiene and how does solid solution behavior affect catalytic activity?

(2) Does the 1,2-addition of oxygen to 1,3-butadiene take place over V_2O_5 and VMoO catalysts, and is it possible to isolate 3,4-epoxy-1-butene or 2,5-dihydrofuran before further reaction to produce products such as furan or maleic anhydride?

(3) What are the catalytic effects of water added to the reactant stream, and how are these explained in terms of surface sites and reaction chemistry?

1.2. Research Objectives

The objective of this research was to provide an understanding of the oxidation of 1,3-butadiene using VMoO catalysts to answer the above questions. The low-temperature oxidation of 1,3-butadiene was studied over V_2O_5 and VMoO catalysts. The solid solution of MoO_3 in V_2O_5 was the focus for this research, as it has already exhibited

electrophilic addition in the oxidation of benzene to maleic anhydride. A peroxide-based sol-gel technique was used to synthesize these compounds, aimed at controlling the stoichiometry, phase composition, and homogeneity. Structure, surface area, reaction products, and water addition were investigated for these catalysts in the reaction of air and 1,3-butadiene. The reaction pathway of 1,3-butadiene to maleic anhydride over solid-solution VMoO catalysts was studied by feeding product gases to the reactant stream and relating their products to those of 1,3-butadiene. Water effects on the catalytic system were determined using several characterization techniques, reactor studies, and temperature-programmed desorption. Additionally, combinatorial sputter deposition was used to examine phase structure and composition of mixed vanadium and molybdenum oxides, and correlations to the active phase compositions for selective oxidation of 1,3-butadiene were made.

1.3. Dissertation Organization

The dissertation consists of six chapters and one appendix. Figures and references are located at the end of each chapter. Chapter 1 gives a brief overview of the industrial and scientific benefit of studying 1,3-butadiene selective oxidation over VMoO catalysts and the specific research goals of the author's work. Chapter 2 is an in-depth literature review, focusing on the several key areas related to the main topic, including structural characteristics of VMoO catalysts, mechanistic studies over VMoO catalysts, selective oxidation reaction pathway studies involving C_4 hydrocarbons (emphasizing 1,3-butadiene to maleic anhydride) and main areas still to be investigated. Chapter 3 and Chapter 4 are papers suitable for publication in scientific journals, based on the author's

research on reaction pathway of 1,3-butadiene to maleic anhydride, surface adsorption studies and the effect of water addition to the reactant system. Chapter 5 is a paper suitable for publication in a scientific journal and represents work in the area of combinatorial chemistry, based on a novel preparation method of catalysts using magnetron sputtering. Chapter 6 draws general conclusions and suggests areas of future research activities. The research presented represents original work conducted by the author.

1.4. References

1. Bordes, E., "Structure-Activity and Selectivity Relationships in Heterogeneous Catalysis", R.K. Grasselli and A.W. Sleight eds., Elsevier 797 (1991).

2. Monnier, J. R., 3rd World Congress on Oxidation Catalysis, 135-146, 1997 Elsevier Science B.V., (R.K. Grasselli, St.T. Oyama, A.M. Gaffney and J.E. Lyons, eds.)

3. Bielanski, A. and J. Haber, "Oxygen in Catalysis", New York : M. Dekker, 1991.

4. Bartek, Joseph Peter; Grasselli, Robert Karl; Cepulis, Rimvydas L. *Eur. Pat. Appl.* 1981, 17 pp. CODEN: EPXXDW EP 23382 19810204 CAN 95:80710 AN 1981:480710

5. Farha, Floyd E., Jr.; Johnson, Marvin M.; Tabler, Donald C. *U.S Pat. App.* 1975, 5 pp. CODEN: USXXAM US 3894055 19750708 CAN 83:178797 AN 1975:578797

6. Centi, G. and F. Trifiro, *Journal of Molecular Catalysis* **35** 255-265, (1986).

7. Mars, P. and D.W.v. Krevelen, *Chem. Eng. Sci. Suppl.* **3**, 41 (1954).

CHAPTER 2

LITERATURE REVIEW

2.1. Redox Mechanism in Selective Oxidation

The first reduction – reoxidation mechanism was proposed by Mars and van Krevelen in 1954. The redox cycle is a two-step process involving (1) the hydrocarbon reacting with the oxide surface, leaving a reduced surface and the product and (2) reoxidation of the reduced surface by gas-phase oxygen to its original state (see Figure 1). Surface oxygen species were considered to be responsible for the oxidation.

This mechanism is generally accepted for reactions involving metal oxide catalysts, however the specific oxide species involved in the reaction, surface mobility of oxygen species, oxygen interactions, or structural effects were not taken into account in this mechanism. Research by Haber et al. later distinguished reduction-reoxidation reactions into two forms, identified by active oxygen species - nucleophilic and electrophilic.

Nucleophilic oxidation was described to use oxygen species directly from the crystal lattice (the O^{2-} species.) The generally accepted mechanism for nucleophilic oxidation proposed by Haber et al. contained a number of consecutive elementary steps. First, catalyst surface cations activated hydrocarbon species, forming surface allylic species. This was followed by hydrogen abstraction and nucleophilic attack by the active oxygen species in the surface crystal lattice. When the product desorbed from the surface, a vacancy site was formed. This site was proposed to be replenished by oxygen diffusion through the bulk lattice or migration of adsorbed surface oxygen species to the vacancy site. Each of these different steps was associated with different active sites on

the catalyst surface. High valence centers such as Mo^{+6} and V^{+5} were generally responsible for oxygen insertion, while cations with lower valence sites, such as Ni^{+2} and Bi^{+2} were designated responsible for activating the hydrocarbon.

In the selective oxidation of 1-butene, nucleophilic oxidation takes place. In this stepwise process, lattice oxygen attacks a highly electropositive region. Hydrocarbons must first be activated via dehydrogenation on the catalyst surface, forming an allylic species. The allylic species undergoes further dehydrogenation to form 1,3-butadiene. Oxygen insertion transforms this intermediate into a number of other reactive intermediates before the final products, such as maleic anhydride, are formed. A generalized reaction pathway is shown below.

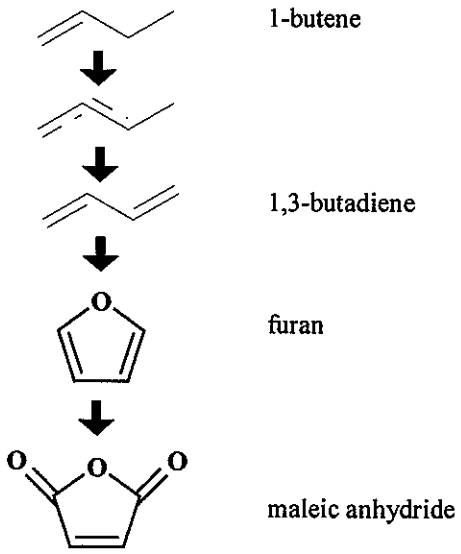

The surface sites active for hydrogen abstraction and oxygen insertion are different from those responsible for hydrocarbon activation, meaning both sites have to be present for the partial oxidation to occur. Furthermore, the number of active sites in the immediate region of the allylic species is dependant on the degree of oxidation (i.e. if the density of

active sites is too high, oxidation to carbon oxides takes place before the hydrocarbon desorbs.) When the product desorbs, either adsorbed gas-phase or bulk lattice oxygen replenishes the surface vacancy site, completing the redox cycle.

Adsorbed oxygen species, which consist of O_2^-, O^- and O_2^{2-}, are highly electrophilic reactants. These oxygen surface species attack hydrocarbons in regions of high electron density (i.e., the π-bonds). At lower temperatures, olefins react with peroxide species to form saturated aldehydes or with atomic oxygen to form epoxides. The presence of highly reactive allylic hydrogen in the olefin also determined the extent of reaction. The epoxidation of ethylene oxide is a good example of an electrophilic addition. Various mechanisms have been used to describe this process, one which describes molecular oxygen absorbing onto the Ag catalyst surface. The diatomic molecule is oriented perpendicular to the surface, becoming polarized with the positive pole sticking out from the surface. The protruding oxygen atom attacks the high electron density region of the C=C bond and splits from the catalyst surface to form ethylene oxide and an atomic oxygen species. Other studies indicated atomic oxygen as the favorable species in epoxidation.

The formation of an electrophilic oxygen species was not limited to gas-phase chemisorption of oxygen. Transfer of lattice oxygen to the surface was possible through dissociation of the solid or under reducing conditions. This phenomenon was observed in the oxidation of o-xylene over V_2O_5 catalysts. At temperatures below 350°C, electrophilic surface oxygen formed only combustion products from o-xylene, while at higher temperatures, the more selective nucleophilic route to phthalic anhydride was

observed.[1] An illustration of lattice and gas-phase oxygen forming electrophilic species is given in Figure 2. When temperature is low and there are no reactive allylic C-H bonds available, electrophilic species should not attack bonds so aggressively to form only combustion products.

2.2. Effects of Water Addition to Catalytic Systems

Three main effects of water can be characterized into three effects: adsorptive, structural, and chemical. Depending on the catalytic system, these effects can either promote or inhibit the desired catalytic activity.

The role of water in the selective oxidation of propylene to acrolein, acrylic acid and other products was extensively studied by Saleh-Alhamed et al.[2, 3] Over a Sb/Sn/V oxide catalyst (composition 2/1/1, respectively) at 340°C, reactor studies showed that with the addition of 10% water, reaction rate to acrolein and acrylic acid more than doubled, while rate to combustion products was decreased by a factor of 2.The addition of water also did not appear to alter the reaction order with respect to propylene. Water, concentration did have an effect on rates of formation, as above 5% in the feed began to show decreases in all rates, particularly acrylic acid. It was proposed that water vapor had strong competitive adsorption with either sites where acrylic acid was formed or stored. Temperature-programmed desorption studies were used to further elucidate the behavior of water. The pre-adsorption of water appeared to inhibit strong bonding sites, responsible for C-C scission and total combustion, while also converting moderate strength adsorption sites into weak adsorption sites. This was assigned as a minor effect, as normal temperatures used in this catalytic oxidation was proposed to make weaker

adsorption sites irrelevant. The main effect of water, therefore, was attributed to the competitive adsorption between acrylic acid and water on strong adsorption sites.

Aoki et al. studied water addition in the MoO_3/SiO_2 catalytic system used for MTA (methane to alcohol) conversion.[4] EXAFS measurements and analysis were used to propose the MoO_3/SiO_2 structure, upon water saturation, had structures resembling silimolybdic acid (SMA) crystallites. The high activity in the presence of water vapor was attributed to the formation of silimolybdic acid (SMA) on the catalyst surface, which was proposed to inhibit further reaction of methanol or formaldehyde to carbon oxides. At the temperatures studied, SMA is normally not stable, however it was proposed a combination of high catalyst dispersion and excess water vapor in fact stabilized SMA. Here a chemical change clearly took place on the surface, with water addition causing a bulk structural transformation.

Isotopic studies done by Moro-oka et al. involving propylene oxidation over SnO_2-MoO_3 catalysts showed the addition of ^{18}O-labeled water to the reactant stream resulted in labeled acetone but non-labeled acrolein. The explanation for the effect of water addition was that water dissociatively adsorbed on the catalyst surface so that surface OH species were formed, which acted as new sources of reactive oxygen.[5] This effect was proposed to exist in an adsorbed phase, as bulk phase (lattice) oxygen was responsible for acrolein production at higher temperatures. In fact, most of these experiments were performed between 100-300°C, with lower temperatures favoring acetone formation. It was concluded the available oxygen for acetone formation was not bulk lattice oxygen, but surface oxygen species that could readily exchange with

adsorbing water oxygen. This type of effect can be characterized as more of a chemical effect, that while not altering the overall catalyst bulk structure, water does chemically interact with the surface to donate oxygen, taking part in the redox cycle.

2.3. Selective Oxidation of 1,3 Butadiene

Centi and Trifiro examined the two possible reaction mechanisms (electrophilic and nucleophilic) for the selective oxidation of 1,3-butadiene over V-P-O catalysts. The two proposed mechanisms are outlined in figure 3. This research indicated that the electrophilic route was the more plausible one for this reaction, for the following reasons. (i) Comparisons between the reactivity of 1,3-butadiene and furan showed similar activities toward maleic anhydride. Examining the second (electrophilic) mechanism, this behavior is valid. Both 1,3-butadiene and furan require the addition of oxygen and the removal of hydrogen. (ii) experimental results showed the rate of furan formation to be dependent on both butadiene and oxygen, indicating a dependence on gas-phase oxygen (iii) oxidation to furan and maleic anhydride takes place without the presence of catalyst (at higher temperatures), which would imply oxygen species present in the gas phase (radicals or non-lattice species) are important for this process. The high regions of electronegativity in 1,3-butadiene and furan support this argument. (iv) in the oxidation of butadiene, a small amount of crotonaldehyde is formed (this is not the case in furan oxidation) which again indicates that O-insertion is the first step. (v) Catalysts containing Ag are well known for electrophilic oxidation and show high selectivity to furan from 1,3-butadiene. From these arguments, it was concluded that electrophilic oxidation followed by allylic dehydrogenation is the best explanation of the mechanism for

selective oxidation of 1,3-butadiene to furan and maleic anhydride. [6] This paper does not consider the 1,2-addition of surface oxygen species, which would most likely strengthen the argument for an electrophilic mechanism. All of the products observed (particularly crotonaldehyde) are explainable through this mechanism.

The Ag surface is well known for its catalytic properties in electrophilic oxidations. Madix et al. studied the Ag (110) and (111) surfaces for several selective oxidations. Temperature programmed desorption studies of the epoxidation of norbornene to norbornene oxide over Ag (110) indicated that the rate-limiting step was the reaction of norbornene with atomic oxygen on the surface. Several groups investigated the addition of absorbed oxygen to 1,3-butadiene. Two possible mechanisms were investigated; 1,4-addition and 1,2-addition to form 2,5-dihydrofuran and 3,4-epoxy-1-butene, respectively. Absorption studies of 1,3-butadiene onto an oxygen-covered Ag (110) surface suggested a 1,4-addition to form 2,5-dihydrofuran.[7] In agreement with these results, Jørgensen et al. used extended Hückel calculations to show 1,4-addition is thermodynamically favored to 1,2-addition.[8] Nevertheless, Monnier observed 3,4-epoxy-1-butene in the oxidation of 1,3-butadiene over Ag (110) catalysts. In fact, it appeared that the 1,2-addition of oxygen was preferred mechanism, and 3,4-epoxy-1-butene was an intermediate in producing 2,5-dihydrofuran and the other products.

Comparing the reaction mechanisms for 1,2 and 1,4-addition to butadiene through kinetic studies and product analysis, Monnier concluded that electrophilic 1,2-addition accounted for all the oxidation products, as outlined in figure 4. It was proposed that

pure Ag catalyst surfaces did not allow 3,4-epoxy-1-butene to desorb before converting to 2,5-dihydrofuran, explaining why previous studies assumed 2,5-dihydrofuran as the direct product from 1,3-butadiene.[9] The addition of CsCl to the Ag catalyst surface not only allowed 3,4-epoxy-1-butene to desorb before converting to 2,5-dihydrofuran, but it desorbed with amazing selectivity (96%) at 21% conversion. In fact, using this same catalyst for the epoxidation of styrene to styrene oxide produced the same effect (see Figure 5a), increasing selectivity to the epoxidation product 33%.

A number of other non-allylic olefins were tested using this catalyst. The reaction of oxygen and 4-vinylpyridine, 4-vinyltoluene, norbornene and bicyclo[2,2,2]oct-2-ene over the CsCl promoted Ag catalyst were all tested for epoxidation products. As shown in Figure 5, only 4-vinyltoluene did not predominantly produce the epoxidation product. In fact, only combustion products were detected. This was explained by the presence of the para $-CH_3$ group containing 3 allylic hydrogens. These C-H bonds will break easily during oxidation. This indicates compounds such as propylene and 1-butene would not form epoxidation products using this catalyst because the presence of the allylic C-H bonds would lead to total combustion (as has been shown to be the case.)[10]

2.4. The VMoO Catalytic System

In the 1930's, the oxidation of benzene was commercialized using promoted V_2O_5-MoO_3 catalysts. In the near 50 years when this was the primary source of maleic anhydride, a vast amount of research has been done on many aspects of this process and specifically the V_2O_5-MoO_3 catalytic system. Still, with decades of research on this catalyst for this specific reaction, many questions remain. Structurally, the phase

composition of these mixed oxide catalysts has been investigated extensively, yet in some cases questions still remain as to what intermediate VMoO compounds exist. Questions regarding the identity of the active sites (such as whether the V=O bond is a necessary component in selective oxidation) have been left unanswered. Identification of active catalytic sites - whether the V=O bond is a necessary component for selective oxidation - has been a source of further discrepancy. The nature of the active oxygen species (such as whether adsorbed or lattice oxygen is inserted into the hydrocarbon) is still unknown.

2.4.1. Structure and composition in VMoO catalysts

A general phase diagram of the V_2O_5-MoO_3 system is illustrated in Figure 6. As shown in the phase diagram, at the eutectic temperature (611°C) the solubility limit of MoO_3 in V_2O_5 is about 30 mol %. This solid solution is a substitutional type, keeping the same metal to oxygen ratio as the parent structure, V_2O_5. Therefore in formation of the solid solution, either the reduction Mo^{+6} to Mo^{+5} or V^{+5} to V^{+4} must take place. Experiments done by Bielanski et. al. used EPR measurements to confirm the existence of the V^{+4} cations (and lack of Mo^{+5}) in the solid solutions.[11] Under 10 mol % MoO_3 the structure is orthorhombic (denoted phase α), and at higher solid solution concentrations the crystal structure distorts to monoclinic (denoted phase α').[12,13] These two structures are represented in Figures 7 and 8. In these studies, no appreciable solid solution of V_2O_5 in MoO_3 was observed. However, there has been evidence of a compound of substituted vanadium into the reduced Mo_4O_{11} structure where vanadium occupies ¼ of the molybdenum positions, corresponding to a VMo_3O_{11} structure (3 Mo^{+6} ions, 1 V^{+4} ion).[14]

There has been a great deal of controversy describing the intermediate phase (designated β) composition. In 1966, Eick and Kihlborg proposed the crystal structure of V_2MoO_8. This structure is very similar to V_2O_5 with rows of corner sharing molybdenum octahedra inserted along the b and c-axis of the lattice (Figure 9).[15] Other groups proposed a slightly reduced $V_9Mo_6O_{40}$ phase, with 6 Mo^{+6} ions, 8 V^{+5} ions and 1 V^{+4} ion. Under solid state synthesis conditions, the evolution of oxygen from the mixtures of MoO_3 and V_2O_5 powders above 30% $MoO_3/(MoO_3 + V_2O_5)$indicated some amount of reduction taking place, specifically V^{+5} changing to V^{+4}. [16, 17, 18]

Phase transformations of a VMoO solid solution (10 mol % MoO_3 in V_2O_5) was monitored in the selective oxidation of benzene to maleic anhydride. This catalyst was subjected to mild reduction with benzene, and then immersed in epoxy resin. From this resin, 600-700Å slices were cut from the surface layers. After reduction with benzene, x-ray analysis indicated that the first layer (slice) was mostly MoO_3 along with the reduced phase $Mo_{17}O_{47}$. The second layer contained both these phases plus $V_9Mo_6O_{40}$. Subsequent layers contained this VMoO intermediate phase and reduced vanadium oxide V_3O_7. After 16 months in an industrial reactor, the surface catalyst layers contained several reduced molybdenum oxides, as well as two different VMoO phases, $V_9Mo_6O_{40}$ and $V_6Mo_4O_{25}$.[19] It is apparent that multiple phases and contact arrangements are possible in these compounds.

Catalytic activity enhancement may be linked to these structural changes in the V_2O_5- MoO_3 arrangement. Bielanski et al. proposed mobile molybdenum and vanadium cations during reduction and reoxidation conditions, which could account for the

previously discussed phase segregation. Using point x-ray microprobe analysis, three spots on a crystallite cut from the V_2O_5-MoO_3 compound were examined. Under oxidation conditions, molybdenum concentration decreased by 50% in samples containing bulk 10 mol % MoO_3. When the catalyst was reduced, the molybdenum concentration increased to almost 30% more than the fresh catalyst. The driving force behind this segregation is the surplus or deficiency of surface oxygen atoms during the redox cycle. Mobile V cations will move through interstitial channels to areas of high oxygen concentration, which means onto the surface in the case of oxidative conditions and into the bulk during reduction conditions.[20] If this segregation is in fact taking place, then the catalytic system would be constantly changing its composition through the reduction-reoxidation cycle, adding further complexities to this system. The ability for these cations to diffuse through the structure is proposed to be an interstitial channel within the V_2O_5 structure of width 2.2Å. This channel, larger in diameter than the radius of both Mo and V cations, running along the (010) and (001) directions.

2.4.2. Role of oxygen species in VMoO catalyst for benzene oxidation

The role of the V=O bond in the structure of VMoO catalysts has been examined by several groups. In the V_2O_5 structure, the V=O bond is the shortest (1.58 Å) and also the strongest. It has been a source of controversy whether this oxygen is a participant in benzene oxidation. Tarama et al proposed that the exposed V=O bonds were the most reactive. Using IR, this group noted that the V=O signal appeared as a sharp band in the 1025 cm^{-1} range. As MoO_3 was added to the catalyst, this band shifted lower, indicating a substitutional-type solid solution of MoO_3 in V_2O_5 taking place with exchange of Mo

for V positions in V=O sites. This group also noticed under reduction conditions, the V=O peak decreased in intensity, suggesting that the reduction gas stripped away the doubly-bonded oxygen relatively easily.[21] From these results the conclusion was made that the ease in breaking the double-bonded oxygen was directly related to the catalytic activity.

Bielanski and Inglot also examined the role of the M = O (M represents either Mo or V) double bond in mixed oxide catalysts of vanadium and molybdenum. Three compositions were examined – pure V_2O_5, 33.1 mol % MoO_3 in V_2O_5 (solid solution) and $V_9Mo_6O_{40}$. Infrared (IR) spectroscopy was used to identify the double bonds V = O and Mo = O at ca. 1025 cm^{-1} and 985 cm^{-1}, respectively. Comparing fresh catalysts to catalysts reduced by the reactive gases or nitrogen, two things are noted. First, for pure V_2O_5 and the solid solution of MoO_3 in V_2O_5, reduction causes the bands characteristic to the double bond (V=O or Mo=O) to be lost (fresh $V_9Mo_6O_{40}$ did not exhibit IR bands for M = O.) Secondly, catalytic activity is much higher for these reduced catalysts. For V_2O_5 alone, benzene conversion of 50% was not observed for fresh catalyst until 666°C with no maleic anhydride produced, while reduced catalysts observed 50% conversion at 279°C with 39% selectivity to maleic anhydride. Of the three catalysts, the solid solution exhibited the best selectivity. The $V_9Mo_6O_{40}$ catalysts had significant activity as a fresh catalyst. From these results this group concluded that the double bonded oxygen are not the catalytically active centers. It is noted that although the oxygen itself might not be the active center, the exposed vanadium atom in the vacancy site might be necessary to activate (adsorb) the benzene molecule. In fact, the presence of a V=O bond is suggested

by these researchers to inhibit benzene adsorption.[22, 23] Considering that activity is directly related to the degree of reduction of these catalysts, discrepancies in data reported from different research groups can be explained by varying initial catalyst state (a low activity could be correlated to a pretreatment under oxygen.)

As discussed earlier, reducing conditions can transform lattice oxygen into adsorbed electrophilic species. Whether that oxygen stays adsorbed on the surface as an electrophilic species depends on the chemisorption properties of the material. The temperature and pressure dependence of oxygen chemisorption in V_2O_5 was investigated volumetrically. In the temperature range of 100-450°C, maxima for chemisorbed species occurred at 250°C and 400°C. Surface coverage at 250°C was θ=0.015. The adsorption characteristics were best fitted with a Langmuir model,

$$C_a = \frac{K(P - P_e)}{1 + K(P - P_e)}$$

where K, K' are constants, C_a the number of adsorbed molecules, P pressure and P_e the initial equilibrium pressure. At the low temperature range (0-300°C), the formation of adsorbed O^{2-} species from the crystal lattice is correlated from the V^{+4} to V^{+5} oxidation.[24]

Volkov studied oxygen chemisorption in the V_2O_5-MoO_3 system. Anodic and cathodic current measurements were correlated to the amount of chemisorbed species on each phase composition. Both currents were highest for V_2O_5 and solid solutions of MoO_3 in V_2O_5 (specifically the saturation point), and near zero for the intermediate phase and pure MoO_3. An additional maximum was found near 10 mol % MoO_3. Addition of MoO_3 to the V_2O_5 structure reduced the V^{+5} to V^{+4} to accommodate the Mo^{+6} cations

replacing V^{+5} cations in the structure. At the saturation point, not only was the reduction from Mo insertion maximized, but the amount of weakly-bound oxygen was highest, leading to evolved and chemisorbed oxygen species. This group described reduction of V_2O_5 and V_2O_5- MoO_3 as

$$V_2O_5 + ye^- \rightarrow V_2O_{5-y} + yO^-$$

and

$$(V_{1-x}Mo_x)_2O_{5+y} + ze^- \rightarrow (V_{1-x}Mo_x)_2O_{5+y-z} + zO^-,$$

respectively In both cases the released species was described as chemisorbed atomic oxygen.[25] From these equations, reduction and/or the amount of Mo present directly effected the amount of released oxygen. It should be noted that these equations referred to V_2O_5-based structures, i.e. V_2O_5 and solid solutions of MoO_3 in V_2O_5.

2.5. Solid-Solution Metal Oxide Catalysts

While pure metal oxides usually provide some of the desired catalytic functions, it is often the case that promoted or multiphase materials provide much higher activity compared to their single-phase counterparts. One explanation for this phenomena was based on the proposed occurrence of solid solutions. Metal oxide solid solutions maintain a parent crystal orientation but have substitutional or interstitial "foreign" cations. The presence of the additional cations often causes changes in the oxidation state of the pure substance cations, as is in the case with V_2O_5-MoO_3. The parent V_2O_5 structure has Mo^{+6} ions substituted for certain V^{+5} sites. In order for the structure to maintain overall charge neutrality, either the Mo^{+6} cation must reduce to Mo^{+5} or the V^{+5}

must reduce to V^{+4}. As discussed before, the amount of oxygen available may be increased as Mo is incorporated into the V_2O_5 lattice.

In mixed Bi-Ce molybdates, maximum catalytic activity for the nucleophilic (amm)oxidation of propylene was achieved at the solubility limits of the solid solutions. In this case, there were two solubility limits, one of cerium in bismuth molybdate, the other bismuth in cerium molybdate. The enhancement in activity, based on Grasselli et al., is that all the required functional sites were present in the solid solution structure. Bismuth cations were responsible for α-H abstraction from propylene, molybdenum ions were responsible for propylene chemisorption and oxygen (or nitrogen) insertion and the cerium redox couple enhanced oxygen and electron mobility in the catalyst (allowing more rapid vacancy reoxidation/reconstruction.) This "job distribution" of various atoms was proposed to be optimized with the maximum amounts of each component.[26,27]

Interfacial phenomena were also examined between solid solutions of bismuth-cerium molybdate catalysts used for propylene ammoxidation. In this catalytic system, the existence of a coherent interface between phases was postulated to promote oxygen diffusion across the grain boundary; however this was not the primary effect of the coherent interface. Thermodynamically, the two phases in contact minimized the amount of free energy across the interface. In this case the formation of a uniform non-ideal solid-solution was postulated. It was proposed necessary for the material to contain a maximum amount of Bi and Ce cations per molybdate center to maximize catalytic activity. [28]

Structural transformations of metal-doped antimony oxides were investigated by Grasselli et al. The α–β transformation of Sb_2O_4 was lowered by 800°C when Mo is present in the Sb_2O_4 lattice. The Mo cations present in the Sb_2O_4 structure are reported to exist interstitially. Low temperature α–β transformation was also observed when trace amounts of vanadium were introduced to the Sb_2O_4 system. In this case, however, V was incorporated substitutionally for Sb^{+3} cations. Considering the nature of the incorporation of V and Mo into the Sb_2O_4 structure, it was proposed that both V and Mo existed in Sb_2O_4.[29]

2.6. Interfacial Phenomenon in Multiphase Oxide Catalysts for Selective Oxidation

Several multiphase catalytic systems have been studied for the influence of interfacial materials on overall activity. The contact region between different phases can enhance the catalytic activity of metal oxide catalysts. This interfacial region is difficult to characterize, resulting in varying explanations for catalytic enhancement. In some cases physical and chemical properties were used to correlate interfacial phenomena with catalytic activity.

The interfacial phenomena in multiphase materials of V_2O_5 and TiO_2 and their effects on catalytic performance have been examined. In selective oxidation of o-xylene to phthalic anhydride, an enhancement of catalytic activity and selectivity was observed when using the V_2O_5-TiO_2 (anatase) catalyst. Thermogravimetric studies of TiO_2 (anatase) supported V_2O_5 revealed that at 600°C in nitrogen, the unexpected, simultaneous, reduction of V_2O_5 and TiO_2 anatase-to-rutile transformation occurred. These phase transformations do not normally occur in this temperature range.[30] This

phenomenon was explained by a close crystallographic fit between the two bulk phases. This interfacial region lowered the activation energy for these reconstructions to occur. This effect provided the initial step ($V^{+5} \rightarrow V^{+4}$ reduction) of the redox cycle.[31] X-ray diffraction confirmed the existence of the two bulk phases, indicating no detectable interfacial phase. These measurements were misleading, as the region affected in the coherent interface could only be a few angstroms thick, too small for a bulk technique such as XRD to detect. TEM studies were used to examine the interface itself and verify the nature of the contact region. The interface reacted under the electron beam, making it difficult to provide indisputable evidence of a crystallographic fit. It should be noted the reaction to the electron beam was only observed at the interface, indicating the presence of an enhanced, more dynamic, structure.[32, 33] A crystallographic fit between two phases will only occur if the contacting lattice planes were similar enough so that the bond strain between phases is minimal, no more that a few percent.

Nickel molybdate catalysts exhibited synergistic effects in several hydrocarbon oxidations, predominantly when excess MoO_3 was present with $NiMoO_4$. When using standard catalyst preparation methods for multiphase metal oxides, complex morphologies and contact arrangements make it difficult to characterize the interface. Zou and Schrader used thin film metal oxides created via reactive sputtering to investigate this interfacial region in the selective oxidation of 1,3-butadiene. Thin films of uniform composition were constructed, consisting of α-MoO_3, α-$NiMoO_4$, and bi-layered films of α-$NiMoO_4$ and α-MoO_3 deposited on silicon wafers. Control over stoichiometry and crystal structure provided by reactive sputtering allowed specific

phases and interfacial regions to be created. These films were characterized by XRD, LRS, XPS, XRF, SEM and TEM. An enhancement of activity and selectivity was observed in layered α-$NiMoO_4$ over α-MoO_3 compared to other thin films. Laser Raman characterization of this thin film indicated Raman bands for α-MoO_3, α-$NiMoO_4$ and a material with similar bands to β-$NiMoO_4$ at 949 cm^{-1}. XRD detected trace amounts of (220) β-$NiMoO_4$, as well as (0k0) α-MoO_3 and (110), (220), and (330) multiple reflections for α-$NiMoO_4$. Other trace signals for α-$NiMoO_4$ and α-MoO_3 were also observed. The coherent interface is proposed, from these results, to be the (010) plane of α-MoO_3 and the (110) plane of α-$NiMoO_4$. When compared to thin films of α-MoO_3, α-$NiMoO_4$, β-$NiMoO_4$ and layered α-MoO_3 over α-$NiMoO_4$, the layered α-$NiMoO_4$ over α-MoO_3 film had higher selectivity to furan, 2(5H)-furanone, and maleic anhydride at similar conversions. These results supported that the enhancement of catalytic activity in MoO_3-rich $NiMoO_4$ (precipitated) catalysts was a result of a coherent interface. It was not, however, only the presence of the interface that was necessary for enhanced selectivity. Thin films of α-$NiMoO_4$ with α-MoO_3 overlayers were active but produced mostly combustion products. It was suggested that with a α-$NiMoO_4$ overlayer it is possible that (i) the formation of theβ-$NiMoO_4$-like interfacial material also provided more active and selective sites or (ii) combustion sites on the (010) face of α-MoO_3 (Mo=O bonds) were blocked by the overlayer of α-$NiMoO_4$, while the more selective sites remained available.[34, 35]

Studies of interfacial phenomena were also done on the $NiMoO_4$-MoO_3 catalytic system by Lezla et al. The method of preparation used had a critical effect on whether the desired enhancement occurred. Different preparation methods were used to make several $NiMoO_4$-MoO_3 catalysts, including precipitation, mechanical mixture, sol-gel, impregnation and evaporation to dryness. In these studies, the synergetic effects were greatest from catalysts prepared through precipitation with the atomic ratio of Mo/Ni at approximately 1.27. High-resolution TEM studies of these active materials indicated (020) α-$NiMoO_4$ directly in contact with (200) α-MoO_3 (4,000,000x magnification). The crystallographic misfit between these phases was calculated to be a few percent. This coherent interface was identified as the source of enhanced catalytic activity. The researchers attributed the redox couple of Mo^{+6}/Mo^{+5} was facilitated by the interface, enhancing the activity for propane oxidation. Thermal analysis was used to understand the differences in preparation conditions and distinguish what necessary conditions needed to be present in making active catalysts. The determined important factor in preparation was to make α-MoO_3 crystallites with a α-$NiMoO_4$ overlayer. Conclusions were drawn that the best preparation methods were those that allowed developed α-MoO_3 crystallites to be coated with smaller crystallites of α-$NiMoO_4$.[36] These studies made it difficult to examine the actual nature of the coherent interface. Any hybrid phase at the interface was not detectable by XRD, and HRTEM studies even cannot characterize the interface composition, as it will be on the order of angstroms thick. It should be noted that high-temperature β-$NiMoO_4$ catalysts having the optimal ratio Mo/Ni=1.27 were 14 times less active at similar temperatures than their α-$NiMoO_4$ counterparts.

The results from the two studies on the nickel molybdate system appear somewhat conflicting. The results by Zou and Schrader indicate that a β-$NiMoO_4$-like material is formed at the interface; Lezla et al. indicated that this phase was detrimental to the catalytic activity of their reaction. It is probable that the β-$NiMoO_4$-like material is found only between the (010) plane of α-MoO_3 and the (110) plane of α-$NiMoO_4$. In fact, calculations done by Zou and Schrader showed a transition between (110) α-$NiMoO_4$ to (110) β-$NiMoO_4$ to (010) α-MoO_3 would have a very low crystallographic misfit. The planes Lezla et al. observed under HRTEM were (020) α-$NiMoO_4$ over (200) α-MoO_3. Perhaps it is more favorable to have a different interfacial material between these planes. It is likely a reduced MoO_3 phase existed at the interface in the Lezla et al. studies, which would facilitate the Mo^{+6} to Mo^{+5} transition favorable for the redox cycle in propane oxidation.

The previously discussed segregation in the V_2O_5-MoO_3 system has led to studies examining possibilities of crystallographic fits between V_2O_5-MoO_3 solid solutions and the intermediate (β) phase. Samples of V_2O_5-MoO_3 made from the fusion of pure oxides were tested for electrical resistivity. If the phases in contact are viewed as an electrical circuit, the nature of the grain boundary was proposed to affect the conductivity of the substance as a whole (see Figure 10). In essence, a lower crystallographic misfit between two grains b and b' would lower the resistance R_c from one grain to the other. Two likely crystallographic fits were determined - the (001) plane of V_2O_5 with the (001) plane of V_2MoO_8 and the (001) plane of V_2O_5 with the (100) plane of V_2MoO_8. The interfacial material was proposed to be 'hybrid' crystals, which was not specifically characterized.

The fit between (001) plane of V_2O_5 and the (100) plane of V_2MoO_8 was proposed to block the interstitial columns that allowed cation diffusion. This prevented further segregation in the catalyst. XRD was used to monitor cation segregation using compounds with different concentrations of MoO_3 in V_2O_5. Segregation was not detected for a solid solution concentration of 30 mol % MoO_3, while in the 10 mol % MoO_3 segregation still occurred. In this case it was concluded that only the crystallographic fit between the (001) planes of V_2O_5 and V_2MoO_8 existed. Visualization of these possible fits is given in Figure 11.[37]

2.7. List of Figures

1. Mars and van Krevelen redox cycle
2. Lattice and gas-phase formation of surface oxygen species.
3. Reaction pathways for 1,3 butadiene to furan and maleic anhydride by (a) nucleophilic addition or (b) combined nucleophilic and electrophilic addition.[6]
4. Reaction pathway(s) for 1,3-butadiene over Ag catalyst. Arrow thicknesses represent relative rates.[9]
5. Epoxidation reactions using CsCl-promoted Ag catalysts of (a) styrene (b) 4-vinylpyridine (c) 4-vinyltoluene (d) norbonene and (e) bicyclo [2,2,2] oct-2-ene.[38]
6. Phase diagram of V_2O_5 - MoO_3 system
7. Idealized crystal structure of V_2O_5 or solid solution MoO_3 in V_2O_5 (α) (a) as octahedra in the (001) plane. (b) as octahedra in the (010) plane. (c) single vanadium and oxygen coordination. [39]

The fit between (001) plane of V_2O_5 and the (100) plane of V_2MoO_8 was proposed to block the interstitial columns that allowed cation diffusion. This prevented further segregation in the catalyst. XRD was used to monitor cation segregation using compounds with different concentrations of MoO_3 in V_2O_5. Segregation was not detected for a solid solution concentration of 30 mol % MoO_3, while in the 10 mol % MoO_3 segregation still occurred. In this case it was concluded that only the crystallographic fit between the (001) planes of V_2O_5 and V_2MoO_8 existed. Visualization of these possible fits is given in Figure 11.[37]

2.7. List of Figures

1. Mars and van Krevelen redox cycle
2. Lattice and gas-phase formation of surface oxygen species.
3. Reaction pathways for 1,3 butadiene to furan and maleic anhydride by (a) nucleophilic addition or (b) combined nucleophilic and electrophilic addition.[6]
4. Reaction pathway(s) for 1,3-butadiene over Ag catalyst. Arrow thicknesses represent relative rates.[9]
5. Epoxidation reactions using CsCl-promoted Ag catalysts of (a) styrene (b) 4-vinylpyridine (c) 4-vinyltoluene (d) norbonene and (e) bicyclo [2,2,2] oct-2-ene.[38]
6. Phase diagram of V_2O_5 - MoO_3 system
7. Idealized crystal structure of V_2O_5 or solid solution MoO_3 in V_2O_5 (α) (a) as octahedra in the (001) plane. (b) as octahedra in the (010) plane. (c) single vanadium and oxygen coordination. [39]

8. Idealized crystal structure of solid solution MoO3 in V2O5 (α') (a) as octahedra in the (001) plane. (b) as octahedra in the (010) plane.[13]
9. Idealized Crystal structure of V_2MoO_8 (a) as octahedra in the (001) plane. (b) as octahedra in the (010) plane.[39]
10. Circuit representation of interfacial region.[40]
11. Crystallographic fits between (001) V_2MoO_8 and (001) V_2O_5.[41]

2.8. References

1. Bielanski, A and J. Haber, "Oxygen in Catalysis", 150.

2 Saleh-Alhamed, R. R. Hudgins and P. L. Silveston, *Applied Catalysis A: General* **127**, 177 (1995).

3 Saleh-Alhamed, R. R. Hudgins and P. L. Silveston, *Journal of Catalysis*.**161**, 430 (1996).

4. Aoki, K., M. Ohmae, T. Nanba, K. Takeishi, N. Azuma, A. Ueno, H. Ohfune, H. Hayashi, Y. Udagawa, *Catalysis Today* **45**, 29 (1998).

5 Moro-oka, Y, Y. Takita, and A. Ozaki, *Journal of Catalysis* **27**, 177 (1972).

6. Centi, G. and F. Trifiro, *Journal of Molecular Catalysis* **35** 255-265, (1986).

7. Roberts, J.T., A.J. Capote and R.J. Madix, *J. Am. Chem. Soc.* **113**, 9848-9851 (1991).

8. Schiøtt, B. and K. A. Jørgensen, *J. Phys Chem.* **97**, 10738-10741 (1993).

9. Monnier, J. R., 3rd World Congress on Oxidation Catalysis, 138, 1997 Elsevier Science B.V., (R.K. Grasselli, St.T. Oyama, A.M. Gaffney and J.E. Lyons, eds.)

10. Monnier, J. R., 3rd World Congress on Oxidation Catalysis, 142-143, 1997 Elsevier Science B.V., (R.K. Grasselli, St.T. Oyama, A.M. Gaffney and J.E. Lyons, eds.)

11. Bielanski, A., K. Dyrek, I. Kracik and E. Wenda, *Bull. Pol. Ac. Chem.* **19**, 512 (1971).

12. Kihlborg, L., *Acta Chim. Scand.* **21**, 2495 (1967).

13. Bielanski, A. and M. Najbar, *Applied Catalysis A: General* **157**, 254 (1997).

14. Andrushkevich, T., M. Plyasova, G. Kustnetsova, A. Bondareva, T. Gorshkova, I Olenkova and N. Lebedeva, *React. Kinet. Catal. Lett.* **12** 463 (1979).

15. Eick, H.A. and L. Kihlborg, *Acta Chemica Scandinavica* **20,** 1658-1666 (1966).

16. Bielanski, A., K. Dyrek, J. Pozniczek and E. Wenda, *Bull. Pol Sci.* **19/8,** 507-512 (1971).

17. Bielanski, A. and M. Najbar, *Polish Journal of Chemistry* **52,** 383-384 (1978).

18. Bielanski, A. and M. Najbar, *Applied Catalysis A: General* **157**, 224 (1997).

19. M. Najbar and E. Bielanska, Reactivity of Solids: Proceedings of the 9th Int. Symposium on the reactivity of solids (K. Dyrek, J. Haber, and J. Nowotny, eds.), Elsvier, Amsterdam, 1982, 657.

20. Bielanski, A., J. Camra and M. Najbar, *Journal of Catalysis* **57**, 326-330 (1979).

21. Tarama, K., S. Teranishi, S. Yoshida and N. Tamura, *Proceedings of the Third International Congess on Catalysis*, Amsterdam 1964, North Holland, 1965, p.282.

22. Bielanski, A. and A. Inglot, *Bull. Acad. Polon. Sci., Ser. Sci. Chim* **22,** 773 (1974).

23. Bielanski, A. and A. Inglot, *React. Kinet. Catal. Lett.* **6/1,** 83-87 (1977).

24. Rey, L., L. A. Gambaro and H. J. Thomas, *Journal of Catalysis* **87**, 520-523 (1984).

25. Volkov, V. L., Russian Journal of Physical Chemistry, **59**, 247-249 (1985).

26. Grasselli, R. K., *Applied Catalysis* **15**, 127-139 (1985).

27. Bradzil, J. F. and R. K. Grasselli, *Journal of Catalysis* **79**, 104-117 (1983).

28. Bradzil, J. F. and R. K. Grasselli, *Journal of Catalysis* **79**, 104-117 (1983).

29. Teller, R. G., M. R. Antonio, J. F. Bradzil and R. K. Grasselli, *Journal of Solid State Chemistry* **64**, 249-260 (1986).

30. Courtine, P. and E. Bordes, *Applied Catalysis A: General* **157**, 50 (1997).

31. Vejux, A. and P. Courtine, *Journal of Solid State Chemistry* **23**, 93 (1978).

32. Vejux, A. and P. Courtine, *Journal of Solid State Chemistry* **63**, 179 (1986).

33. Bordes, E., and P. Courtine, *Journal of Catalysis* **57**, 236 (1979).

34. Zou, J. and G.L. Schrader, *Journal of Catalysis* **161**, 667-686 (1996).

35. Zou, J. and G.L. Schrader, *Thin Solid Films* **324**, 52-62 (1998).

36. Lezla, O., E Bordes, P Courtine and G. Hecquet, *Journal of Catalysis* **170**, 346-356 (1997).

37. Najbar, M. and K. Stadnicka, *J. Chem. Soc., Faraday Trans. I* **79**, 27-37 (1983).

38. Monnier, J. R., 3rd World Congress on Oxidation Catalysis, 142, 1997 Elsevier Science B.V., (R.K. Grasselli, St.T. Oyama, A.M. Gaffney and J.E. Lyons, eds.)

39. Haber, J., M. Witko and R. Tokarz, *Applied Catalysis A: General* **157**, 3-22 (1997).

40. Najbar, M. and K. Stadnicka, *J. Chem. Soc., Faraday Trans. I* **79**, 28 (1983).

41. Najbar, M. and K. Stadnicka, *J. Chem. Soc., Faraday Trans. I* **79**, 34 (1983).

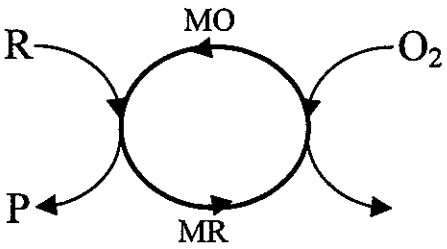

R - Reactant (hydrocarbon)
P - Product
MO - Oxide catalyst, normal oxidation state
MR - Oxide catalyst, reduced state

Figure 1

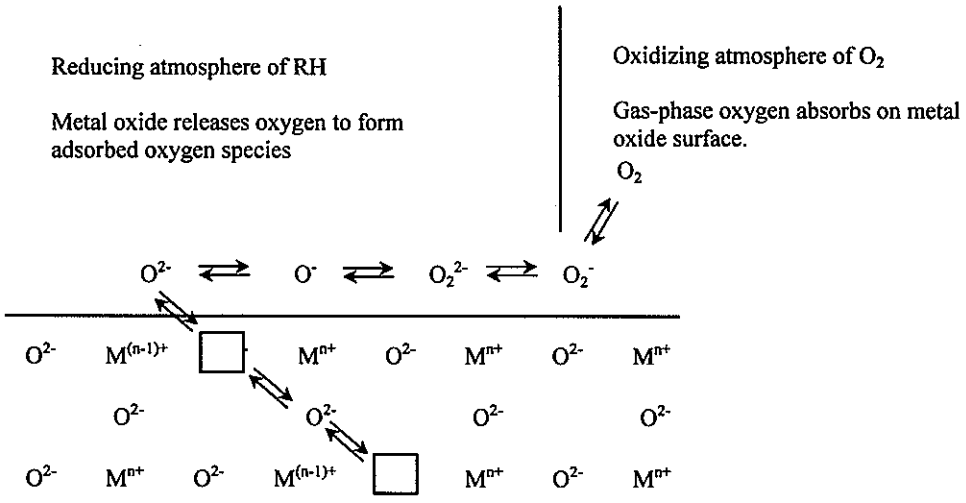
Reducing atmosphere of RH
Metal oxide releases oxygen to form adsorbed oxygen species
Oxidizing atmosphere of O_2
Gas-phase oxygen absorbs on metal oxide surface.
O_2
O^{2-}
O^-
O_2^{2-}
O_2^-
$M^{(n-1)+}$
M^{n+}

Figure 2

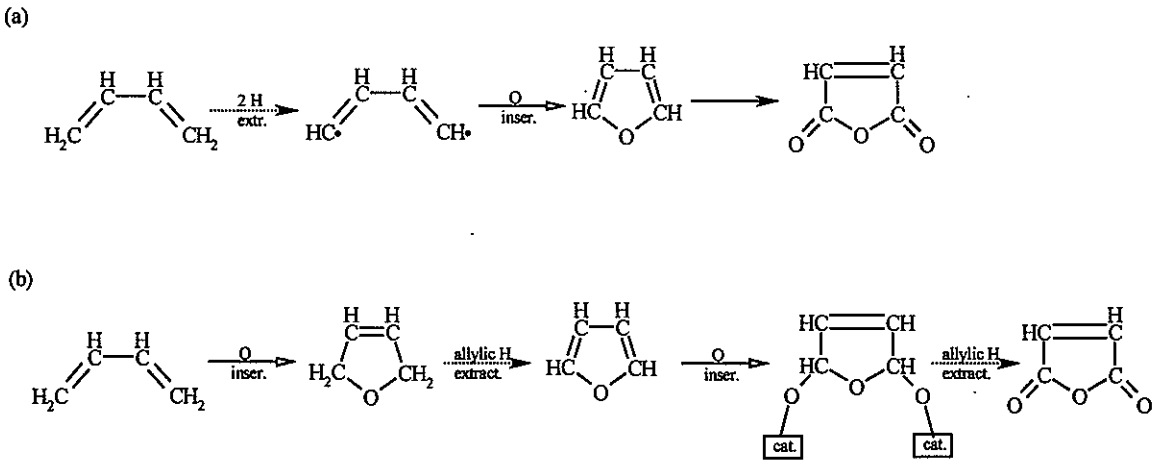
(a)
2 H extr.
O inser.
(b)
O inser.
allylic H extract.
O inser.
allylic H extract.
cat.
cat.

Figure 3

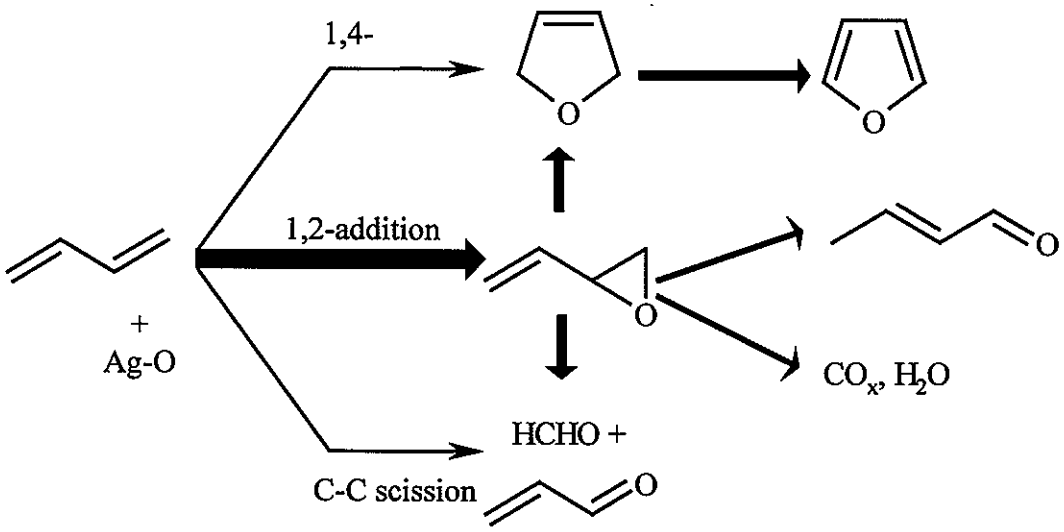

Figure 4

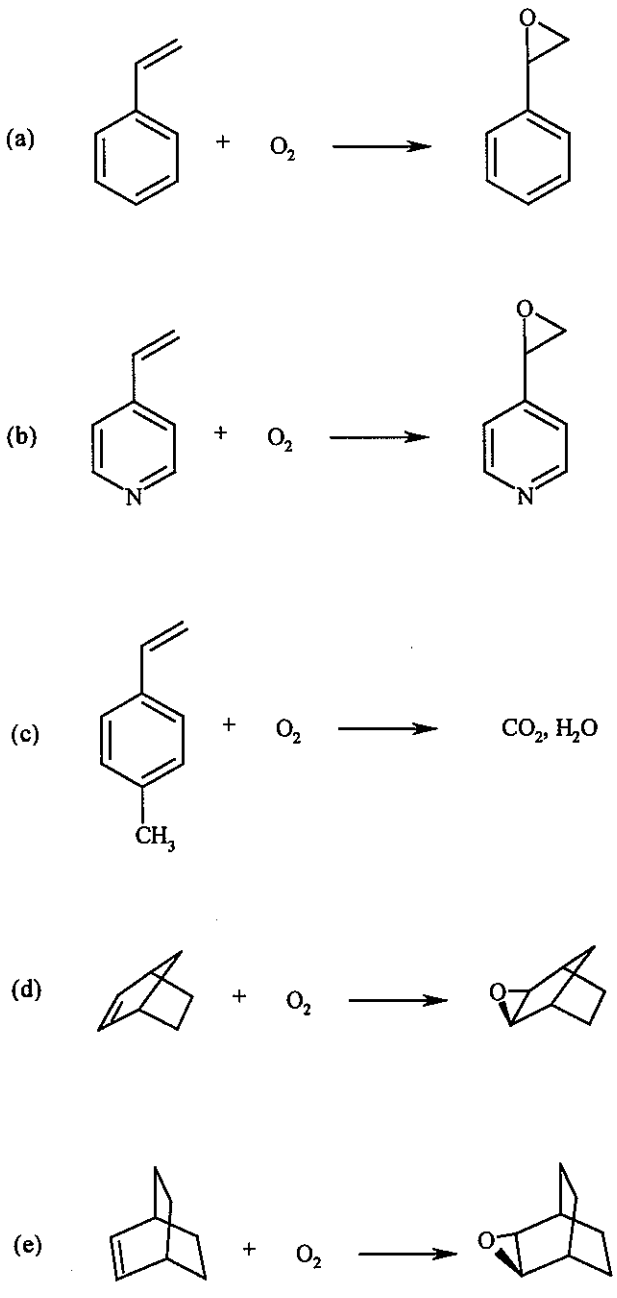

Figure 5

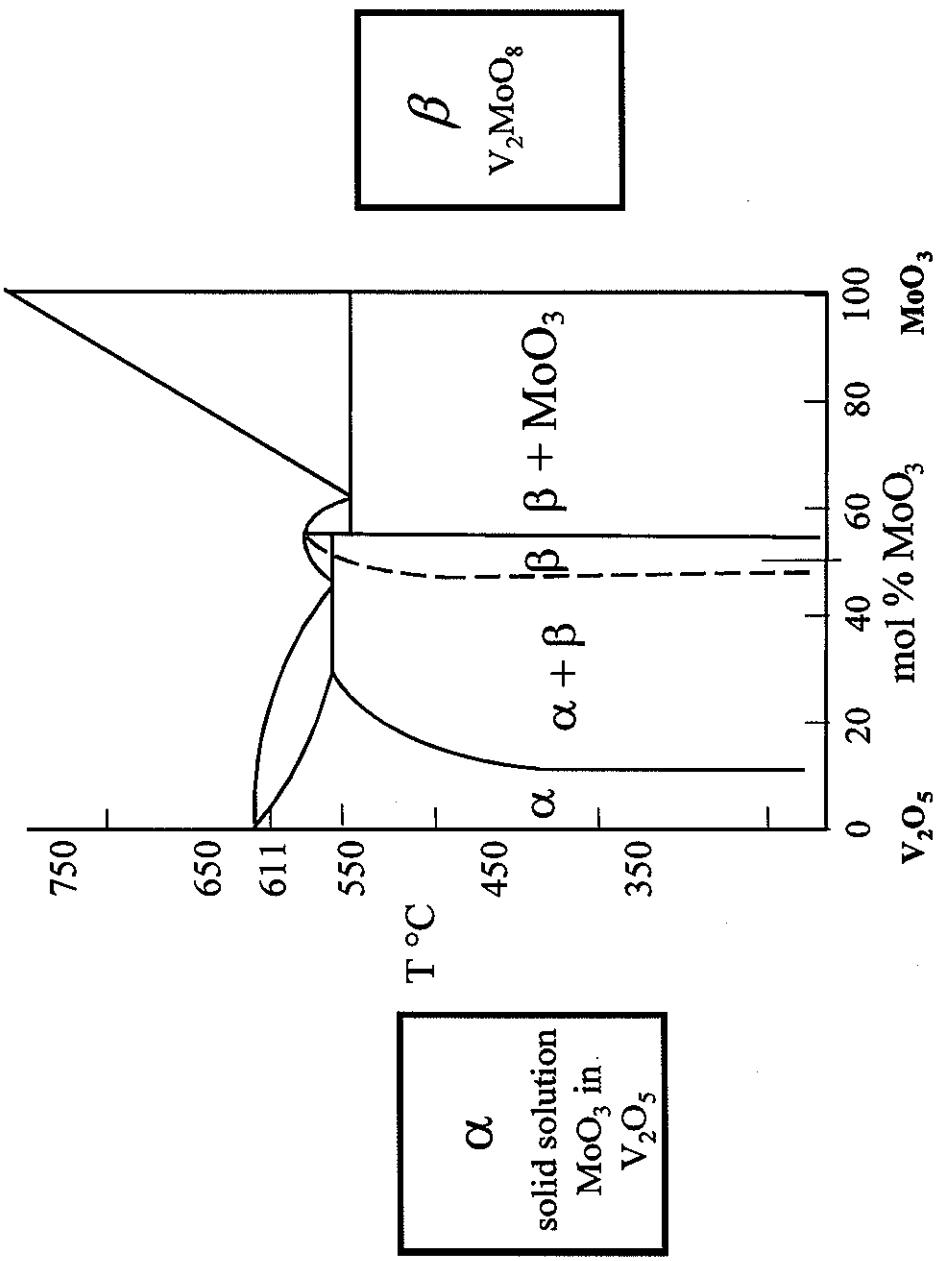
β
V2MoO8
β + MoO3
β
α + β
α
α
solid solution
MoO3 in
V2O5
T °C
750
650
611
550
450
350
0
20
40
60
80
100
V2O5
mol % MoO3
MoO3

Figure 6

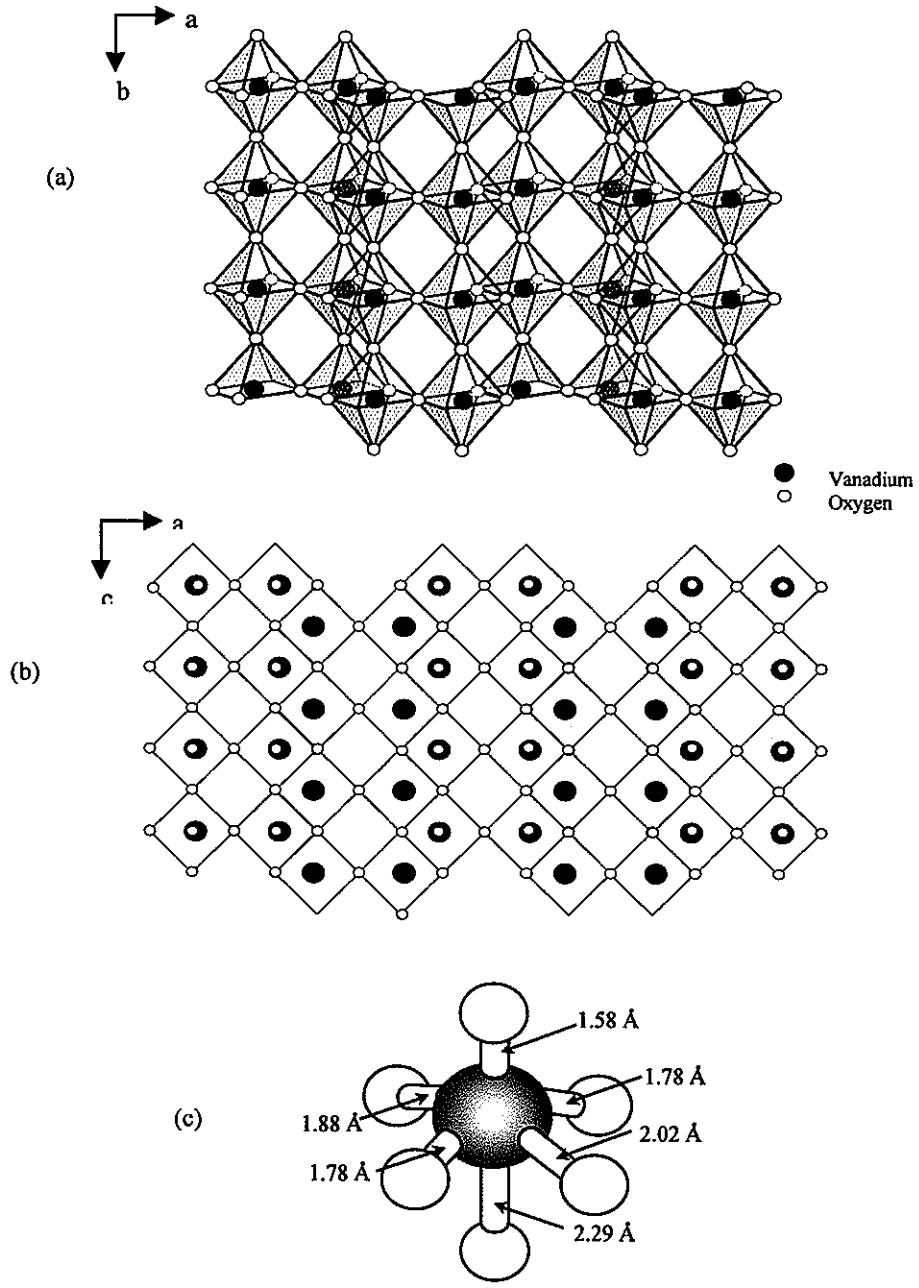

Figure 7

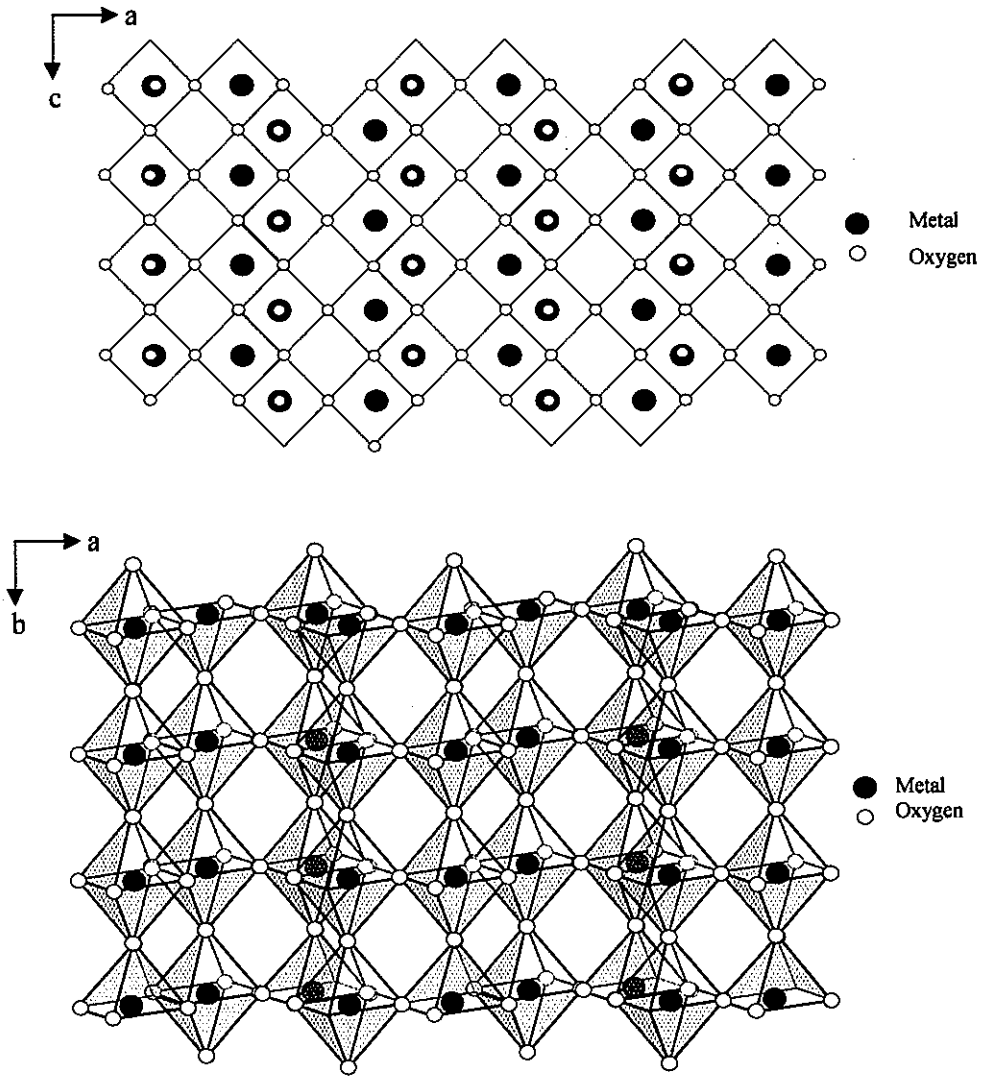

Figure 8

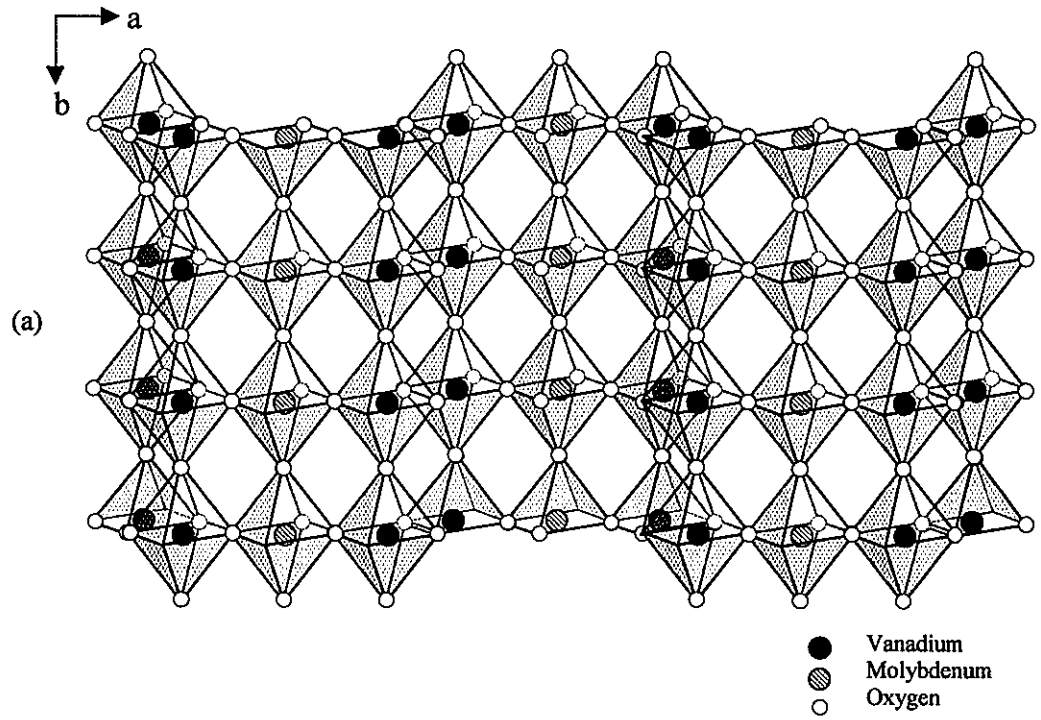

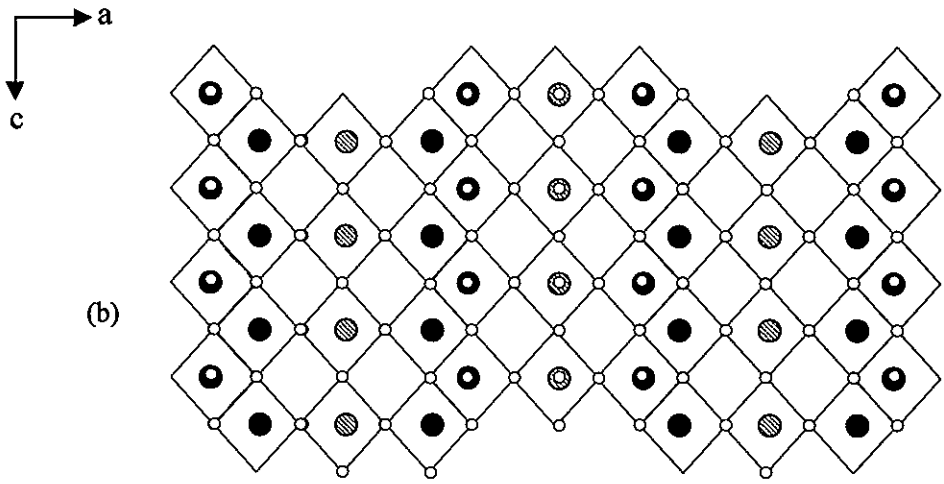

Figure 9

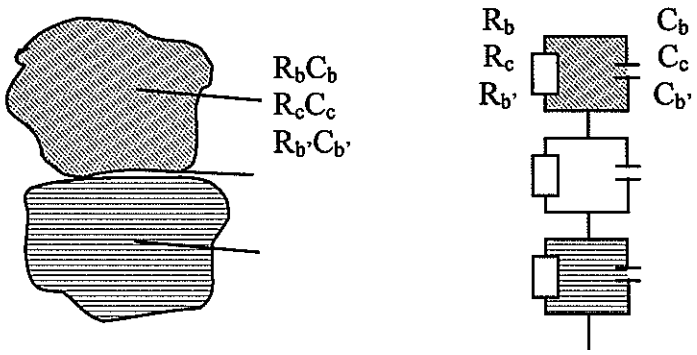

Figure 10

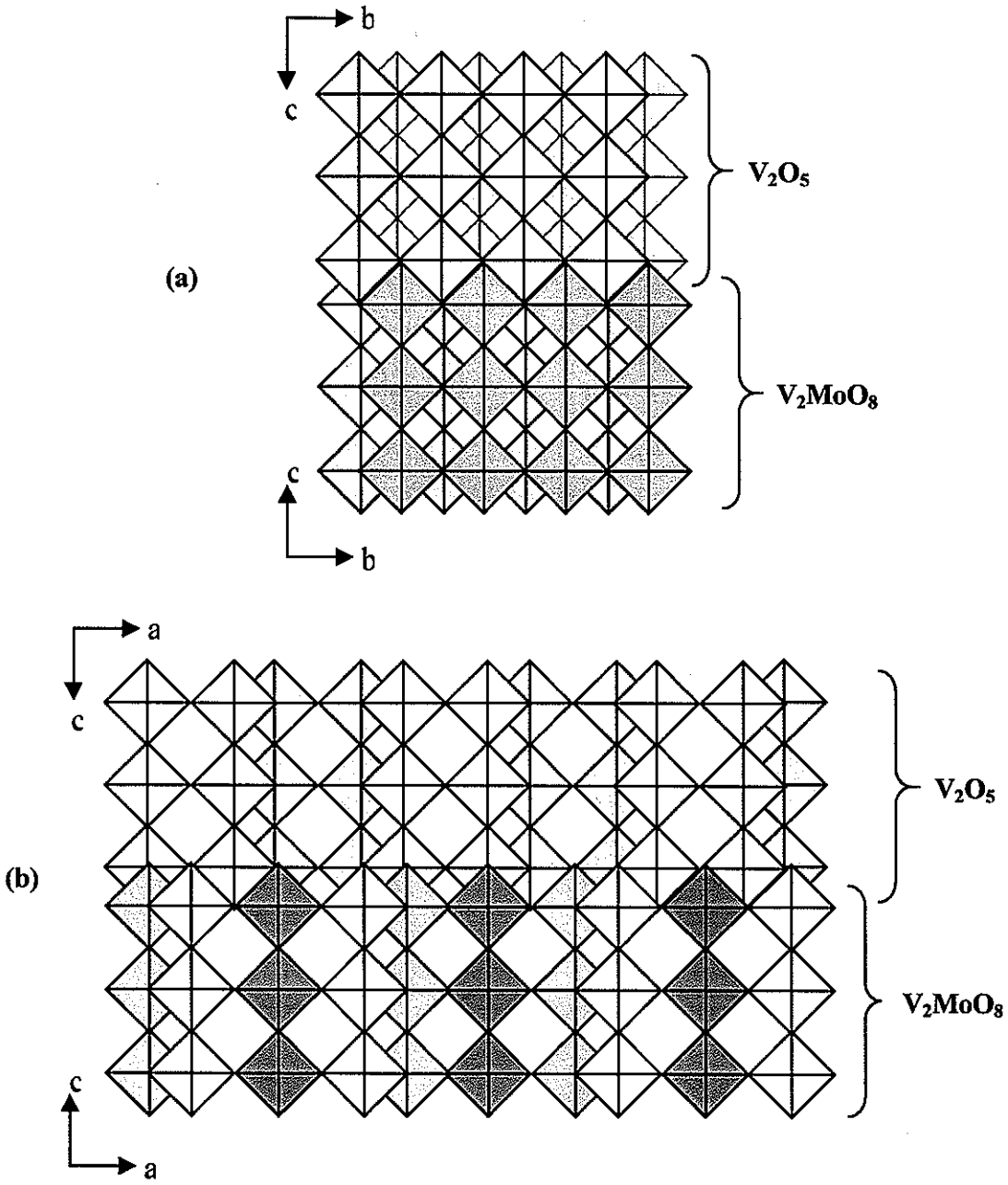

Figure 11

CHAPTER 3
1,3-BUTADIENE SELECTIVE OXIDATION OVER VMoO CATALYSTS: NEW INSIGHTS INTO THE REACTION PATHWAY

A manuscript submitted to the *Journal of Catalysis*

William D. Schroeder, C. J. Fontenot, and G.L. Schrader

Department of Chemical Engineering and Ames Laboratory – USDOE

Iowa State University Ames, IA 50011

3.1. Abstract

The partial oxidation of 1,3-butadiene has been investigated over VMoO catalysts synthesized by sol-gel techniques. Surface areas were 9-14 m^2/g, and compositions were within the solid solution regime, i.e. below 15.0 mol % (MoO_3) in V_2O_5. Laser Raman and XRD data indicated that solid solutions were formed, and pre- and post-reaction XPS data indicated that catalyst surfaces were reduced by the 1,3-butadiene-in-air feeds. The reaction pathway for 1,3-butadiene partial oxidation to maleic anhydride was shown to involve intermediates such as 3,4-epoxy-1-butene, crotonaldehyde, furan, and 2-butene-1,4-dial. The addition of water to the reaction stream substantially increased catalyst activity and improved selectivity to crotonaldehyde and furan at specific reaction temperatures.

key words: hydrocarbon selective oxidation, mixed metal oxide catalysts, 1,3-butadiene partial oxidation

3.2. Introduction

The conversion of 1,3-butadiene to maleic anhydride and other partially oxidized hydrocarbons has been examined using several selective oxidation catalysts. However, there is no generally accepted reaction pathway, particularly regarding the role of specific intermediates and the sequential conversion steps. Most studies have emphasized maleic anhydride production: other compounds such as furan and 3,4-epoxy-1-butene are potentially valuable products also.

Centi and Trifiro suggested a simple consecutive pathway for 1,3-butadiene conversion over VPO catalysts (1):

1,3-butadiene → 2,5-dihydrofuran → furan → maleic anhydride

1,4-Cycloaddition of oxygen to 1,3-butadiene produced 2,5-dihydrofuran, followed by allylic H-abstraction to form furan. Maleic anhydride was produced by further oxygen insertion into the 2- and 5-positions. Crotonaldehyde was also detected in these studies but was considered only to be a side product.

Investigations of 1,3-butadiene oxidation over Ag catalysts indicated that 1,4-addition was not the first step in the oxidation of 1,3-butadiene; rather, 1,2-addition was postulated to produce 3,4-epoxy-1-butene (2,3). Conversion of 1,3-butadiene was inhibited by the epoxide. Reaction of 3,4-epoxy-1-butene over unpromoted Ag catalysts formed furan, crotonaldehyde, acrolein, and CO_2, although only 55% of the converted 3,4-epoxy-1-butene could be accounted for. Experiments using 2,5-dihydrofuran as a feed additive indicated that furan, crotonaldehyde, and CO_2 were formed. Although 3,4-epoxy-1-butene did not produce 2,5-dihydrofuran (and vice versa), it was proposed that

the epoxide was the initial 1,3-butadiene oxidation product. Monnier suggested that 3,4-epoxy-1-butene was unable to desorb from the catalyst surface before cyclization to 2,5-dihydrofuran, isomerization to crotonaldehyde, or hydrogenolysis to acrolein. Addition of small amounts of CsCl or CsF produced a highly selective catalyst for 3,4-epoxy-1-butene production from 1,3-butadiene (96% selectivity at 21% conversion). This catalyst proved to also be efficient in the epoxidation of several other compounds, such as styrene, 4-vinylpyridine, and norborene (2,3). The increase in selectivity was attributed to a lowering of the epoxide desorption energy. Attempts to use these catalysts for the selective oxidation of compounds with allylic hydrogen (propylene, butenes, etc) were unsuccessful. Apparently, strongly electrophilic oxygen present on the modified Ag surface produced only combustion products.

In other studies over Ag surfaces, the catalytic oxidation of 1,3-butadiene has been considered to be a 1,4-addition where both C=C bonds interact with surface oxygen to form 2,5-dihydrofuran. Studies by Madix et al. postulated that for single-crystal Ag (110) surfaces, a stabilized intermediate species was formed which could desorb as 2,5-dihydrofuran. This reaction was compared to a Diels-Alder mechanism for acetylene and 1,3-butadiene conversion to benzene in which interaction of acetylene with the terminal C=C bonds of 1,3-butadiene formed a cyclic structure. In the same fashion, the active oxygen on the catalyst surface was believed to interact with the terminal C=C bonds of 1,3-butadiene to form 2,5-dihydrofuran (4).

Other selective oxidation products generated from 1,3-butadiene have also been detected, suggesting the formation of maleic anhydride by multiple pathways. Akimoto

et al. observed that over supported molybdena catalysts, maleic anhydride was formed by two temperature-dependent pathways: via 2,5-dihydrofuran with subsequent conversion to furan, or via 2,5-dihydrofuran only (5). More recent work by several research groups has suggested that these multiple pathways were a result of ring opening of cyclic compounds and subsequent reaction of "open-chain" compounds. Re-cyclization or the partial oxidation intermediates could then produce maleic anhydride. Crew and Madix performed ^{18}O labeling experiments over a Ag (110) catalyst using furan as the reactant (6). In their experiments furan underwent ring opening before maleic anhydride formation. Xue and Schrader conducted transient *in situ* FTIR studies over $(VO)_2P_2O_7$ to demonstrate similar pathways for the oxidation of methyl vinyl ketone, crotonaldehyde, 1,3-butadiene, 2,5-dihydrofuran, furan and 2(5H)-furanone (7). Cyclic compounds [2,5-dihydrofuran, furan, and 2(5H)-furanone] were converted to maleic anhydride, but only after initial ring cleavage produced open-chain carbonyl compounds such as crotonaldehyde or 2-butene-1,4-dial. In addition, crotonaldehyde and methyl vinyl ketone formed maleic anhydride with no evidence of prior cyclization. Hönicke proposed multiple pathways to maleic anhydride over V_2O_5 catalysts (Figure 1). Furan was produced directly from crotonaldehyde, 2,5-dihydrofuran, and 2,3-dihydrofuran, and the immediate precursors for maleic anhydride were 2-butene-1,4-dial, 2(5H)-furanone, and furan (8, 9).

The objective of our current research has been to further elucidate the reaction pathway for 1,3-butadiene selective oxidation to valuable products such as maleic anhydride and furan. VMoO catalysts have been prepared which can produce these key

products as well as other important reaction intermediates. Several characterization techniques have been utilized to examine the catalytic solid solution materials. Addition of water has also been shown to affect the selectivity of the VMoO catalysts for intermediates such as furan and crotonaldehyde.

3.3. Materials and Methods

3.3.1. Preparation of VMoO catalysts by sol-gel synthesis

Samples having compositions of 3.5 (Catalyst A) and 14.0 mol % MoO_3 in V_2O_5 (Catalyst B) were prepared using a hydrogen peroxide-based, sol-gel preparation method (10, 11, 12, 13). $(NH_4)_2MoO_4$ (Fisher Scientific) was added to de-ionized water and gently heated to ensure complete dissolution. In a separate flask, V_2O_5 (99.9%, Alfa-Aesar) was added to de-ionized water and stirred. After approximately 5 minutes, a 30 % aqueous solution of H_2O_2 (Fischer Scientific) was added to the V_2O_5-H_2O slurry. Within minutes the solution turned from orange to clear red, and the molybdate solution was added. The solution turned dark red and then light orange or yellow. After a few minutes, a colloidal gel formed and settled on the bottom of the flask under a layer of solvent. The gel of Catalyst A was brown while the gel of Catalyst B was dark green. Once the gel had formed, the remaining water was poured off the samples, and the gels were covered with n-pentane. After 3 days, the catalysts were allowed to dry at ambient conditions and then calcined for 4 h at 350°C. The calcined powder appeared green-black and shiny.

3.3.2. Catalyst characterization

3.3.2.1. Surface area measurements

Surface areas were measured using the BET method. A Micromeretics ASAP 2000 surface analysis system was used with N_2 as the adsorbate.

3.3.2.2. Laser Raman spectroscopy

Laser Raman spectroscopy (LRS) was performed in a backscattering mode using a fiber-optic probe head coupled to a Kaiser Holospec f/1.8 spectrometer. A Coherent 532-50 diode-pumped solid state laser was the excitation source (532 nm, 50 mW at the source), and a Princeton Instruments CCD (1100x330) detector system was used with Winspec acquisition and processing software.

3.3.2.3. X-ray diffraction (XRD)

XRD was performed using a Scintag 2000 diffractometer utilizing Cu K_α radiation. Standard powder diffraction was performed for the solid state synthesis products. Diffraction patterns were recorded using θ-2θ scans between 10-70° with 0.050° step size in 2θ and 2.0 second count per step time.

3.3.2.4. X-ray photoelectron spectroscopy

X-ray photoelectron spectroscopy (XPS) was performed using a Physical Electronics Multitechnique system with monochromatic Al at 29.35 eV. The base pressure for the analyzer system was less than 3×10^{-10} Torr. Post-reaction catalyst samples were sealed in their reactor tubes under He and transferred to a glove box under an inert atmosphere. Samples were then loaded into the analysis chamber without exposure to the atmosphere.

3.3.3. Reactor studies

Reactions were performed using the system shown in Figure 2. The gas feed composition ranged from 0.5-1.4% 1,3-butadiene (Matheson, C.P. grade) in 77-92% air (Air Products, zero grade.) and 8-22% He (Air Products, zero grade). Hydrocarbon product feeds were introduced to the reactor system using a He-swept liquid saturator in which both temperature and He flow could be adjusted. For low temperatures (less than -20°C), a liquid N_2 cooled ethanol bath was required. For saturator temperatures above –20°C, a commercial ethylene glycol temperature bath was used (Brinkmann Instruments). These hydrocarbon feeds were maintained below 0.15% of the total feed (51% air and balance He). A 2.5% water additive level was introduced into the feed by directing the air stream through a saturator at 22°C. Helium was added to maintain a constant flow rate.

Catalysts were pressed and sieved (ca. 0.15 g, 40/100 mesh) before being loaded into the continuous flow reactor (6 mm I.D., quartz). Differential conversion conditions were maintained for all 1,3-butadiene studies. Small amounts of quartz wool were packed above and below the catalyst bed. Temperatures were maintained between 110°C and 300°C using a programmable temperature controller (Omega Engineering). Feed and effluent lines were heated to 150°C to prevent product condensation. Total flow rates regulated from 70 to 200 sccm using mass flow controllers.

The Varian 3600 gas chromatograph used a Carbosphere 80/100 packed column for the thermal conductivity (TCD) and a CP-Select 624 CB mega-bore capillary column (Varian, Inc.) for the flame ionization detector (FID). For these studies, the percent conversion of 1,3-butadiene was defined as

$$\frac{\text{moles } 1,3-\text{butadiene reacted}}{\text{moles } 1,3-\text{butadiene fed}} \times 100.$$

Percent selectivity to a specific product was defined as

$$\frac{\text{moles product}}{\text{moles } 1,3-\text{butadiene reacted}} \times \frac{1}{\gamma} \times 100,$$

where γ was the stoichiometric carbon atom ratio of 1,3-butadiene (4) to a product.

3.4. Results

3.4.1. Characterization of VMoO catalysts

3.4.1.1. Surface area

The pre-reaction surface area of Catalyst A was determined to be 9.1 m^2/g. Post-reaction surface area was 8.3 m^2/g. Pre-reaction surface area Catalyst B was determined to be 13.4 m^2/g. Post-reaction surface area was 12.0 m^2/g.

3.4.1.2. Laser Raman spectroscopy

Raman spectra for pre- and post-reaction catalysts have been presented in Figure 3. For Catalyst A, low wavenumber bands at 406, 300, 283 and 201 cm^{-1} were characteristic of vanadium-oxygen bending vibrations (14). The 990, 689 and 523 cm^{-1} peaks were likely related to stretching vibrations (995, 701 and 527 cm^{-1} for V_2O_5) and were assigned to terminal V=O, edge-sharing V-O, and corner sharing V-O-V stretching frequencies, respectively. The downward shift of these bands has been explained in terms of solid solution formation (23). Post-reaction Raman characterization indicated only a small shift of the 700 cm^{-1} peak to 693 cm^{-1}.

For Catalyst B, the Raman spectrum was similar to that for V_2O_5. However, a somewhat larger shift of the 995 cm^{-1} band to 987 cm^{-1} was observed. Raman band positions following reaction were virtually unchanged.

3.4.1.3. X-ray diffraction

X-ray powder patterns have been presented in Figure 4 (also for crystalline V_2O_5). XRD results for Catalyst A prior to reaction were similar to V_2O_5 except for small shifts in d-spacing. The d-spacing measurements for selected representative Miller indices of the pre- and post-reaction catalysts have been reported in Table 1. Incorporation of Mo in the vanadia catalysts resulted in expansion of the d-spacing in the (100) and (010) directions and contraction in the (001) direction. Post-reaction XRD characterization indicated little change in the long range order of Catalyst A or B.

3.4.1.4. X-Ray photoelectron spectroscopy

Results from X-ray photoelectron spectroscopy (XPS) of Catalysts A and B before and after reaction have been presented in Table 2, and the spectra for the vanadium region of the spectrum have been provided in Figures 5 and 6. The strong oxygen (O 1s) signal on the catalyst surfaces was used to calibrate the XPS spectra (15). For the pre-reaction materials, V binding energies decreased with addition of Mo. Following reaction, there was an additional decrease in V binding energies. The data for Figures 5 and 6 were fitted to the standard doublets for V^{+5} (V $2p_{3/2}$ at 517.4 eV and V $2p_{1/2}$ at 525.0 eV) and V^{+4} (V $2p_{3/2}$ at 515.4 eV and V $2p_{1/2}$ at 523.0 eV) (16, 17).

For Catalyst A, V^{+5} was predominant, but a relatively small amount of V^{+4} (about 6 %) was also detected. For the post-reaction spectra, the V bands shifted due to an

increase in V^{+4}. After reaction, approximately 20 % of the intensity of the V signal could be attributed to V^{+4} (Table 2), which revealed significant surface reduction. For Catalyst B, V^{+5} also appeared to dominate the oxidation state of the pre-reaction catalyst, although the proportion of V^{+4} (about 9%) was larger. Post-reaction XPS characterization revealed further reduction (about 12%).

Molybdenum appeared to exist only in the Mo^{+6} oxidation state in Catalysts A and B. Only a single doublet for Mo was observed. Pre and post-reaction Mo binding energies were similar to the doublet for Mo^{+6} based on MoO_3 (Mo $3d_{5/2}$ at 235.8 eV and Mo $3d_{3/2}$ at 232.7 eV) (18).

3.4.2. Reactor studies

3.4.2.1. Effect of catalyst composition

Product selectivities for Catalysts A, B and V_2O_5 at 275°C have been summarized in Figure 7 for 5% conversion of 1,3-butadiene. Reaction products included 3,4-epoxy-1-butene, furan, 2-butenal (crotonaldehyde), acrolein, 2-butene-1,4-dial, maleic anhydride, CO_x, phthalic anhydride, and 2(5H)-furanone. Phthalic anhydride and 2(5H)-furanone were detected in trace quantities (selectivity less than 1%).

For higher Mo concentrations, selectivities to furan and CO_x decreased while selectivity to maleic anhydride tended to increase. Selectivies to 3,4-epoxy-1-butene, 2-butene-1,4-dial, and crotonaldehyde remained relatively unchanged, and the selectivity to 2-butene-1,4-dial decreased slightly.

3.4.2.2. Effects of temperature

Temperature studies between 230-300°C were performed for Catalyst B using a 200 sccm feed of 0.5% 1,3-butadiene in air. Conversion of 1,3-butadiene remained less than 5% for these studies. Product selectivity as a function of temperature has been presented in Figure 8. As temperature increased, selectivities to CO_x and maleic anhydride increased, while selectivities to 3,4-epoxy-1-butene, crotonaldehyde and 2-butene-1,4-dial decreased. Selectivity to furan appeared to reach a maximum around 275-285°C.

3.4.2.3. Reaction of other partially oxidized hydrocarbons

The conversion of 3,4-epoxy-1-butene, crotonaldehyde, furan and 2,5-dihydrofuran were examined from 180 to 280°C. Catalyst B was used for these studies. Concentrations of these feeds were approximately 0.15 % in air with added He to achieve a total flow rate of 105 sccm.

3,4-Epoxy-1-butene

Conversion of 3,4-epoxy-1-butene and product selectivities as a function of temperature have been presented in Figure 9. The reaction products for 3,4-epoxy-1-butene oxidation were crotonaldehyde, furan, 2-butene-1,4-dial, maleic anhydride, and CO_x. At lower temperatures, some 2,5-dihydrofuran was detected (maximum selectivity of about 15% at 180°C, although higher levels were possible at lower temperatures). Conversion of 3,4-epoxy-1-butene was near 20% at 180°C and increased to near 100% around 260°C. Selectivities to crotonaldehyde and 2-butene-1,4-dial appeared to reach

maxima at 200°C; furan reached a maximum near 240°C; and maleic anhydride appeared to approach a maximum at 280°C.

Crotonaldehyde

Conversion of crotonaldehyde and product selectivities have been presented as a function of temperature in Figure 10. Crotonaldehyde produced acrolein, furan, 2-butene-1,4-dial, maleic anhydride, and CO_x. Neither 3,4-epoxy-1-butene nor 2,5-dihydrofuran were detected in the reactor effluent. At higher temperatures, conversion increased and more CO_x was produced while selectivities to furan and 2-butene-1,4-dial achieved maxima around 240°C. The selectivity to maleic anhydride apparently went through a minimum around 225°C.

Furan

Only maleic anhydride and CO_x were produced from furan, but conversion was insignificant until 220°C (Figure 11); at temperatures above 280°C, conversion increased significantly. Selectivity to maleic anhydride decreased with increasing temperature (from almost 95% at 220°C to 60% at 280°C). CO_x selectivity increased with temperature.

2,5-Dihydrofuran

The reaction products for 2,5-dihydrofuran oxidation were furan, maleic anhydride, and CO_x (Figure 12). 3,4-Epoxy-1-butene, crotonaldehyde, acrolein, or 2-butene-1,4-dial were not detected in the reactor effluent stream. As temperature was increased, conversion to 2,5-dihydrofuran increased from 35 to 100%. Selectivity to CO_x

also increased with temperature, while selectivity to furan was nearly 95% at 180°C. Maleic anhydride selectivity appeared to reach a maximum of about 65% around 265°C.

3.4.2.4. Effects of water addition

Addition of 2.5% water to the 1.4% 1,3-butadiene feed resulted in a 40% increase in conversion. Selectivities to furan, crotonaldehyde and 3,4-epoxy-1-butene also increased while those for CO_x and maleic anhydride decreased (Figure 13). Following the water addition experiments, the catalysts were re-examined without added water. Catalyst performances were similar to the prior studies not involving water addition.

3.5. Discussion

Based on these studies, a reaction pathway for the selective oxidation of 1,3-butadiene to maleic anhydride over VMoO catalysts has been proposed (Figure 14). According to this pathway, 1,2-addition of electrophilic oxygen to 1,3-butadiene first produced 3,4-epoxy-1-butene. This initial step was confirmed by the feed additive studies in which conversion of 3,4-epoxy-1-butene also produced compounds formed for 1,3-butadiene oxidation. The role of 3,4-epoxy-1-butene as the initial product of 1,3-butadiene oxidation was further indicated by the temperature variation experiments: as 1,3-butadiene conversion decreased at lower temperatures, selectivity to 3,4-epoxy-1-butene increased.

In the next step of the reaction pathway, 3,4-epoxy-1-butene underwent isomerization to crotonaldehyde, the dominant product at low conversions. The transformation of 3,4-epoxy-1-butene to crotonaldehyde was considered to be an acid-

catalyzed ring-opening of the bond between carbon 3 and oxygen. This was generally achieved by nucleophilic attack:

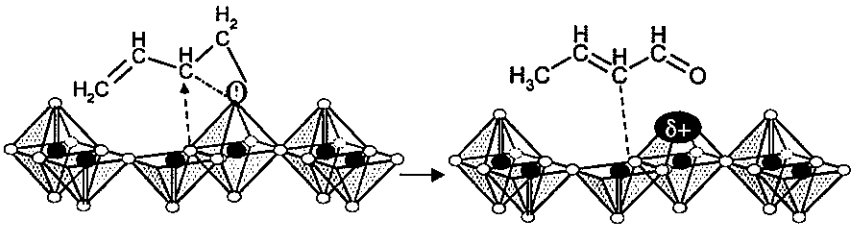

2,5-Dihydrofuran was also a reaction product of 3,4-epoxy-1-butene conversion, but only trace quantities were detected. Feed additive studies using 3,4-epoxy-1-butene supported this understanding. At similar temperatures, 2,5-dihydrofuran was significantly more reactive than 3,4-epoxy-1-butene, crotonaldehyde or furan. Although other researchers have found that 2,5-dihydrofuran oxidation over silver-based epoxidation catalysts produced crotonaldehyde, only furan and maleic anhydride (and CO_x) were detected in our studies (2, 3). The conversion of 3,4-epoxy-1-butene to 2,5-dihydrofuran has been proposed to be only a minor alternate route for the mechanism shown in Figure 14.

Crotonaldehyde produced furan, maleic anhydride, and 2-butene-1,4-dial, and a dual pathway to both furan and 2-butene-1,4-dial has been proposed in Figure 14. Allylic hydrogen abstraction and subsequent ring closure produced furan, and allylic hydrogen abstraction combined with nucleophilic oxygen insertion at the allylic center formed 2-butene-1,4-dial. Temperature studies revealed similarities in selectivity trends for crotonaldehyde and 2-butene-1,4-dial, likely indicating a common precursor.

Reaction of furan produced maleic anhydride and small amounts of 2(5H)-furanone. Xue *et al.* observed ring opening for furan and 2(5H)-furanone for VPO

catalysts, but the VMoO solid solution materials apparently did not catalyze these reactions (7). These transformations, however, could have occurred on the surface with no desorption and detection of the intermediate species. This possibility, however, was discounted since products of ring opening such as crotonaldehyde should have been evolved from the VMoO surface. 2(5H)-furanone was also a possible intermediate in the reaction of furan to maleic anhydride. Our studies indicated that 2(5H)-furanone either was quickly converted to the more stable maleic anhydride species (in a manner similar to 2,5-dihydrofuran) or was strongly adsorbed on the surface. The conversion of 2-butene-1,4-dial to maleic anhydride has been proposed over VPO, Ag, and V_2O_5-based catalysts (6, 8). The instability of 2-butene-1,4-dial and lack of commercial availability made confirmation of this pathway impossible for our planned studies.

For the VMoO catalysts, an increase in molybdenum content increased the selectivity for maleic anhydride but decreased conversion of 1,3-butadiene. The catalyst having a composition expressed as 14.0 mol % MoO_3 in V_2O_5 (near saturation of Mo in V_2O_5) had the highest selectivity for maleic anhydride. Catalysts with lower Mo content produced relatively more furan and crotonaldehyde. Catalyst B apparently had a higher tendency to promote nucleophilic addition reactions resulting in oxidation to maleic anhydride while the active sites in Catalyst A and pure V_2O_5 possessed more electrophilic nature associated with the initial epoxidation step.

The XRD and XPS characterization performed on Catalysts A and B supported formation of solid solutions of Mo in V_2O_5. The lattice expansion in the (100) and (010) planes and contraction in the (001) plane indicated Mo directly replaced V in the VMoO

catalysts (19, 20). This substitution caused an increase in the amount of V^{+4}, detected by XPS. Substitution of Mo into the V_2O_5 structure should involve reduction of V since Mo^{+6} replaces V^{+5}. Bielanski et al. used EPR studies to confirm the V^{+5} to V^{+4} transformation: further reduction to V^{+3} was also believed to occur (21). No evidence of V^{+3} was observed in XPS spectra of our catalysts.

For the VMoO catalysts, an increase in the availability of oxygen resulting from Mo incorporation into the V_2O_5 lattice has been attributed to reduction of V^{+5} to V^{+4} (22). The oxygen associated with these reduced vanadium cations was suggested to be more readily available for nucleophilic oxygen insertion. This postulate appeared to be true using VMoO catalysts as well. The reduction of V^{+5} to V^{+4} facilitated by Mo^{+6} incorporation allows additional V^{+4}-O sites to be available to form maleic anhydride. XPS analysis of the post-reaction catalyst with lower molybdenum content (Catalyst A) showed a higher relative V^{+4} concentration than post-reaction Catalyst B. This indicates the surface of Catalyst A experienced significant reduction, while the surface of Catalyst B was only slightly reduced. A plausible explanation for this behavior is an increase in re-oxidation capacity resulting from the presence of the Mo^{+6} species. If this is the case, the higher Mo content in catalyst B would replenish the catalyst with oxygen at a higher rate, therefore decreasing the extent of reduction during the selective oxidation process. This also may assist in the production of maleic anhydride from furan, as two additional oxygen atoms are necessary to complete this conversion.

Since electrophilic and nucleophilic oxidation transformations are required in this mechanism, the V_2O_5-based structure must have multiple active sites that are responsible

for distinct steps in the reaction pathway. Three different coordinations of oxygen in the orthorhombic V_2O_5 structure have been considered to be reactive for catalytic oxidation: corner sharing V-O-V, edge sharing V-O, and terminal V=O. In Raman studies performed by Ono et al. for n-butane oxidation, edge-sharing V-O were enriched with ^{18}O by re-oxidation of a reduced VMoO catalyst. Raman bands at 995, 701 and 521 cm^{-1} were assigned to V=O, V-O, and V-O-V bonds, respectively, and ^{18}O incorporation into the catalyst caused a downward shift in the vibrational frequencies (23). Since the largest shift was observed for the 521 cm^{-1} peak, the V-O-V sites were believed to be responsible for oxygen insertion during n-butane oxidation. In contrast, IR studies have indicated that the V=O oxygen was the most reactive for benzene oxidation (24). For reducing conditions involving benzene, the IR band at 995 cm^{-1} (characteristic of the V=O oxygen) decreased in intensity and eventually disappeared over time. These disparate results, however, may not necessarily conflict with those of Ono: for a Mars-van Krevelen mechanism, the site responsible for oxygen insertion may not be the same site for oxygen re-incorporation. In the V_2O_5 crystal structure, the vanadyl oxygen (V=O) species is considered to be the most electrophilic and could be responsible for the epoxidation of 1,3-butadiene. Surface oxygen (O^-, $2O^-$, etc.) species would likely also be active for electrophilic oxidation. However, lattice oxygen species (corner sharing V-O-V and edge sharing V-O) are more nucleophilic and are more likely to be involved in the formation of 2-butene-1,4-dial and maleic anhydride (25, 26).

The addition of water to the reactor 1,3-butadiene feed resulted in both higher conversion and selectivitiy to crotonaldehyde and furan. Several groups investigating the

effect of water on C_3 hydrocarbon selective oxidation also observed selectivity changes due to water addition. These differences were mainly attributed to competitive adsorption between water and hydrocarbon intermediates (27,28). Research performed by Ai et al. which focused on the oxidation of 1,3-butadiene to furan over supported heteropoly molybdates determined that the addition of water increased the reaction rate and the yield of furan (29). These researchers proposed that water (steam) removed strongly adsorbed products from the catalyst surface, which resulted in reactivation of catalytic sites and/or release of furan or other intermediates from the catalyst surface. In our studies, competitive adsorption of water may have occurred on specific VMoO catalyst sites where crotonaldehyde was bound as a reaction intermediate. This would explain the selectivity increase for crotonaldehyde when water is added. On the other hand, crotonaldehyde could simply have a lower energy for desorption and thus be the first to be released by the non-site specific adsorption of water. Further investigation of the effect of water will be reported in an additional publication.

3.6. Conclusions

VMoO catalysts produced using a peroxide-based, sol-gel synthesis route resulted in the formation of solid solutions of Mo in V_2O_5 that could be characterized by several techniques such as XRD, LRS and XPS. Of the materials evaluated for catalytic performance, the catalyst with the highest concentration of Mo was the most selective to maleic anhydride, while the catalyst with less Mo produced larger amounts of furan, crotonaldehyde and CO_x. This effect was attributed to increased availability of nucleophilic oxygen associated with V^{+4}-O sites.

Based on experiments performed using 1,3-butadiene and several other product hydrocarbons as feeds, a reaction pathway was proposed for the selective oxidation of 1,3-butadiene to maleic anhydride, including an initial 1,2-addition of oxygen to 1,3-butadiene to produce 3,4-epoxy-1-butene and a dual pathway from crotonaldehyde to produce furan or 2-butene-1,4-dial.

3.7. Acknowledgements

The authors would like to acknowledge Jim Anderegg of the Ames Laboratory for performing XPS experiments and for assisting interpretation. This research was performed under funding from Ames Laboratory – USDOE contract No. W-7405-Eng-82.

3.8. List of Figures

1. Reaction pathway of 1,3-butadiene to maleic anhydride over V_2O_5 proposed by Hönicke et al.
2. Reactor system for selective oxidation of 1,3-butadiene and other hydrocarbons over V-Mo-O catalysts.
3. LRS of VMoO catalysts a) catalyst A pre-reaction b) catalyst A post-reaction c) catalyst B pre-reaction d) catalyst B post-reaction e) V_2O_5 reference. These spectra were all collected in 3 min acquisition times under 50 mW laser power at 532 nm.
4. XRD of VMoO catalysts a) catalyst A pre-reaction b) catalyst A post-reaction c) catalyst B pre-reaction d) catalyst B post-reaction e) V_2O_5 reference.
5. XPS of VMoO catalysts (V region) for a) catalyst A pre-reaction b) catalyst A post-reaction.

6. XPS of VMoO catalysts (V region) for a) catalyst B pre-reaction b) catalyst B post-reaction.
7. Effect of Mo concentration for selective oxidation of 1,3-butadiene at 275°C. Total gas flow rate was 70 sccm (1.4% 1,3-butadiene in air and He) and conversion was near 5.0%.
8. Effect of temperature between 240°C and 300°C for 1,3-butadiene selective oxidation over Catalyst B. Total gas flow rate was 200 sccm (0.5% 1,3-butadiene in air and He).
9. Effect of temperature between 180°C and 280°C for 3,4-epoxy-1-butene selective oxidation over Catalyst B. Total gas flow rate was 105 sccm (0.15% 3,4-epoxybutene in air and He).
10. Effect of temperature between 180°C and 280°C for crotonaldehyde selective oxidation over Catalyst B. Total gas flow rate was 105 sccm (0.15% crotonaldehyde in air and He).
11. Effect of temperature between 180°C and 280°C for furan selective oxidation over Catalyst B. Total gas flow rate was 105 sccm (0.15% furan in air and He).
12. Effect of temperature between 180°C and 280°C for 2,5-dihydrofuran selective oxidation over Catalyst B. Total gas flow rate was 105 sccm (0.15% 2,5-dihydrofuran in air and He).
13. Effect of water addition to reactant feed of 1,3-butadiene in air over Catalyst B. Total gas flow rate was 70 sccm (1.4% 1,3-butadiene in air and He).

14. Proposed reaction pathway for 1,3-butadiene to maleic anhydride over VMoO catalysts.

3.9. List of Tables

1. XRD d-spacing measurements for V_2O_5, Catalyst A and Catalyst B.
2. XPS data for peak positions for vanadium and molybdenum and intensities of fitted V^{+4} and V^{+5} peaks for Catalysts A and B.

3.10. References

1 Centi, G. and F. Trifiro, *Journal of Molecular Catalysis*, **35**, 255 (1986).

2 Monnier, J. R., 3rd World Congress on Oxidation Catalysis, 135 (1997) Elsevier Science B.V., (R.K. Grasselli, St.T. Oyama, A.M. Gaffney and J.E. Lyons, eds.)

3 Monnier, J. R. and P. J. Muehlbauer, U.S. Patent No. 5,081,096 (1992).

4 Roberts, J. T., A. J. Capote, and R. J. Madix, *J. Am. Chem. Soc.* **113**, 9848 (1991).

5 Akimoto, M. and E. Echigoya, *Bull. Chem Soc. Japan* **48**, 3518 (1975).

6 Crew, W.W. and R. J. Madix, *J. Am. Chem. Soc* **115**, 729 (1993).

7 Xue, Z. and G. L. Schrader, *Journal of Catalysis* **184**, 87 (1999).

8 Hönicke, D., *Journal of Catalysis* **105**, 10 (1997).

9 Hönicke, D., *Journal of Catalysis* **105**, 19 (1997).

10 Fontenot, C.J., J. W. Wiench, M. Pruski, and G. L. Schrader, *J. Phys Chem. B* **104**, 11622 (2000).

11 Fontenot, C.J., J. W. Wiench, M. Pruski, and G. L. Schrader, *J. Phys Chem. B*, submitted for publication 2001.

12 Alonso, B. and J. Livage, *Journal of Solid State Chemistry* **148**, 16 (1999).

13 Bradzil, J. F., M. A. Toft, J. P. Bartek, R. G. Teller, and R. M. Cyngier, *Chem. Mater.* **10**, 4100 (1998).

14 Abello, L., Husson, E., Repelin, Y., and Lucazeau, G., *Spectrochimica Acta* **39A/7**, 641 (1983).

15 Mendialdua, J., R. Casanova, and Y. Barbaux, *Journal of Electron Spectroscopy and Related Phenomena* **71**, 249 (1995).

16 Chen, Y., Xie, K., and Liu, Z.X., *Applied Surface Surface* **133**, 221 (1998).

17 Demeter, M, M. Neumann, and W. Reichelt, *Surface Science* **454-456**, 41 (2000).

18 Levasseur, A., P. Vinatier, and D. Gonbeau, *Bull. Mater. Sci.*, **22**, 607 (1999).

19 Kihlborg, L., *Acta Chemica Scandinavica* **21**, 2495 (1967).

20 Hirata, T. and H-Y Zhu, *J. Phys.: Condens. Matter* **4**, 7377 (1992).

21 Bielanski, A., K. Dyrek, I. Kracik, and E. Wenda, *Bull. Pol. Ac. Chem.* **19**, 512 (1971).

22 Bielanski, A. and M. Najbar, *Applied Catalysis A: General* **157**, 223 (1997).

23 Ono, T. and H. Numata, *Journal of Molecular Catalysis A: Chemical* **116,** 421 (1997).

24 Bielanski, A. and A. Inglot, *React. Kinet. Catal. Lett.* **6/1**, 83 (1977)

25 Haber, J., M. Witko, and R. Tokarz, *Applied Catalysis A: General* **157**, 3 (1997).

26 Witko, J.M., R. Tokarz, and J. Haber, *Applied Catalysis A: General* **157**, 23 (1997).

27 Tichý, J, J. Küstka, and J. Machek, *Collection Czechoslovak Chem. Commun.* **48**, 698 (1983)

28 Stein, B., C. Weimer, J. Gaube, *3rd World Congress on Oxidation Catalysis*, 393 (1997) Elsevier Science B.V., (R.K. Grasselli, St.T. Oyama, A.M. Gaffney and J.E. Lyons, eds.

29 Ai, M., *Journal of Catalysis* **67**, 110 (1981).

CHAPTER 3
1,3-BUTADIENE SELECTIVE OXIDATION OVER VMoO CATALYSTS: NEW INSIGHTS INTO THE REACTION PATHWAY

A manuscript submitted to the *Journal of Catalysis*

William D. Schroeder, C. J. Fontenot, and G.L. Schrader

Department of Chemical Engineering and Ames Laboratory – USDOE

Iowa State University Ames, IA 50011

3.1. Abstract

The partial oxidation of 1,3-butadiene has been investigated over VMoO catalysts synthesized by sol-gel techniques. Surface areas were 9-14 m^2/g, and compositions were within the solid solution regime, i.e. below 15.0 mol % (MoO_3) in V_2O_5. Laser Raman and XRD data indicated that solid solutions were formed, and pre- and post-reaction XPS data indicated that catalyst surfaces were reduced by the 1,3-butadiene-in-air feeds. The reaction pathway for 1,3-butadiene partial oxidation to maleic anhydride was shown to involve intermediates such as 3,4-epoxy-1-butene, crotonaldehyde, furan, and 2-butene-1,4-dial. The addition of water to the reaction stream substantially increased catalyst activity and improved selectivity to crotonaldehyde and furan at specific reaction temperatures.

key words: hydrocarbon selective oxidation, mixed metal oxide catalysts, 1,3-butadiene partial oxidation

3.2. Introduction

The conversion of 1,3-butadiene to maleic anhydride and other partially oxidized hydrocarbons has been examined using several selective oxidation catalysts. However, there is no generally accepted reaction pathway, particularly regarding the role of specific intermediates and the sequential conversion steps. Most studies have emphasized maleic anhydride production: other compounds such as furan and 3,4-epoxy-1-butene are potentially valuable products also.

Centi and Trifiro suggested a simple consecutive pathway for 1,3-butadiene conversion over VPO catalysts (1):

1,3-butadiene → 2,5-dihydrofuran → furan → maleic anhydride

1,4-Cycloaddition of oxygen to 1,3-butadiene produced 2,5-dihydrofuran, followed by allylic H-abstraction to form furan. Maleic anhydride was produced by further oxygen insertion into the 2- and 5-positions. Crotonaldehyde was also detected in these studies but was considered only to be a side product.

Investigations of 1,3-butadiene oxidation over Ag catalysts indicated that 1,4-addition was not the first step in the oxidation of 1,3-butadiene; rather, 1,2-addition was postulated to produce 3,4-epoxy-1-butene (2,3). Conversion of 1,3-butadiene was inhibited by the epoxide. Reaction of 3,4-epoxy-1-butene over unpromoted Ag catalysts formed furan, crotonaldehyde, acrolein, and CO_2, although only 55% of the converted 3,4-epoxy-1-butene could be accounted for. Experiments using 2,5-dihydrofuran as a feed additive indicated that furan, crotonaldehyde, and CO_2 were formed. Although 3,4-epoxy-1-butene did not produce 2,5-dihydrofuran (and vice versa), it was proposed that

the epoxide was the initial 1,3-butadiene oxidation product. Monnier suggested that 3,4-epoxy-1-butene was unable to desorb from the catalyst surface before cyclization to 2,5-dihydrofuran, isomerization to crotonaldehyde, or hydrogenolysis to acrolein. Addition of small amounts of CsCl or CsF produced a highly selective catalyst for 3,4-epoxy-1-butene production from 1,3-butadiene (96% selectivity at 21% conversion). This catalyst proved to also be efficient in the epoxidation of several other compounds, such as styrene, 4-vinylpyridine, and norborene (2,3). The increase in selectivity was attributed to a lowering of the epoxide desorption energy. Attempts to use these catalysts for the selective oxidation of compounds with allylic hydrogen (propylene, butenes, etc) were unsuccessful. Apparently, strongly electrophilic oxygen present on the modified Ag surface produced only combustion products.

In other studies over Ag surfaces, the catalytic oxidation of 1,3-butadiene has been considered to be a 1,4-addition where both C=C bonds interact with surface oxygen to form 2,5-dihydrofuran. Studies by Madix et al. postulated that for single-crystal Ag (110) surfaces, a stabilized intermediate species was formed which could desorb as 2,5-dihydrofuran. This reaction was compared to a Diels-Alder mechanism for acetylene and 1,3-butadiene conversion to benzene in which interaction of acetylene with the terminal C=C bonds of 1,3-butadiene formed a cyclic structure. In the same fashion, the active oxygen on the catalyst surface was believed to interact with the terminal C=C bonds of 1,3-butadiene to form 2,5-dihydrofuran (4).

Other selective oxidation products generated from 1,3-butadiene have also been detected, suggesting the formation of maleic anhydride by multiple pathways. Akimoto

et al. observed that over supported molybdena catalysts, maleic anhydride was formed by two temperature-dependent pathways: via 2,5-dihydrofuran with subsequent conversion to furan, or via 2,5-dihydrofuran only (5). More recent work by several research groups has suggested that these multiple pathways were a result of ring opening of cyclic compounds and subsequent reaction of "open-chain" compounds. Re-cyclization or the partial oxidation intermediates could then produce maleic anhydride. Crew and Madix performed ^{18}O labeling experiments over a Ag (110) catalyst using furan as the reactant (6). In their experiments furan underwent ring opening before maleic anhydride formation. Xue and Schrader conducted transient *in situ* FTIR studies over $(VO)_2P_2O_7$ to demonstrate similar pathways for the oxidation of methyl vinyl ketone, crotonaldehyde, 1,3-butadiene, 2,5-dihydrofuran, furan and 2(5H)-furanone (7). Cyclic compounds [2,5-dihydrofuran, furan, and 2(5H)-furanone] were converted to maleic anhydride, but only after initial ring cleavage produced open-chain carbonyl compounds such as crotonaldehyde or 2-butene-1,4-dial. In addition, crotonaldehyde and methyl vinyl ketone formed maleic anhydride with no evidence of prior cyclization. Hönicke proposed multiple pathways to maleic anhydride over V_2O_5 catalysts (Figure 1). Furan was produced directly from crotonaldehyde, 2,5-dihydrofuran, and 2,3-dihydrofuran, and the immediate precursors for maleic anhydride were 2-butene-1,4-dial, 2(5H)-furanone, and furan (8, 9).

The objective of our current research has been to further elucidate the reaction pathway for 1,3-butadiene selective oxidation to valuable products such as maleic anhydride and furan. VMoO catalysts have been prepared which can produce these key

products as well as other important reaction intermediates. Several characterization techniques have been utilized to examine the catalytic solid solution materials. Addition of water has also been shown to affect the selectivity of the VMoO catalysts for intermediates such as furan and crotonaldehyde.

3.3. Materials and Methods

3.3.1. Preparation of VMoO catalysts by sol-gel synthesis

Samples having compositions of 3.5 (Catalyst A) and 14.0 mol % MoO_3 in V_2O_5 (Catalyst B) were prepared using a hydrogen peroxide-based, sol-gel preparation method (10, 11, 12, 13). $(NH_4)_2MoO_4$ (Fisher Scientific) was added to de-ionized water and gently heated to ensure complete dissolution. In a separate flask, V_2O_5 (99.9%, Alfa-Aesar) was added to de-ionized water and stirred. After approximately 5 minutes, a 30 % aqueous solution of H_2O_2 (Fischer Scientific) was added to the V_2O_5-H_2O slurry. Within minutes the solution turned from orange to clear red, and the molybdate solution was added. The solution turned dark red and then light orange or yellow. After a few minutes, a colloidal gel formed and settled on the bottom of the flask under a layer of solvent. The gel of Catalyst A was brown while the gel of Catalyst B was dark green. Once the gel had formed, the remaining water was poured off the samples, and the gels were covered with n-pentane. After 3 days, the catalysts were allowed to dry at ambient conditions and then calcined for 4 h at 350°C. The calcined powder appeared green-black and shiny.

3.3.2. Catalyst characterization

3.3.2.1. Surface area measurements

Surface areas were measured using the BET method. A Micromeretics ASAP 2000 surface analysis system was used with N_2 as the adsorbate.

3.3.2.2. Laser Raman spectroscopy

Laser Raman spectroscopy (LRS) was performed in a backscattering mode using a fiber-optic probe head coupled to a Kaiser Holospec f/1.8 spectrometer. A Coherent 532-50 diode-pumped solid state laser was the excitation source (532 nm, 50 mW at the source), and a Princeton Instruments CCD (1100x330) detector system was used with Winspec acquisition and processing software.

3.3.2.3. X-ray diffraction (XRD)

XRD was performed using a Scintag 2000 diffractometer utilizing Cu K_α radiation. Standard powder diffraction was performed for the solid state synthesis products. Diffraction patterns were recorded using θ-2θ scans between 10-70° with 0.050° step size in 2θ and 2.0 second count per step time.

3.3.2.4. X-ray photoelectron spectroscopy

X-ray photoelectron spectroscopy (XPS) was performed using a Physical Electronics Multitechnique system with monochromatic Al at 29.35 eV. The base pressure for the analyzer system was less than 3×10^{-10} Torr. Post-reaction catalyst samples were sealed in their reactor tubes under He and transferred to a glove box under an inert atmosphere. Samples were then loaded into the analysis chamber without exposure to the atmosphere.

3.3.3. Reactor studies

Reactions were performed using the system shown in Figure 2. The gas feed composition ranged from 0.5-1.4% 1,3-butadiene (Matheson, C.P. grade) in 77-92% air (Air Products, zero grade.) and 8-22% He (Air Products, zero grade). Hydrocarbon product feeds were introduced to the reactor system using a He-swept liquid saturator in which both temperature and He flow could be adjusted. For low temperatures (less than -20°C), a liquid N_2 cooled ethanol bath was required. For saturator temperatures above –20°C, a commercial ethylene glycol temperature bath was used (Brinkmann Instruments). These hydrocarbon feeds were maintained below 0.15% of the total feed (51% air and balance He). A 2.5% water additive level was introduced into the feed by directing the air stream through a saturator at 22°C. Helium was added to maintain a constant flow rate.

Catalysts were pressed and sieved (ca. 0.15 g, 40/100 mesh) before being loaded into the continuous flow reactor (6 mm I.D., quartz). Differential conversion conditions were maintained for all 1,3-butadiene studies. Small amounts of quartz wool were packed above and below the catalyst bed. Temperatures were maintained between 110°C and 300°C using a programmable temperature controller (Omega Engineering). Feed and effluent lines were heated to 150°C to prevent product condensation. Total flow rates regulated from 70 to 200 sccm using mass flow controllers.

The Varian 3600 gas chromatograph used a Carbosphere 80/100 packed column for the thermal conductivity (TCD) and a CP-Select 624 CB mega-bore capillary column (Varian, Inc.) for the flame ionization detector (FID). For these studies, the percent conversion of 1,3-butadiene was defined as

$$\frac{\text{moles 1,3 – butadiene reacted}}{\text{moles 1,3 – butadiene fed}} \times 100.$$

Percent selectivity to a specific product was defined as

$$\frac{\text{moles product}}{\text{moles 1,3 – butadiene reacted}} \times \frac{1}{\gamma} \times 100,$$

where γ was the stoichiometric carbon atom ratio of 1,3-butadiene (4) to a product.

3.4. Results

3.4.1. Characterization of VMoO catalysts

3.4.1.1. Surface area

The pre-reaction surface area of Catalyst A was determined to be 9.1 m^2/g. Post-reaction surface area was 8.3 m^2/g. Pre-reaction surface area Catalyst B was determined to be 13.4 m^2/g. Post-reaction surface area was 12.0 m^2/g.

3.4.1.2. Laser Raman spectroscopy

Raman spectra for pre- and post-reaction catalysts have been presented in Figure 3. For Catalyst A, low wavenumber bands at 406, 300, 283 and 201 cm^{-1} were characteristic of vanadium-oxygen bending vibrations (14). The 990, 689 and 523 cm^{-1} peaks were likely related to stretching vibrations (995, 701 and 527 cm^{-1} for V_2O_5) and were assigned to terminal V=O, edge-sharing V-O, and corner sharing V-O-V stretching frequencies, respectively. The downward shift of these bands has been explained in terms of solid solution formation (23). Post-reaction Raman characterization indicated only a small shift of the 700 cm^{-1} peak to 693 cm^{-1}.

For Catalyst B, the Raman spectrum was similar to that for V_2O_5. However, a somewhat larger shift of the 995 cm^{-1} band to 987 cm^{-1} was observed. Raman band positions following reaction were virtually unchanged.

3.4.1.3. X-ray diffraction

X-ray powder patterns have been presented in Figure 4 (also for crystalline V_2O_5). XRD results for Catalyst A prior to reaction were similar to V_2O_5 except for small shifts in d-spacing. The d-spacing measurements for selected representative Miller indices of the pre- and post-reaction catalysts have been reported in Table 1. Incorporation of Mo in the vanadia catalysts resulted in expansion of the d-spacing in the (100) and (010) directions and contraction in the (001) direction. Post-reaction XRD characterization indicated little change in the long range order of Catalyst A or B.

3.4.1.4. X-Ray photoelectron spectroscopy

Results from X-ray photoelectron spectroscopy (XPS) of Catalysts A and B before and after reaction have been presented in Table 2, and the spectra for the vanadium region of the spectrum have been provided in Figures 5 and 6. The strong oxygen (O 1s) signal on the catalyst surfaces was used to calibrate the XPS spectra (15). For the pre-reaction materials, V binding energies decreased with addition of Mo. Following reaction, there was an additional decrease in V binding energies. The data for Figures 5 and 6 were fitted to the standard doublets for V^{+5} (V $2p_{3/2}$ at 517.4 eV and V $2p_{1/2}$ at 525.0 eV) and V^{+4} (V $2p_{3/2}$ at 515.4 eV and V $2p_{1/2}$ at 523.0 eV) (16, 17).

For Catalyst A, V^{+5} was predominant, but a relatively small amount of V^{+4} (about 6 %) was also detected. For the post-reaction spectra, the V bands shifted due to an

increase in V^{+4}. After reaction, approximately 20 % of the intensity of the V signal could be attributed to V^{+4} (Table 2), which revealed significant surface reduction. For Catalyst B, V^{+5} also appeared to dominate the oxidation state of the pre-reaction catalyst, although the proportion of V^{+4} (about 9%) was larger. Post-reaction XPS characterization revealed further reduction (about 12%).

Molybdenum appeared to exist only in the Mo^{+6} oxidation state in Catalysts A and B. Only a single doublet for Mo was observed. Pre and post-reaction Mo binding energies were similar to the doublet for Mo^{+6} based on MoO_3 (Mo $3d_{5/2}$ at 235.8 eV and Mo $3d_{3/2}$ at 232.7 eV) (18).

3.4.2. Reactor studies

3.4.2.1. Effect of catalyst composition

Product selectivities for Catalysts A, B and V_2O_5 at 275°C have been summarized in Figure 7 for 5% conversion of 1,3-butadiene. Reaction products included 3,4-epoxy-1-butene, furan, 2-butenal (crotonaldehyde), acrolein, 2-butene-1,4-dial, maleic anhydride, CO_x, phthalic anhydride, and 2(5H)-furanone. Phthalic anhydride and 2(5H)-furanone were detected in trace quantities (selectivity less than 1%).

For higher Mo concentrations, selectivities to furan and CO_x decreased while selectivity to maleic anhydride tended to increase. Selectivies to 3,4-epoxy-1-butene, 2-butene-1,4-dial, and crotonaldehyde remained relatively unchanged, and the selectivity to 2-butene-1,4-dial decreased slightly.

3.4.2.2. Effects of temperature

Temperature studies between 230-300°C were performed for Catalyst B using a 200 sccm feed of 0.5% 1,3-butadiene in air. Conversion of 1,3-butadiene remained less than 5% for these studies. Product selectivity as a function of temperature has been presented in Figure 8. As temperature increased, selectivities to CO_x and maleic anhydride increased, while selectivities to 3,4-epoxy-1-butene, crotonaldehyde and 2-butene-1,4-dial decreased. Selectivity to furan appeared to reach a maximum around 275-285°C.

3.4.2.3. Reaction of other partially oxidized hydrocarbons

The conversion of 3,4-epoxy-1-butene, crotonaldehyde, furan and 2,5-dihydrofuran were examined from 180 to 280°C. Catalyst B was used for these studies. Concentrations of these feeds were approximately 0.15 % in air with added He to achieve a total flow rate of 105 sccm.

3,4-Epoxy-1-butene

Conversion of 3,4-epoxy-1-butene and product selectivities as a function of temperature have been presented in Figure 9. The reaction products for 3,4-epoxy-1-butene oxidation were crotonaldehyde, furan, 2-butene-1,4-dial, maleic anhydride, and CO_x. At lower temperatures, some 2,5-dihydrofuran was detected (maximum selectivity of about 15% at 180°C, although higher levels were possible at lower temperatures). Conversion of 3,4-epoxy-1-butene was near 20% at 180°C and increased to near 100% around 260°C. Selectivities to crotonaldehyde and 2-butene-1,4-dial appeared to reach

maxima at 200°C; furan reached a maximum near 240°C; and maleic anhydride appeared to approach a maximum at 280°C.

Crotonaldehyde

Conversion of crotonaldehyde and product selectivities have been presented as a function of temperature in Figure 10. Crotonaldehyde produced acrolein, furan, 2-butene-1,4-dial, maleic anhydride, and CO_x. Neither 3,4-epoxy-1-butene nor 2,5-dihydrofuran were detected in the reactor effluent. At higher temperatures, conversion increased and more CO_x was produced while selectivities to furan and 2-butene-1,4-dial achieved maxima around 240°C. The selectivity to maleic anhydride apparently went through a minimum around 225°C.

Furan

Only maleic anhydride and CO_x were produced from furan, but conversion was insignificant until 220°C (Figure 11); at temperatures above 280°C, conversion increased significantly. Selectivity to maleic anhydride decreased with increasing temperature (from almost 95% at 220°C to 60% at 280°C). CO_x selectivity increased with temperature.

2,5-Dihydrofuran

The reaction products for 2,5-dihydrofuran oxidation were furan, maleic anhydride, and CO_x (Figure 12). 3,4-Epoxy-1-butene, crotonaldehyde, acrolein, or 2-butene-1,4-dial were not detected in the reactor effluent stream. As temperature was increased, conversion to 2,5-dihydrofuran increased from 35 to 100%. Selectivity to CO_x

also increased with temperature, while selectivity to furan was nearly 95% at 180°C. Maleic anhydride selectivity appeared to reach a maximum of about 65% around 265°C.

3.4.2.4. Effects of water addition

Addition of 2.5% water to the 1.4% 1,3-butadiene feed resulted in a 40% increase in conversion. Selectivities to furan, crotonaldehyde and 3,4-epoxy-1-butene also increased while those for CO_x and maleic anhydride decreased (Figure 13). Following the water addition experiments, the catalysts were re-examined without added water. Catalyst performances were similar to the prior studies not involving water addition.

3.5. Discussion

Based on these studies, a reaction pathway for the selective oxidation of 1,3-butadiene to maleic anhydride over VMoO catalysts has been proposed (Figure 14). According to this pathway, 1,2-addition of electrophilic oxygen to 1,3-butadiene first produced 3,4-epoxy-1-butene. This initial step was confirmed by the feed additive studies in which conversion of 3,4-epoxy-1-butene also produced compounds formed for 1,3-butadiene oxidation. The role of 3,4-epoxy-1-butene as the initial product of 1,3-butadiene oxidation was further indicated by the temperature variation experiments: as 1,3-butadiene conversion decreased at lower temperatures, selectivity to 3,4-epoxy-1-butene increased.

In the next step of the reaction pathway, 3,4-epoxy-1-butene underwent isomerization to crotonaldehyde, the dominant product at low conversions. The transformation of 3,4-epoxy-1-butene to crotonaldehyde was considered to be an acid-

catalyzed ring-opening of the bond between carbon 3 and oxygen. This was generally achieved by nucleophilic attack:

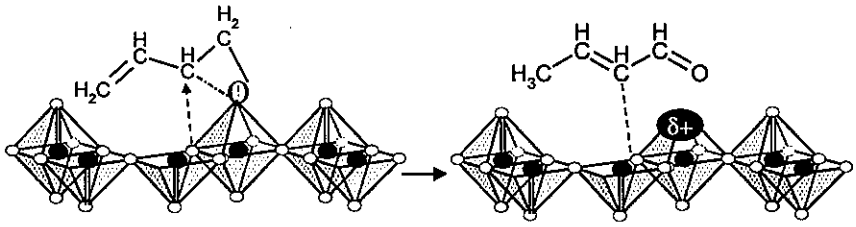

2,5-Dihydrofuran was also a reaction product of 3,4-epoxy-1-butene conversion, but only trace quantities were detected. Feed additive studies using 3,4-epoxy-1-butene supported this understanding. At similar temperatures, 2,5-dihydrofuran was significantly more reactive than 3,4-epoxy-1-butene, crotonaldehyde or furan. Although other researchers have found that 2,5-dihydrofuran oxidation over silver-based epoxidation catalysts produced crotonaldehyde, only furan and maleic anhydride (and CO_x) were detected in our studies (2, 3). The conversion of 3,4-epoxy-1-butene to 2,5-dihydrofuran has been proposed to be only a minor alternate route for the mechanism shown in Figure 14.

Crotonaldehyde produced furan, maleic anhydride, and 2-butene-1,4-dial, and a dual pathway to both furan and 2-butene-1,4-dial has been proposed in Figure 14. Allylic hydrogen abstraction and subsequent ring closure produced furan, and allylic hydrogen abstraction combined with nucleophilic oxygen insertion at the allylic center formed 2-butene-1,4-dial. Temperature studies revealed similarities in selectivity trends for crotonaldehyde and 2-butene-1,4-dial, likely indicating a common precursor.

Reaction of furan produced maleic anhydride and small amounts of 2(5H)-furanone. Xue *et al.* observed ring opening for furan and 2(5H)-furanone for VPO

catalysts, but the VMoO solid solution materials apparently did not catalyze these reactions (7). These transformations, however, could have occurred on the surface with no desorption and detection of the intermediate species. This possibility, however, was discounted since products of ring opening such as crotonaldehyde should have been evolved from the VMoO surface. 2(5H)-furanone was also a possible intermediate in the reaction of furan to maleic anhydride. Our studies indicated that 2(5H)-furanone either was quickly converted to the more stable maleic anhydride species (in a manner similar to 2,5-dihydrofuran) or was strongly adsorbed on the surface. The conversion of 2-butene-1,4-dial to maleic anhydride has been proposed over VPO, Ag, and V_2O_5-based catalysts (6, 8). The instability of 2-butene-1,4-dial and lack of commercial availability made confirmation of this pathway impossible for our planned studies.

For the VMoO catalysts, an increase in molybdenum content increased the selectivity for maleic anhydride but decreased conversion of 1,3-butadiene. The catalyst having a composition expressed as 14.0 mol % MoO_3 in V_2O_5 (near saturation of Mo in V_2O_5) had the highest selectivity for maleic anhydride. Catalysts with lower Mo content produced relatively more furan and crotonaldehyde. Catalyst B apparently had a higher tendency to promote nucleophilic addition reactions resulting in oxidation to maleic anhydride while the active sites in Catalyst A and pure V_2O_5 possessed more electrophilic nature associated with the initial epoxidation step.

The XRD and XPS characterization performed on Catalysts A and B supported formation of solid solutions of Mo in V_2O_5. The lattice expansion in the (100) and (010) planes and contraction in the (001) plane indicated Mo directly replaced V in the VMoO

catalysts (19, 20). This substitution caused an increase in the amount of V^{+4}, detected by XPS. Substitution of Mo into the V_2O_5 structure should involve reduction of V since Mo^{+6} replaces V^{+5}. Bielanski et al. used EPR studies to confirm the V^{+5} to V^{+4} transformation: further reduction to V^{+3} was also believed to occur (21). No evidence of V^{+3} was observed in XPS spectra of our catalysts.

For the VMoO catalysts, an increase in the availability of oxygen resulting from Mo incorporation into the V_2O_5 lattice has been attributed to reduction of V^{+5} to V^{+4} (22). The oxygen associated with these reduced vanadium cations was suggested to be more readily available for nucleophilic oxygen insertion. This postulate appeared to be true using VMoO catalysts as well. The reduction of V^{+5} to V^{+4} facilitated by Mo^{+6} incorporation allows additional V^{+4}-O sites to be available to form maleic anhydride. XPS analysis of the post-reaction catalyst with lower molybdenum content (Catalyst A) showed a higher relative V^{+4} concentration than post-reaction Catalyst B. This indicates the surface of Catalyst A experienced significant reduction, while the surface of Catalyst B was only slightly reduced. A plausible explanation for this behavior is an increase in re-oxidation capacity resulting from the presence of the Mo^{+6} species. If this is the case, the higher Mo content in catalyst B would replenish the catalyst with oxygen at a higher rate, therefore decreasing the extent of reduction during the selective oxidation process. This also may assist in the production of maleic anhydride from furan, as two additional oxygen atoms are necessary to complete this conversion.

Since electrophilic and nucleophilic oxidation transformations are required in this mechanism, the V_2O_5-based structure must have multiple active sites that are responsible

for distinct steps in the reaction pathway. Three different coordinations of oxygen in the orthorhombic V_2O_5 structure have been considered to be reactive for catalytic oxidation: corner sharing V-O-V, edge sharing V-O, and terminal V=O. In Raman studies performed by Ono et al. for n-butane oxidation, edge-sharing V-O were enriched with ^{18}O by re-oxidation of a reduced VMoO catalyst. Raman bands at 995, 701 and 521 cm^{-1} were assigned to V=O, V-O, and V-O-V bonds, respectively, and ^{18}O incorporation into the catalyst caused a downward shift in the vibrational frequencies (23). Since the largest shift was observed for the 521 cm^{-1} peak, the V-O-V sites were believed to be responsible for oxygen insertion during n-butane oxidation. In contrast, IR studies have indicated that the V=O oxygen was the most reactive for benzene oxidation (24). For reducing conditions involving benzene, the IR band at 995 cm^{-1} (characteristic of the V=O oxygen) decreased in intensity and eventually disappeared over time. These disparate results, however, may not necessarily conflict with those of Ono: for a Mars-van Krevelen mechanism, the site responsible for oxygen insertion may not be the same site for oxygen re-incorporation. In the V_2O_5 crystal structure, the vanadyl oxygen (V=O) species is considered to be the most electrophilic and could be responsible for the epoxidation of 1,3-butadiene. Surface oxygen (O^-, $2O^-$, etc.) species would likely also be active for electrophilic oxidation. However, lattice oxygen species (corner sharing V-O-V and edge sharing V-O) are more nucleophilic and are more likely to be involved in the formation of 2-butene-1,4-dial and maleic anhydride (25, 26).

The addition of water to the reactor 1,3-butadiene feed resulted in both higher conversion and selectivitiy to crotonaldehyde and furan. Several groups investigating the

effect of water on C_3 hydrocarbon selective oxidation also observed selectivity changes due to water addition. These differences were mainly attributed to competitive adsorption between water and hydrocarbon intermediates (27,28). Research performed by Ai et al. which focused on the oxidation of 1,3-butadiene to furan over supported heteropoly molybdates determined that the addition of water increased the reaction rate and the yield of furan (29). These researchers proposed that water (steam) removed strongly adsorbed products from the catalyst surface, which resulted in reactivation of catalytic sites and/or release of furan or other intermediates from the catalyst surface. In our studies, competitive adsorption of water may have occurred on specific VMoO catalyst sites where crotonaldehyde was bound as a reaction intermediate. This would explain the selectivity increase for crotonaldehyde when water is added. On the other hand, crotonaldehyde could simply have a lower energy for desorption and thus be the first to be released by the non-site specific adsorption of water. Further investigation of the effect of water will be reported in an additional publication.

3.6. Conclusions

VMoO catalysts produced using a peroxide-based, sol-gel synthesis route resulted in the formation of solid solutions of Mo in V_2O_5 that could be characterized by several techniques such as XRD, LRS and XPS. Of the materials evaluated for catalytic performance, the catalyst with the highest concentration of Mo was the most selective to maleic anhydride, while the catalyst with less Mo produced larger amounts of furan, crotonaldehyde and CO_x. This effect was attributed to increased availability of nucleophilic oxygen associated with V^{+4}-O sites.

Based on experiments performed using 1,3-butadiene and several other product hydrocarbons as feeds, a reaction pathway was proposed for the selective oxidation of 1,3-butadiene to maleic anhydride, including an initial 1,2-addition of oxygen to 1,3-butadiene to produce 3,4-epoxy-1-butene and a dual pathway from crotonaldehyde to produce furan or 2-butene-1,4-dial.

3.7. Acknowledgements

The authors would like to acknowledge Jim Anderegg of the Ames Laboratory for performing XPS experiments and for assisting interpretation. This research was performed under funding from Ames Laboratory – USDOE contract No. W-7405-Eng-82.

3.8. List of Figures

1. Reaction pathway of 1,3-butadiene to maleic anhydride over V_2O_5 proposed by Hönicke et al.
2. Reactor system for selective oxidation of 1,3-butadiene and other hydrocarbons over V-Mo-O catalysts.
3. LRS of VMoO catalysts a) catalyst A pre-reaction b) catalyst A post-reaction c) catalyst B pre-reaction d) catalyst B post-reaction e) V_2O_5 reference. These spectra were all collected in 3 min acquisition times under 50 mW laser power at 532 nm.
4. XRD of VMoO catalysts a) catalyst A pre-reaction b) catalyst A post-reaction c) catalyst B pre-reaction d) catalyst B post-reaction e) V_2O_5 reference.
5. XPS of VMoO catalysts (V region) for a) catalyst A pre-reaction b) catalyst A post-reaction.

6. XPS of VMoO catalysts (V region) for a) catalyst B pre-reaction b) catalyst B post-reaction.
7. Effect of Mo concentration for selective oxidation of 1,3-butadiene at 275°C. Total gas flow rate was 70 sccm (1.4% 1,3-butadiene in air and He) and conversion was near 5.0%.
8. Effect of temperature between 240°C and 300°C for 1,3-butadiene selective oxidation over Catalyst B. Total gas flow rate was 200 sccm (0.5% 1,3-butadiene in air and He).
9. Effect of temperature between 180°C and 280°C for 3,4-epoxy-1-butene selective oxidation over Catalyst B. Total gas flow rate was 105 sccm (0.15% 3,4-epoxybutene in air and He).
10. Effect of temperature between 180°C and 280°C for crotonaldehyde selective oxidation over Catalyst B. Total gas flow rate was 105 sccm (0.15% crotonaldehyde in air and He).
11. Effect of temperature between 180°C and 280°C for furan selective oxidation over Catalyst B. Total gas flow rate was 105 sccm (0.15% furan in air and He).
12. Effect of temperature between 180°C and 280°C for 2,5-dihydrofuran selective oxidation over Catalyst B. Total gas flow rate was 105 sccm (0.15% 2,5-dihydrofuran in air and He).
13. Effect of water addition to reactant feed of 1,3-butadiene in air over Catalyst B. Total gas flow rate was 70 sccm (1.4% 1,3-butadiene in air and He).

14. Proposed reaction pathway for 1,3-butadiene to maleic anhydride over VMoO catalysts.

3.9. List of Tables

1. XRD d-spacing measurements for V_2O_5, Catalyst A and Catalyst B.
2. XPS data for peak positions for vanadium and molybdenum and intensities of fitted V^{+4} and V^{+5} peaks for Catalysts A and B.

3.10. References

1 Centi, G. and F. Trifiro, *Journal of Molecular Catalysis*, **35**, 255 (1986).

2 Monnier, J. R., 3rd World Congress on Oxidation Catalysis, 135 (1997) Elsevier Science B.V., (R.K. Grasselli, St.T. Oyama, A.M. Gaffney and J.E. Lyons, eds.)

3 Monnier, J. R. and P. J. Muehlbauer, U.S. Patent No. 5,081,096 (1992).

4 Roberts, J. T., A. J. Capote, and R. J. Madix, *J. Am. Chem. Soc.* **113**, 9848 (1991).

5 Akimoto, M. and E. Echigoya, *Bull. Chem Soc. Japan* **48**, 3518 (1975).

6 Crew, W.W. and R. J. Madix, *J. Am. Chem. Soc* **115**, 729 (1993).

7 Xue, Z. and G. L. Schrader, *Journal of Catalysis* **184**, 87 (1999).

8 Hönicke, D., *Journal of Catalysis* **105**, 10 (1997).

9 Hönicke, D., *Journal of Catalysis* **105**, 19 (1997).

10 Fontenot, C.J., J. W. Wiench, M. Pruski, and G. L. Schrader, *J. Phys Chem. B* **104**, 11622 (2000).

11 Fontenot, C.J., J. W. Wiench, M. Pruski, and G. L. Schrader, *J. Phys Chem. B*, submitted for publication 2001.

12 Alonso, B. and J. Livage, *Journal of Solid State Chemistry* **148**, 16 (1999).

13 Bradzil, J. F., M. A. Toft, J. P. Bartek, R. G. Teller, and R. M. Cyngier, *Chem. Mater.* **10**, 4100 (1998).

14 Abello, L., Husson, E., Repelin, Y., and Lucazeau, G., *Spectrochimica Acta* **39A/7**, 641 (1983).

15 Mendialdua, J., R. Casanova, and Y. Barbaux, *Journal of Electron Spectroscopy and Related Phenomena* **71**, 249 (1995).

16 Chen, Y., Xie, K., and Liu, Z.X., *Applied Surface Surface* **133**, 221 (1998).

17 Demeter, M, M. Neumann, and W. Reichelt, *Surface Science* **454-456**, 41 (2000).

18 Levasseur, A., P. Vinatier, and D. Gonbeau, *Bull. Mater. Sci.*, **22**, 607 (1999).

19 Kihlborg, L., *Acta Chemica Scandinavica* **21**, 2495 (1967).

20 Hirata, T. and H-Y Zhu, *J. Phys.: Condens. Matter* **4**, 7377 (1992).

21 Bielanski, A., K. Dyrek, I. Kracik, and E. Wenda, *Bull. Pol. Ac. Chem.* **19**, 512 (1971).

22 Bielanski, A. and M. Najbar, *Applied Catalysis A: General* **157**, 223 (1997).

23 Ono, T. and H. Numata, *Journal of Molecular Catalysis A: Chemical* **116,** 421 (1997).

24 Bielanski, A. and A. Inglot, *React. Kinet. Catal. Lett.* **6/1**, 83 (1977)

25 Haber, J., M. Witko, and R. Tokarz, *Applied Catalysis A: General* **157**, 3 (1997).

26 Witko, J.M., R. Tokarz, and J. Haber, *Applied Catalysis A: General* **157**, 23 (1997).

27 Tichý, J, J. Küstka, and J. Machek, *Collection Czechoslovak Chem. Commun.* **48**, 698 (1983)

28 Stein, B., C. Weimer, J. Gaube, *3rd World Congress on Oxidation Catalysis*, 393 (1997) Elsevier Science B.V., (R.K. Grasselli, St.T. Oyama, A.M. Gaffney and J.E. Lyons, eds.

29 Ai, M., *Journal of Catalysis* **67**, 110 (1981).

CHAPTER 4
EFFECT OF WATER ADDITION IN SELECTIVE OXIDATION OF 1,3-BUTADIENE OVER VMoO CATALYSTS

A manuscript prepared for the *Journal of Catalysis*

William D. Schroeder and Glenn L. Schrader

Department of Chemical Engineering and Ames Laboratory – USDOE

Iowa State University Ames, IA 50011

4.1. Abstract

The effects of water on the partial oxidation of 1,3-butadiene to maleic anhydride were investigated over a sol-gel derived VMoO catalyst. Catalyst composition was 14.0 mol % MoO_3:(V_2O_5 + MoO_3). Water addition levels of 0-12% in the reactant feed of butadiene, air and He caused significant increases in catalytic activity and improved selectivity to crotonaldehyde and furan. These effects were attributed to competitive adsorption between hydrocarbon products and water and acid site formation through water dissociative adsorption. Using TPD experiments, five distinct adsorption sites were observed and associated with terminal V=O, corner sharing V-O-V, and edge sharing V-O oxygen. It appeared that no significant bulk structural effects occurred with the addition of water.

key words: hydrocarbon selective oxidation, steam addition, water adsorption effects, 1,3-butadiene partial oxidation.

4.2. Introduction

The addition of water (steam) to both catalytic and non-catalytic gas phase reactions has been performed for years. The effect of water is often system specific, dependent on reactant feed, catalyst structure and composition, etc. Several studies have demonstrated that the addition of water to the reactant stream has significant effects on catalytic selectivity and activity in selective oxidation. However, the effect of water on the reaction pathway has not been clearly identified for many hydrocarbon selective oxidation reactions. The role of water vapor was studied extensively by Hudgins et al. for the selective oxidation of propylene over Sb/Sn/V oxide catalysts at 340°C. Results showed that with the addition of water, an increase in reaction rate occurred, as well as a shift in selectivities to acrolein and acrylic acid. Water was proposed to competitively adsorb onto the surface, in effect releasing oxygenated compounds and simultaneously activating new sites more suited for acrylic acid formation (1, 2).

Isotopic studies done by Moro-oka et al. involving propylene oxidation over SnO_2-MoO_3 catalysts showed that $H_2{}^{18}O$ in the reactant stream produced ^{18}O-labeled acetone but non-labeled acrolein. The explanation for the effect was that water dissociatively adsorbed on the catalyst so that surface OH species were formed, which served as a new source of reactive oxygen (3). It was concluded the available oxygen for acetone formation was not bulk lattice oxygen, but surface oxygen species that could readily exchange with adsorbing water oxygen.

Bulk catalyst structure and composition have also been shown to alter with water addition. In the case of VPO catalysts, room temperature addition of water to the reactant

stream had been shown to cause bulk structural changes from α_I, α_{II}, δ or γ-$VOPO_4$ to $VOPO_4$-$2H_2O$ (4). In fact, under extended treatment with water, further transformation to V_2O_5 was observed. This behavior was attributed to water diffusion in to catalyst structure, where it facilitated a crystallographic shear structure by removing phosphorous and oxygen (as HPO_4) from the catalyst bulk (5). Previous water effect studies on VPO catalytic performance showed a decrease in conversion and an increase in maleic anhydride selectivity. Suggested sources for the altered catalytic behavior included competitive adsorption between water and oxygen on the catalyst surface, water participation in the reaction itself, changes in catalyst surface area, and the aforementioned phase transformation (6, 7, 8).

The adsorption of water onto V_2O_5 surfaces has been studied and modeled extensively. Most studies agree that on crystalline V_2O_5, molecular adsorption is favorable. The preferred location of the molecular adsorption of water, remains somewhat in question. Theoretical models by Yin et al. indicated that water preferably undergoes molecular adsorption over the vanadyl oxygen O_A (9).

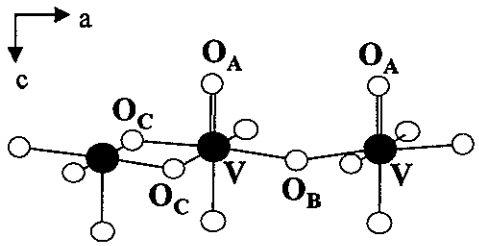

Using periodical density function calculations it was proposed that H-bonding between a single hydrogen and surface V_2O_5 oxygen occurs. Compared to calculations performed for water adsorption on corner-sharing O_B or edge-sharing O_C oxygen atoms, water

adsorbed onto the vanadyl O_A site provide near 100% higher charge transfer, directly related to a higher adsorption potential. Other studies modeled the H_2O-V_2O_5 system and proposed both water hydrogen atoms are bonded to the surface. Activation energy calculations performed by Ranea et al. indicated the favorable adsorption sites were; 1. water H-bonded to two adjacent O_A sites (in the b-direction), oriented parallel with the (001) plane of V_2O_5, and 2. water H-bonded to two adjacent O_A sites (in the a-direction), oriented perpendicular with the (001) plane of V_2O_5. Other studies by Witko et al. proposed molecular adsorption to take place over O_B sites (10). On a non-ideal V_2O_5 surface, defects, steps, and/or reduced sites may facilitate dissociative adsorption, in which (11, 12)

$$H_2O + O^{2-} \rightarrow 2\,OH^-.$$

In the previously discussed theoretical studies, dissociative adsorption appears to be very unfavorable over an ideal (001) surface.

From earlier 1,3-butadiene selective oxidation studies using VMoO catalysts, a reaction pathway was proposed that included intermediate oxidation products 3,4-epoxy-1-butene, crotonaldehyde, furan and 2-butene-1,4-dial. The addition of 2.5% water to the overall 1,3-butadiene feed resulted in a significant increase in conversion 1,3-butadiene and selectivity to crotonaldehyde and furan. Selectivities to maleic anhydride and carbon oxides decreased with the addition of water. Characterization of the catalytic materials indicated they were solid solutions of Mo in V_2O_5, in which Mo^{+6} replaced V^{+5} in the overall V_2O_5 structure. Upon addition of Mo, a reduction of V^{+5} to V^{+4} took place to maintain charge neutrality.

The objective of our research has been to determine the role that water plays in the catalytic enhancement of 1,3-butadiene selective oxidation over sol-gel derived VMoO solid solution catalysts. Structural, chemical and adsorptive properties of water are investigated as possible explanations to explain the effects of water.

4.3. Materials and Methods

4.3.1. Preparation of V_2O_5-MoO_3 compounds using sol-gel synthesis

The catalyst used in these studies contained 14.0 mol % MoO_3 in V_2O_5 and were prepared using a hydrogen peroxide-based, sol-gel preparation method (13, 14, 15, 16). $(NH_4)_2MoO_4$ (Fisher Scientific) was added to de-ionized water and gently heated to ensure complete dissolution. In a separate flask, V_2O_5 (99.9%, Alfa-Aesar) was added to de-ionized water and stirred. After approximately 5 minutes, a 30 % aqueous solution of H_2O_2 (Fischer Scientific) was added to the V_2O_5-H_2O slurry. Within minutes the solution turned from orange to clear red, and the molybdate solution was added. The solution turned dark red and then light orange or yellow. Once the gel had formed, the remaining water was poured off the samples, and the gels were covered with n-pentane. After 3 days, the catalysts were allowed to dry at ambient conditions and then calcined for 4 h at 350°C. Catalyst surface area (pre and post-reaction) was approximately 13.0 m^2/g. The calcined powder appeared green-black and shiny. These catalysts were characterized as substitutional solid solutions of MoO_3 in V_2O_5 and exhibited catalytic behavior for the selective oxidation of 1,3-butadiene in previous work (17).

4.3.2. Catalysts characterization

4.3.2.1. Laser Raman spectroscopy

Laser Raman spectroscopy (LRS) was performed in a backscattering mode using a fiber-optic probe head coupled to a Kaiser Holospec f/1.8 spectrometer. A Coherent 532-50 diode-pumped solid state laser was the excitation source (532 nm, 50 mW at the source), and a Princeton Instruments CCD (1100x330) detector system was used with Winspec acquisition and processing software.

4.3.2.2. X-ray photoelectron spectroscopy

X-ray photoelectron spectroscopy (XPS) was done using a Physical Electronics Multitechnique system with monochromatic Al at 29.35 eV. Base pressure for the analyzer system was less than 3 x 10^{-10} Torr. Post-reaction catalyst samples were sealed in their reactor tubes under He and transferred to a glove box under an inert atmosphere. Samples were then loaded into the analysis chamber without atmospheric exposure.

4.3.3. Reactor studies

4.3.3.1 Catalytic performance

Catalytic performance, step change and TPD experiments were performed using the reactor system shown in Figure 1. The gas feed composition for catalytic performance studies was 1.4% 1,3-butadiene (Matheson, C.P. grade) in 77% air (Air Products, zero grade.) and 22% He (Air Products, zero grade). Water and other hydrocarbon feeds were introduced to the reactor system using a He-swept liquid saturator in which the amount added to the feed stream was controlled using both liquid temperature and helium flow. For low temperatures (less than -20°C), a liquid N_2 cooled ethanol bath was used. For

saturator temperatures above –20°C, a commercial ethylene glycol temperature bath was used (Brinkmann Instruments model RM 6). Water was added in levels between 0.1% to 12%. Product hydrocarbons used as reactants (3,4-epoxy-1-butene, crotonaldehyde, furan, and 2,5-dihydrofuran) were in concentrations no more than 0.15% of the total feed. Added water level for product hydrocarbon feeds was at 2.5%. He make-up gas was used to maintain a constant overall flow rate within studies.

Catalysts were pressed and sieved (40/100 mesh) before being loaded into the continuous flow reactor (6 mm I.D., quartz). Small amounts of quartz wool were packed above and below the catalyst bed, which could be heated 1 h to the desired temperature in air or an air-He mixture. Between 0.15 and 0.30 g catalyst was used. Temperatures were maintained from 65°C to 420°C using a programmable temperature controller (Omega Engineering). Feed and effluent lines were maintained at 150°C to prevent condensation of products. Total flow rate ranged from 70 to 105 sccm using mass flow controllers.

The gas chromatograph (Varian 3600) used a Carbosphere 80/100 packed column for the thermal conductivity (TCD) and a WCOT fused silica (CP-Select 624 CB) megabore column for the flame ionization detector (FID).

For these studies, the percent conversion was defined as

$$\frac{\text{moles 1,3 – butadiene reacted}}{\text{moles 1,3 – butadiene fed}} \times 100.$$

Percent selectivity was defined as

$$\frac{\text{moles product}}{\text{moles 1,3 – butadiene reacted}} \times \frac{1}{\gamma} \times 100,$$

where γ in the carbon atom ratio of 1,3-butadiene to product.

Water step change experiments were performed by adding 0.5 or 2.5% water to the reactant feed while performing short method successive GC injections. Step-change experiments were all done using 0.25 g of 14.0 mol % MoO_3 catalyst at 275°C with a 1.4% 1,3-butadiene flow.

4.3.3.2 Temperature-programmed desorption

TPD studies were performed by flowing pure helium over a catalyst bed held at 65°C to which hydrocarbon pulses were introduced. Water was added to the system feed through a separate saturator held at 25°C, also at 10 sccm He flow. Approximately 0.25 g catalyst was used for TPD studies. Temperature ramping rate was 1.2°C per minute from adsorption temperature to 420°C. Conditioning was performed prior to adsorption procedure, in which the catalyst was heated to 420°C under 50% air flow and held for 1 hour. After conditioning, two different adsorption procedures were used: 1) following hydrocarbon adsorption onto the catalyst surface the temperature ramp was started (after sufficient time to remove any non-adsorbed hydrocarbon), and 2) water was pre-adsorbed onto the catalyst surface after which procedure 1 was performed. Desorption products were measured using successive GC injections. It should be noted that upon adsorption of any of the hydrocarbons used, a small amount of maleic anhydride was detected in the reactor effluent during the adsorption process. In previous studies using low feed concentrations (<0.15%) of product hydrocarbons, selectivity to maleic anhydride was quite high even at lower temperatures (17). It is probable that some (or all) the desorbing species may have immediately reacted to form maleic anhydride, which was detected in

the reactor effluent. This type of behavior was reported over V_2O_5 catalyst TPD studies using ethanol and ethylene, in which carbon oxides were the dominant product detected in the temperature ramp (18).

4.4. Results

4.4.2. Characterization

4.4.2.1. Laser Raman spectroscopy

Laser Raman spectra have been provided in Figure 2. The pre-reaction catalyst had peaks assigned to a solid solution of Mo in V_2O_5, with Raman bands at 990, 689, 523, 406, 300, 283 and 201 cm^{-1}. Water addition appeared to have no effect on post-reaction Raman signal, indicating that local bulk structure was unaffected by water addition.

4.4.2.2. X-ray photoelectron spectroscopy

X-ray photoelectron spectra have been provided in Figure 3. The strong oxygen (O 1s) signal detected was used to calibrate the XPS spectra (19). For the pre-reaction materials, XPS in the vanadium region had peaks at 517.1 eV and 524.7 eV. The shape and position of the XPS in the Vanadium region indicated a downward shift in the standard V^{+5} doublet (V $2p_{3/2}$ at 517.4 eV and V $2p_{1/2}$ at 525.0 eV), due to V^{+4} (V $2p_{3/2}$ at 515.4 eV and V $2p_{1/2}$ at 523.0 eV) present from the solid solution formation (20, 21). XPS results for this catalyst has been discussed in greater detail in another publication (17). Following reaction, overall peak intensities decreased, but peak positions were comparable to the pre-reaction catalyst. Water addition appeared to have no effect on post-reaction catalyst XPS.

4.4.3. Reactor studies

1,3-Butadiene feed

Reaction products from 1,3-butadiene feed included 3,4-epoxy-1-butene, furan, 2-butenal (crotonaldehyde), acrolein, 2-butene-1,4-dial, maleic anhydride, CO_x, phthalic anhydride, and 2(5H)-furanone. Phthalic anhydride and 2(5H)-furanone were in trace quantities (less than 1% selectivity).

The effects of water addition on conversion and selectivity of 1,3-butadiene feed over 0.15 g catalyst at 275°C is presented in Figure 4. Water was added to the feed stream at levels between 0-12%. With only 0.1% water addition, conversion increased from 5% to 6%. Selectivity to crotonaldehyde increased from 9% to 13% while selectivity to CO_x decreased from 39% to 35%. As water level increased, conversion continued to increase until a maximum of 8% conversion at 6% water addition. Conversion showed a slight decrease when water levels were increased from 6% to 12%. Crotonaldehyde achieved a maximum selectivity around 6% water addition, while furan selectivity started to significantly increase at water levels above 6%. Maleic anhydride selectivity decreased as water addition levels increased from 2.5% to 12%. After an initial increase in 3,4-epoxy-1-butene levels with the addition of 0.1% water, selectivity to 3,4-epoxy-1-butene decreased with increasing water addition. 2-Butene-1,4-dial remained at relatively constant selectivity, with an increase between 6% and 12% water addition.

Water step-change experiments

Results from step-change water addition experiments have been provided in Figures 5 and 6. With 0.5% water added to the feed, conversion 1,3-butadiene immediately increased from 7.5% to 10%, as shown in Figure 6. At the same time crotonaldehyde increased in selectivity to 21%, while maleic anhydride and CO_x decreased from 20% to 18% and 33 to 28%, respectively. 3,4-Epoxy-1-butene and furan showed small (<1%) increases in selectivity as well. Upon the addition of 2.5% water to the feed, conversion 1,3-butadiene increased from 6% to 10%, and selectivity crotonaldehyde increased from 17% to 25.5%. Selectivity to and maleic anhydride and COx decreased from 21% to 16.5% and 29.5% to 25%, respectively. In each step-change experiment, conversion and selectivities immediately returned to near their original (no water added) values when the water feed was cutoff.

3,4-Epoxybutene as feed

The addition of water to a 3,4-epoxy-1-butene feed resulted in a significant increase in conversion (near 50% conversion at 180°C and 100% conversion at 220°C) as presented in Figure 7. Selectivity to crotonaldehyde, 2-butene-1,4-dial, and 2,5-dihydrofuran apparently reached maxima at temperatures below 180°C. The maximum selectivity to furan (27 %) appeared around 200°C. The maximum selectivity for maleic anhydride was approximately 48% near 240°C. The selectivities to 2,5-dihydrofuran and 2-butene-1,4-dial decreased with water addition. Furan, however, reached a selectivity almost 10% higher (at a lower temperature), and crotonaldehyde appeared to exhibit similar behavior in approaching a maximum at temperatures below 180°C.

Crotonaldehyde as feed

Results for adding water to crotonaldehyde feeds are given in Figure 8. With water addition, conversion increased dramatically, near 99% at 240°C compared to 35% without water addition. Furan selectivity reached a maximum of 48% near 200°C (from 24% near 240°C without water addition), and the temperature for the maximum selectivity to 2-butene-1,4-dial shifted from about 240°C to 180°C with the addition of water. At around 250°C, maleic anhydride selectivity reached a maximum of approximately 54%; a minimum of about 14% was observed near 200°C.

Furan as feed

The addition of water to the reactant stream containing furan resulted in a significant increase in conversion, as shown in Figure 9 (almost 75% at 220°C and reaches 100% near 240°C. Maleic anhydride selectivity was 92% at 180°C and decreased at higher temperatures.

2,5-Dihydrofuran as feed

Experiments were performed for water addition to the feed stream of 2,5-dihydrofuran (Figure 10). Conversion increased over all temperature ranges. Water addition also increased selectivity to CO_x. Furan selectivity sharply decreased at 180°C so that at 240°C only trace amounts could be detected. It appeared that furan selectivity could exceed 80% below 180°C. Selectivity to maleic anhydride reached a maximum at 230°C near 50% selectivity, which was lower than the maximum selectivity without water addition.

The effects of water addition in reactor studies that used 3,4-epoxy-1-butene or crotonaldehyde feeds are presented in Table 1. Maximum selectivity to furan or maleic anhydride increased in both cases with the addition of water, while selectivity to 2-butene-1,4-dial decreased. At 220°C, the addition of water to the reactant stream caused an increase in conversion of 49% and 63% for 3,4-epoxy-1-butene and crotonaldehyde, respectively.

4.4.4. Temperature-programmed desorption studies

TPD studies were done at over 14.0 mol % MoO_3 in V_2O_5 catalyst using 1,3-butadiene, crotonaldehyde and furan as adsorbing species. Results of these studies are presented in Figures 11 through 16. The predominant desorption hydrocarbon was maleic anhydride. It was also observed that generally, for some maleic anhydride desorption peaks, there were also trace amounts of 1,3-butadiene, furan, and/or crotonaldehyde. If maleic anhydride had a lower desorption potential, it was likely that these larger maleic anhydride peaks in fact represented other partially oxidized hydrocarbons like furan or crotonaldehyde that desorbed and reacted very quickly to form maleic anhydride.

1,3-Butadiene adsorption

The detected desorption product was predominantly maleic anhydride, with small amounts of 1,3-butadiene, furan and crotonaldehyde. As can be seen in Figure 11, there were distinct maleic anhydride peaks near 125°C, 225°C, and 305°C. 1,3-Butadiene showed desorption peaks near 175°C and 350°C. Furan and crotonaldehyde appeared to have a single desorption peak at approximately 125°C. Pre-adsorption of water resulted

in higher amounts of desorbed products for each species, save the 125°C peak for maleic anhydride, which appeared smaller in magnitude.

Crotonaldehyde adsorption

Results from TPD studies are presented in Figure 12. Maleic anhydride, furan, and 1,3-butadiene were detected. Crotonaldehyde was not present during TPD in any detectable amount. Maleic anydride appeared to have two peaks, one at 125°C and the other near 225°C. Water pre-adsorption seemed to have insignificant effect on the amount of maleic anhydride desorbed. Furan had a single peak near 115°C, which was near 4 times higher with water pre-adsorption. 1,3-butadiene exhibited a peak near 175°C that also was larger with water pre-adsorption.

Furan adsorption

Data for furan TPD are presented in Figure 13. Maleic anhydride appeared to have three peaks, near 175°C, 250°C and 300°C. 1,3-Butadiene exhibited a desorption peak at 225°C. With water pre-adsorption, the amount maleic anhydride desorbed at 175°C, 250°C and 300°C was less compared to results without water adsorbed, and 1,3-butadiene was virtually undetectable.

Separate desorption spectra for 1,3-butadiene, crotonaldehyde and furan were compared in Figure 14. It appears that there were at least five distinct adsorption sites at 125°C, 175°C, 225-250°C, 275-300°C and 350°C. Water pre-adsorption appeared to have different effects dependant of the adsorbed hydrocarbon species. The results in terms of the five adsorption sites and water effects are summarized in Table 2.

4.5. Discussion

According to TPD studies performed, there appears to be at least five active sites on the VMoO catalyst surface for adsorption and reaction to furan, crotonaldehyde, maleic anhydride, etc. These sites were designated Sites I, II, III, IV, and V, corresponding to respective temperatures of 125°C, 175°C, 225-250°C, 275-300°C and 350°C. Previous studies suggested that a redox mechanism occurred over the VMoO catalyst for this selective oxidation (17). In the absence of air, adsorbing feed 1,3-butadiene, furan, or crotonaldehyde produced maleic anhydride, with their only oxidation source the catalyst itself. Furthermore, small amount of 1,3-butadiene were detected in the desorption gases from furan and crotonaldehyde, indicating these partial oxidation products were used to re-oxidize the catalyst.

Desorption products associated with Site I were crotonaldehyde, furan, and maleic anhydride. Site I was not observed in furan adsorption experiments. Examining the reaction pathway proposed for 1,3-butadiene to maleic anhydride for these catalysts in Chapter 3, it is probable that Site I is the point of furan cyclization from crotonaldehyde. The heterocyclization of crotonaldehyde to furan can be described on a single site in which crotonaldehyde adsorbs through an allylic hydrogen abstraction and catalytic oxygen attack on the allylic center (Figure 15). Following adsorption, the delocalization of charge throughout the adsorbed crotonaldehyde could occur, inducing a $\delta+$ charge onto carbon 4. This would be proceeded by an intramolecular nucleophilic attack of the carbonyl oxygen on the $\delta+$ center, forming furan (22). Considering the chemistry involved in this reaction, Site I is assigned to surface O_B oxygen in the V_2O_5 structure. In

1,3-butadiene oxidation, this site would be involved after epoxide ring cleavage of 3,4-epoxy-1-butene to form crotonaldehyde. As an adsorbing species, furan would exhibit a different chemistry than crotonaldehyde, explaining the lack of Site I behavior for furan TPD experiments.

Site II at 175°C appeared to be associated with 1,3-butadiene, crotonaldehyde and furan. It is likely that Site II was the initial adsorption site to form 3,4-epoxy-1-butene from 1,3-butadiene. In terms of the various oxidative potentials in a V_2O_5-based catalyst, theoretical calculations of an extended vanadium oxide surface indicated the vanadyl O_A oxygen to be the most electrophilic (23). In the case of Site II, O_A is assigned. The function of this fully oxidized site would be epoxidation, prior to further reaction on site I to form crotonaldehyde and furan. Crotonaldehyde adsorption resulted in reduction to 1,3-butadiene, which over an O_A site would be explained by a re-oxidation of an O_A-vacancy. Desorption of maleic anhydride was observed for Site II in furan adsorption experiments, which indicated furan possibly adsorbed onto the O_A site and desorbed without further interaction with the catalyst (before further reaction to maleic anhydride).

The next-strongest adsorption site at 225-250°C appeared to be associated with maleic anhydride. All three adsorbing gases exhibited a peak for Site III, and only furan showed any additional product (1,3-butadiene) than maleic anhydride desorbing. For 1,3-butadine to have desorbed, furan would first have adsorbed onto a vacancy and re-oxidize the catalyst surface. On that site, furan could have oxidized further to form maleic anhydride. In the case of furan adsorption, water pre-adsorption clearly lowered the Site III population, while for 1,3-butadiene adsorption, Site III population appeared to have

increased. The assignment for Site III in the V_2O_5-based structure is proposed to be an O_C vacancy. Site III and Site I appeared to be associated with one another in the respect that instead of desorbing as a cyclized furan or crotonaldehyde, the oxygen of Site I was also added to the desorbing species. This would result in desorbed 2-butene-1,4-dial or 2(5H)-furanone, which would quickly react to form maleic anhydride before leaving the catalyst bed.

Site IV was observed in furan adsorption studies, but not in crotonaldehyde or 1,3-butadiene adsorption studies. It is difficult to determine the nature of this site (other than adsorption capability) because upon desorption, Sites I-III are available for rapid reaction to maleic anhydride. At best Site IV was a minor adsorption site which existed as a shoulder peak in furan studies.

In the 1,3-butadiene adsorption studies, desorbed 1,3-butadiene was detected in addition to maleic anhydride near 350°C. This could have been a strong adsorption site and resulted in further oxidation to maleic anhydride upon 1,3-butadiene desorption. According to quantum chemical calculations by Witko et al., edge-sharing O_C oxygen have a higher bond order than corner sharing O_B and are more difficult to remove from the V_2O_5 structure (23). Considering the chemistry of the oxidation and the energy required for desorption, Site V is assigned to O_C oxygen.

The addition of water to the reactor feed resulted in both higher conversion and selectivity to partial oxidation products such as crotonaldehyde and furan. Competitive adsorption between water and 1,3-butadiene or selective oxidation products thereof was first considered as a possible explanation for these effects. The increased conversion

with the addition of water is proposed to have "cleaned" the surface by re-activating hindered sites. This effect is well known for industrial catalysts, as water is used as a de-coking agent in reactor systems. Conversion stopped increasing near 6% water addition. It is conceivable that at some point the very number of water molecules present in the system would hinder not only partial oxidation products from adsorbing, but also 1,3-butadiene. In TPD studies, it appeared that pre-adsorbed water occupied Site IV, in effect blocking the adsorption site in furan studies. In fact, in all of the furan TPD studies, water caused a decrease in maleic anhydride desorbed. Additional support of competitive adsorption was in 1,3-butadiene and crotonaldehyde TPD from Site I. Water pre-adsorption resulted in more furan and less maleic anhydride to desorb. This behavior clarified reactor study results in which high selectivity to furan was observed at higher water feed concentrations. Water appears to have blocked furan from further reaction to maleic anhydride or other products.

The relative reaction strengths of crotonaldehyde and furan were also taken into consideration when analyzing the results. As a reaction feed, furan exhibited a fairly low activity (no conversion until 240°C) compared to crotonaldehyde (20% conversion at 180°C). In all cases when crotonaldehyde was observed as a desorption product in TPD experiments, it existed in trace amounts. This could have simply been because crotonaldehyde further reacted to furan, or maleic anhydride. It was difficult to attribute water to be in competitive adsorption with crotonaldehyde from our TPD data (as it may be coupled with the furan desorption peak). It was apparent in reactor studies using feeds

of 1,3-butadiene and 3,4-epoxy-1-butene and step-change experiments that the addition of water had a large positive effect on crotonaldehyde selectivity.

It was observed in partial oxidized hydrocarbon feed studies (3,4-epoxy-1-butene and crotonaldehyde) that the addition of water caused an increase in the maximum selectivities to furan and maleic anhydride and a decrease in selectivity to 2-butene-1,4-dial. This indicated that water had a specific effect on the nature of the surface sites. The high increase in selectivity to furan (from 3,4-epoxy-1-butene or crotonaldehyde) or crotonaldehyde (from 1,3-butadiene or 3,4-epoxy-1-butene) suggested a possible increase in the acid character of the catalyst. Both the isomerization of 3,4-epoxy-1-butene and the ring formation of furan are acid-catalyzed reactions. In TPD studies, the pre-adsorption of water increased the amount of furan desorbed from both 1,3-butadiene and crotonaldehyde. Another explanation for the effect of water addition considered is that water dissociatively adsorbed on the catalyst surface. Surface $OH^{\delta-}$ species and $H^{\delta+}$ would be formed, which could exhibit Brønsted acid-base interactions with adsorbing molecules. With a non-ideal V_2O_5-based structure, this type of adsorption is favored (11). These types of reactive centers have been suggested to exist for SnO_2-MoO_3 catalysts based on ^{18}O-H_2O tracer studies for propylene oxidation to acetone (3). Recalling the TPD studies, it seems unlikely that water formed new "different" reactive centers, as desorption curves maintained their peak position with the pre-adsorption of water. It could be possible that water dissociatively desorbed and donated oxygen to existing sites on the surface, particularly Sites III and IV. This behavior is supported in TPD studies, in which 1,3-butadiene adsorption showed and increase in desorption

response at Sites III and IV. Dissociatively adsorbed water could have replenished additional O_B and O_C vacancies. For TPD experiments with furan adsorption, an opposite behavior would be expected, as furan adsorption could be onto one of sites type III or IV, meaning that furan-filled vacancies would block some of the water adsorption sites. This was supported by studies in which 3,4-epoxy-1-butene or crotonaldehyde had significant selectivity increases to furan and maleic anhydride. The addition of oxygen from dissociatively adsorbed water to nucleophilic sites would strengthen the pathway to these products in two possible ways – by adding acidic character to the catalyst surface and providing additional oxygen to the catalyst. The dissociative adsorption of water, however, should also form more electrophilic species responsible for total oxidation (or perhaps epoxidation). At low levels of water addition, 3,4-epoxy-1-butene selectivity increased slightly, while CO_x selectivity decreased significantly. At higher levels of water addition (above 5-6%), CO_x selectivity began to steadily rise. It appears that at lower concentrations of water, competitive adsorption was the dominant effect of water, while at higher water concentrations, dissociative adsorption added additional "chemical" effects to the surface, including acid formation and increased electrophilic nature.

The possibility that bulk structural changes of the VMoO catalyst took place with the addition of water to the reactant feed seemed unlikely. Characterization of pre and post-reaction catalysts with LRS and XPS indicated no detectable difference in bulk or surface structure. An example of bulk structural changes which have been shown to occur with water addition are for previously discussed VPO catalysts in n-butane oxidation to maleic anhydride (24). VPO catalysts have been shown to undergo phase

transformations during reaction, including transformations to both V^{+5} and V^{+4} phases. In studies by Xue et al. using in situ LRS, it was shown that every V^{+5} phase transformed into the dihydrate under an H_2O/air or H_2O/N_2 feed. In the case of VPO catalysts, it has been proposed by several groups that the geometry of the surface is key in the reaction of n-butane to maleic anhydride. In previous studies using VMoO catalysts, reaction conditions induced a slight surface reduction (as shown by XPS), and it appeared the addition of water does not affect the degree of surface reduction to any distinguishable extent, shown in Figure 3. Further support of this postulate is derived from step change studies. Upon water addition, an immediate response in selectivity and conversion occurred. Furthermore, conversion and selectivity immediately reverted to original levels when the water feed was diverted from the reactant stream. It appeared to be unlikely that a structural change (lattice expansion, phase change, etc.) would have occurred with such an abrupt conversion and selectivity response.

4.6. Conclusions

Five distinct adsorption sites were proposed for the selective oxidation of 1,3-butadiene over V_2O_5-based solid solution VMoO catalysts. Site I was proposed to be corner-sharing O_B oxygens responsible for crotonaldehyde adsorption and furan cyclization. Site II was identified as the vanadyl oxygen (O_A), responsible for electrophilic oxidation of 1,3-butadiene to 3,4-epoxy-1-butene. Sites III was proposed to be and O_B or O_C vacancy, formed upon the desorption of 2-butene-1,4-dial. Site IV was not clearly identified and was detected only in furan adsorption studies. Water addition to the reactant feed showed a significant increase in conversion, and a preference to the

formation of crotonaldehyde and furan. Site V appeared to be a strong 1,3-butadiene adsorption site, assigned to O_C oxygen. At high levels of water (12%), selectivity of 1m,3-butadien to furan was near 25%. The effects of water on catalytic performance were explained through competitive adsorption, in which water either undergoes molecular or dissociative adsorption. The dissociative adsorption of water appeared to replenish Sites II and IV, and additionally provided acidic character that promoted acid-catalyzed isomerization of 3,4-epoxy-1-butene and heterocyclization of crotonaldehyde to furan. It appeared that at lower water concentrations, competitive adsorption was the dominant effect of water, while at higher water concentrations, adsorption of water played a more active role in the reaction by forming acidic sites and electrophilic species.

4.7. Acknowledgements

The authors would like to acknowledge Jim Anderegg of the Ames Laboratory for performing XPS experiments and for assisting interpretation. This research was performed under funding from Ames Laboratory – USDOE contract No. W-7405-Eng-82.

4.8. List of Figures

1. Reactor system configuration for temperature-programmed desorption studies
2. Laser Raman Spectra of 14.0 mol % MoO3 in V2O5 catalyst a) pre-reaction, b) post reaction under 1.4% 1,3-butadiene, 54% air and balance He and c) post reaction under 1.4% 1,3-butadiene, 54% air, 2.5% water and balance He.

3. XPS (vanadium region) of 14.0 mol % MoO_3 in V_2O_5 catalyst a) pre-reaction, b) post reaction under 1.4% 1,3-butadiene, 54% air and balance He and c) post reaction under 1.4% 1,3-butadiene, 54% air, 2.5% water and balance He.
4. Effect of water addition level for selective oxidation of 1,3-butadiene at 275°C. Water addition level varied from 0.0 to 12%. Total gas flow rate was 70 sccm (1.4% 1,3-butadiene in air, He and, water).
5. Conversion and selectivity effects from 0.5% water addition step change in 1,3-butadiene oxidation at 275°C. Total gas flow rate was 70 sccm (1.4% 1,3-butadiene in air and He).
6. Conversion and selectivity effects from 2.5% water addition step change in 1,3-butadiene oxidation at 275°C. Total gas flow rate was 70 sccm (1.4% 1,3-butadiene in air and He).
7. Effect of temperature and water addition between 180°C and 280°C for 3,4-epoxy-1-butene selective oxidation. Total gas flow rate was 105 sccm (0.15% 3,4-epoxybutene in air and He).
8. Effect of temperature between 180°C and 280°C for crotonaldehyde selective oxidation. Total gas flow rate was 105 sccm (0.15% crotonaldehyde in air and He). When added, water made up 2.5% of the total feed.
9. Effect of temperature and water addition between 180°C and 280°C for furan selective oxidation. Total gas flow rate was 105 sccm (0.15% furan in air and He). When added, water made up 2.5% of the total feed.

10. Effect of temperature and water addition between 180°C and 280°C for 2,5-dihydrofuran selective oxidation. Total gas flow rate was 105 sccm (0.15% 2,5-dihydrofuran in air and He). When added, water made up 2.5% of the total feed.
11. Temperature-programmed desorption results from 1,3-butadiene adsorbed at 65°C. Solid lines represent GC response from experiments with no water pre-adsorption, dashed lines represent GC response from experiments with water pre-adsorption.
12. Temperature-programmed desorption results from crotonaldehyde adsorbed at 65°C. Solid lines represent GC response from experiments with no water pre-adsorption, dashed lines represent GC response from experiments with water pre-adsorption.
13. Temperature-programmed desorption (maleic anhydride response) results from furan adsorbed at 65°C. Solid lines indicate no water pre-adsorption. Dashed lines indicate water pre-adsorption.
14. Temperature-programmed desorption (maleic anhydride response) results for 1,3-butadiene, crotonaldehyde, and furan adsorbed at 65°C. Solid lines indicate no water pre-adsorption. Dashed lines indicate water pre-adsorption.
15. Possible surface mechanism for Site I adsorption of crotonaldehyde and reaction to furan based on V_2O_5 structure.

4.9. List of Tables

1. Effects of water on catalyst performance studies using 3,4-epoxy-1-butene and crotonaldehyde as feeds.

2. Temperature-programmed desorption results using 1,3-butadiene, crotonaldehyde, and furan as adsorption gases. Gases were adsorbed at 65°C with or without water pre-adsorption.

4.10. References

1 Saleh-Alhamed, R. R. Hudgins and P. L. Silveston, *Applied Catalysis A: General* **127**, 177 (1995).

2 Saleh-Alhamed, R. R. Hudgins and P. L. Silveston, *Journal of Catalysis*.**161**, 430 (1996).

3 Moro-oka, Y, Y. Takita, and A. Ozaki, *Journal of Catalysis* **27**, 177 (1972).

4 Ben Abdelouahab, F., J. C. Volta, R. Olier, *Journal of Catalysis* **148**, 334 (1994).

5 Xue, Z. Y. and G. L. Schrader, *J. Phys Chem. B* **103**, 9459 (1999).

6 Arnold, E. W., III, S. Sundaresan, *Applied Catalysis* **41**, 225 (1988).

7 Lerou, J. J., P. L. Mills, Du Pont Butane Oxidation Process. *In Precision Process Technology*; Weijnen, M. P. C., Drinkenburg, A. A. H., Eds., Kluwer Academic Publishers, Dordrecht, The Netherlands, 175-195 (1993).

8 Contractor, R. M., H. S. Horowitz, G. M. Sisler, E. Bordes, *Catal. Today* **37**, 51 (1997).

9 Yin, X., A. Fahmi, H. Han, A. Endou, S. S. C. Ammal, M. Kubo, K. Teraishi, and A. Miyamoto, *J. Phys. Chem. B* **103**, 3218 (1999).

10 Witko, M., K. Hermann, R. Tokarz, *Book of Abstracts of 215th ACS National Meeting*; COMP 078, Dallas, 1998.

11 Haber, J., M. Witko, and R. Tokarz, *Applied Catalysis A: General* **157**, 3 (1997).

12 Henrich, V. E., P. A. Cox, *The Surface Science of Metal Oxides*, Cambridge University Press: Cambridge 1994, Chapter 6.

13 Fontenot, C. J., J. W. Wiench, M. Pruski, and G. L. Schrader, *J. Phys Chem. B* **104**, 11622 (2000).

14 Fontenot, C. J., J. W. Wiench, M. Pruski, and G. L. Schrader, *J. Phys Chem. B*, submitted for publication 2001.

15 Alonso, B. and J. Livage, *Journal of Solid State Chemistry* **148**, 16 (1999).

16 Bradzil, J. F., M. A. Toft, J. P. Bartek, R. G. Teller, and R. M. Cyngier, *Chem. Mater.* **10**, 4100 (1998).

17 Schroeder, W.D., C.J. Fontenot and G.L. Schrader, *Journal of Catalysis,* submitted 2001.

18 Lewis, K. B., S. T. Oyama, and G. A. Somorjai, *Applied Surface Science* **52**, 241 (1991).

19 Mendialdua, J., R. Casanova, and Y. Barbaux, *Journal of Electron Spectroscopy and Related Phenomena* **71**, 249 (1995).

20 Chen, Y., Xie, K., and Liu, Z.X., *Applied Surface Surface* **133**, 221 (1998).

21 Demeter, M, Neumann, M., and Reichelt, W., *Surface Science* **454-456**, 41 (2000).

22 Joule, J. A., K. Mills, and G. F. Smith, *Heterocyclic Chemistry*, 3rd Edition, "Furans: Reaction and Synthesis", Chapman & Hall, London, UK. pp. 290-292 (1995).

23 Witko, J.M., R. Tokarz, and J. Haber, *Applied Catalysis A: General* **157**, 23 (1997).

24 Xue, Z. and G. L. Schrader, *Journal of Catalysis* **184**, 87 (1999).

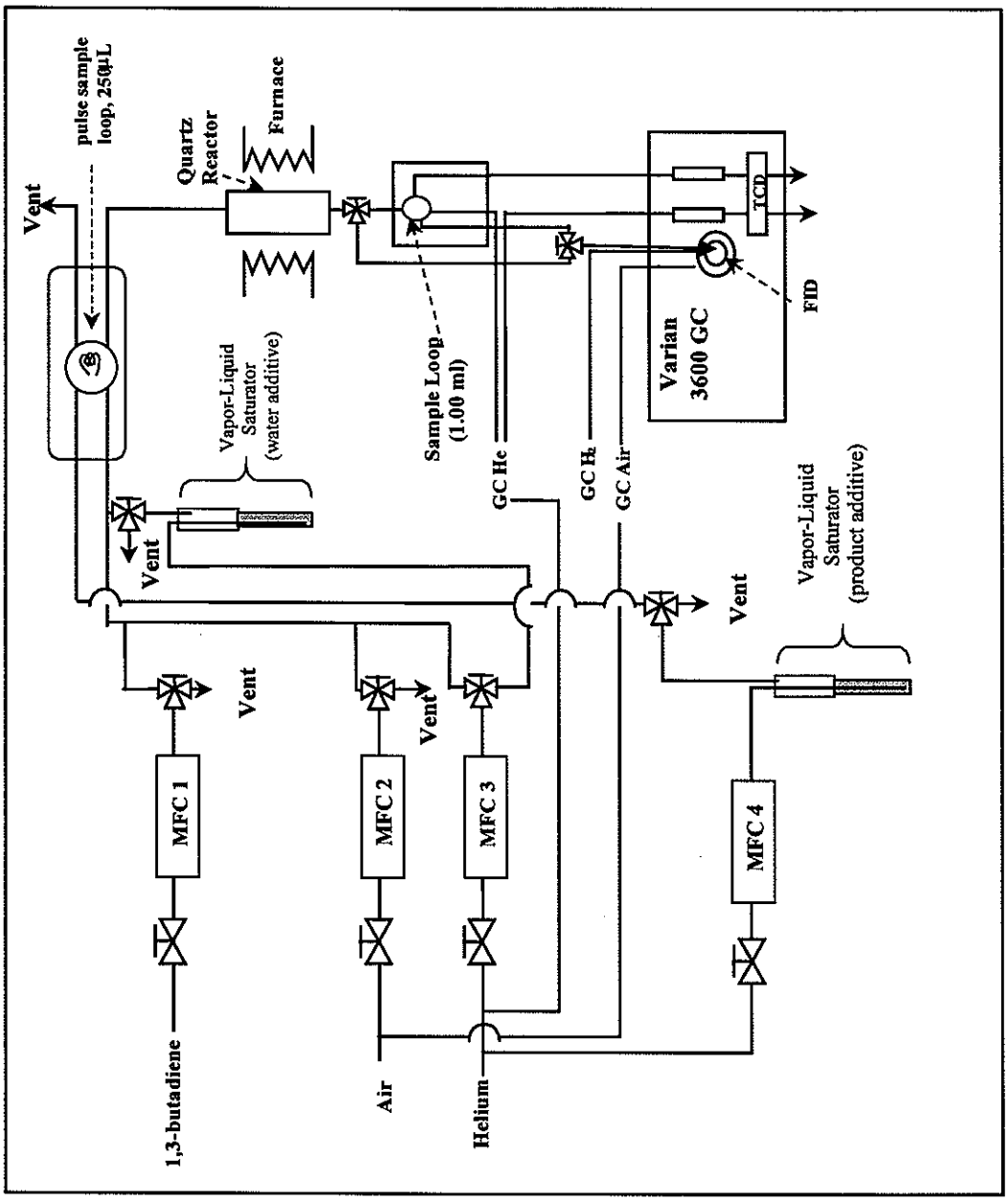
pulse sample loop, 250µL
Quartz Reactor
Furnace
Vent
TCD
FID
Varian 3600 GC
Vapor-Liquid Saturator (water additive)
Sample Loop (1.00 ml)
GC He
GC H2
GC Air
Vent
Vapor-Liquid Saturator (product additive)
Vent
Vent
Vent
MFC 1
MFC 2
MFC 3
MFC 4
1,3-butadiene
Air
Helium

Figure 1

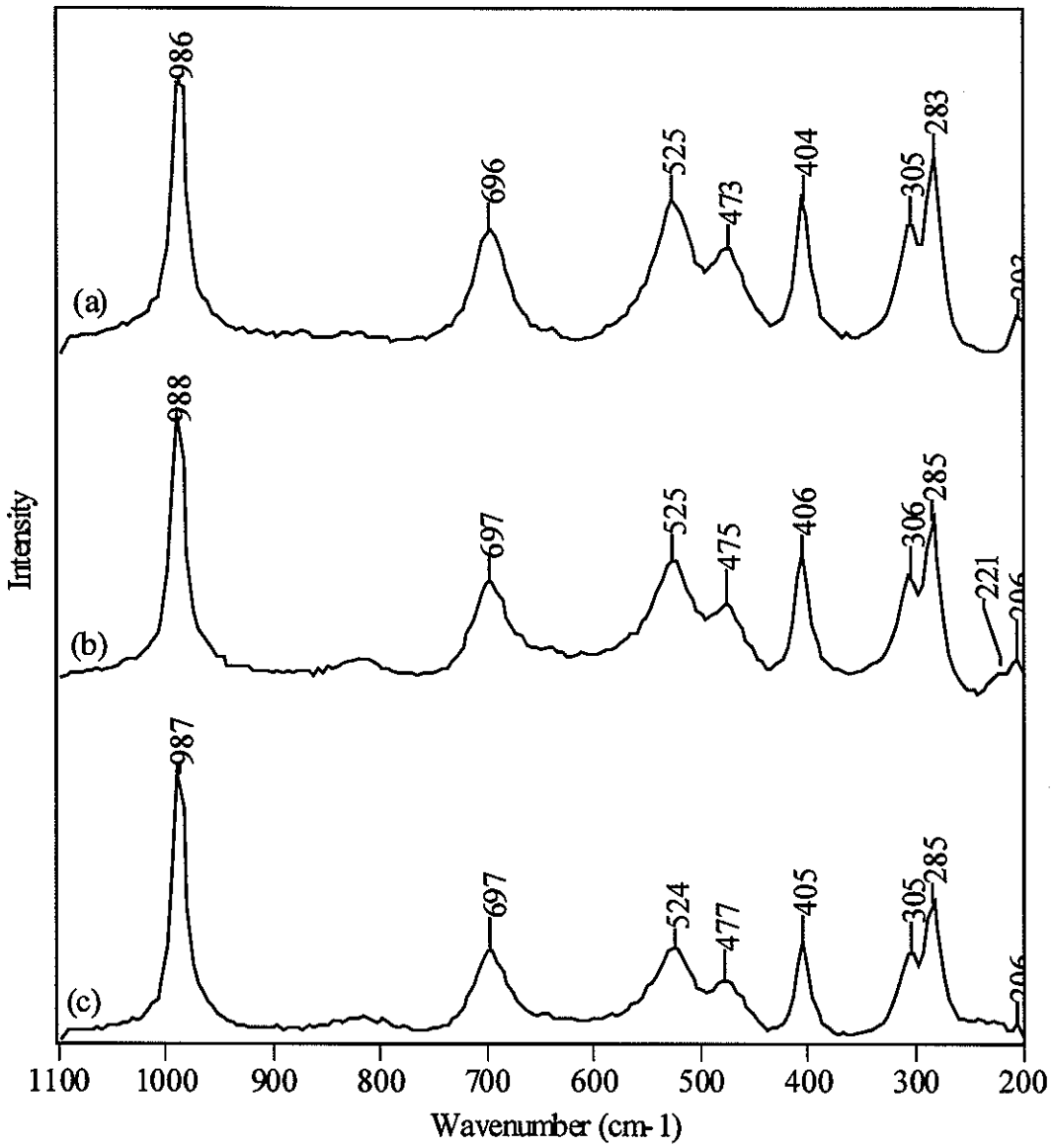
986
696
525
473
404
305
283
(a)
988
697
525
475
406
306
285
221
(b)
987
697
524
477
405
305
285
(c)
Intensity
1100
1000
900
800
700
600
500
400
300
200
Wavenumber (cm-1)

Figure 2

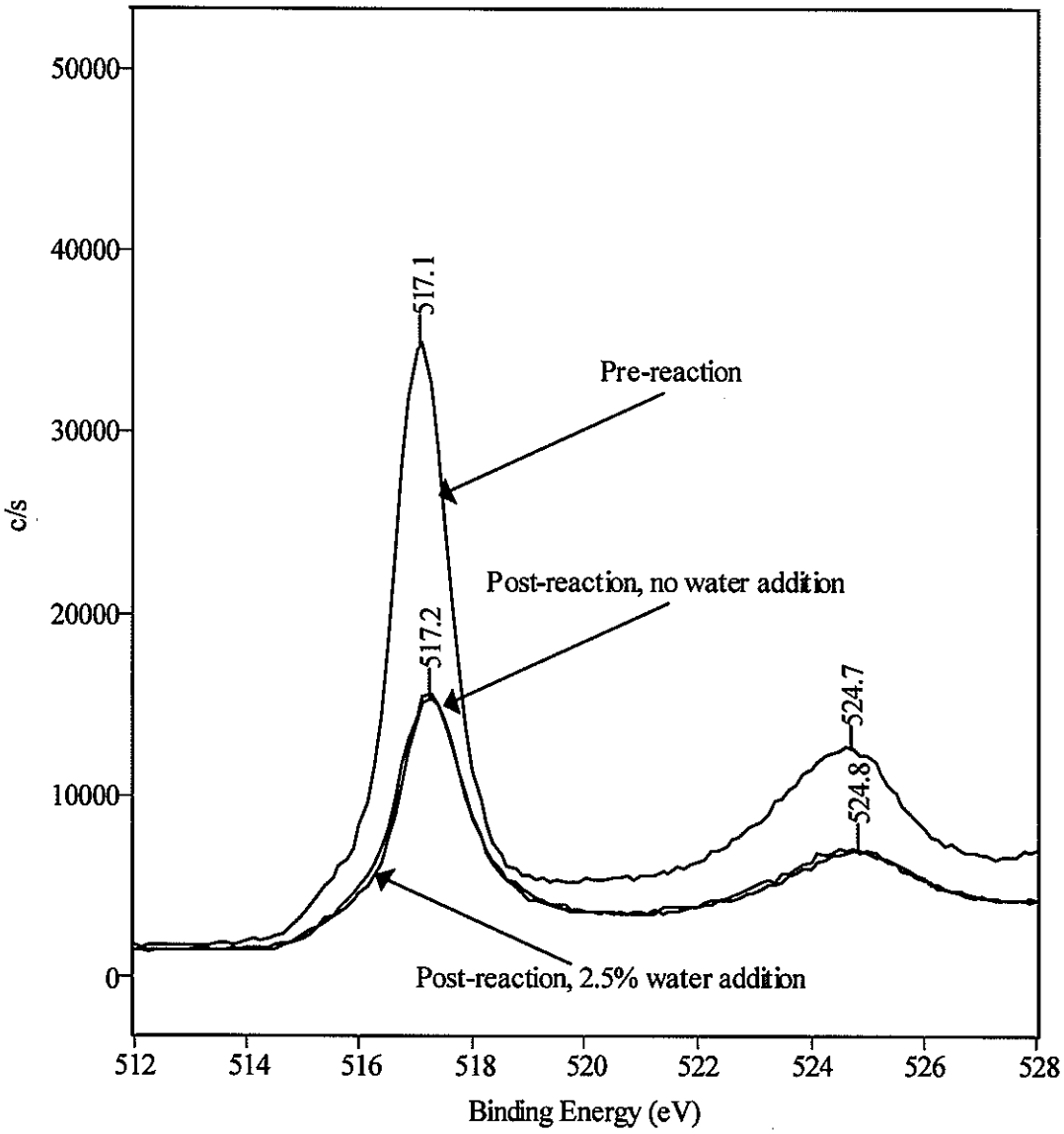
50000
40000
30000
20000
10000
0
c/s
517.1
Pre-reaction
Post-reaction, no water addition
517.2
524.7
524.8
Post-reaction, 2.5% water addition
512
514
516
518
520
522
524
526
528
Binding Energy (eV)

Figure 3

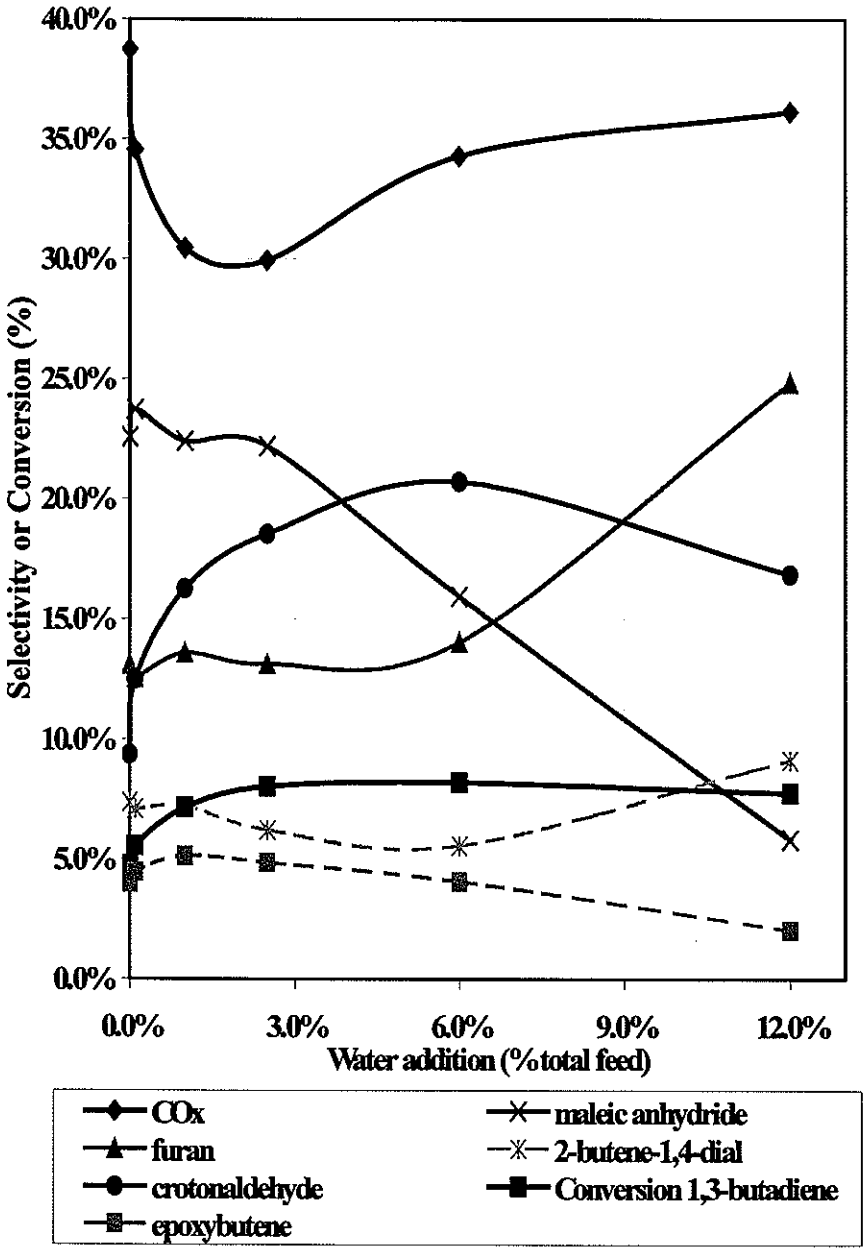
40.0%
35.0%
30.0%
25.0%
20.0%
15.0%
10.0%
5.0%
0.0%
Selectivity or Conversion (%)
0.0%
3.0%
6.0%
9.0%
12.0%
Water addition (% total feed)
COx
maleic anhydride
furan
2-butene-1,4-dial
crotonaldehyde
Conversion 1,3-butadiene
epoxybutene

Figure 4

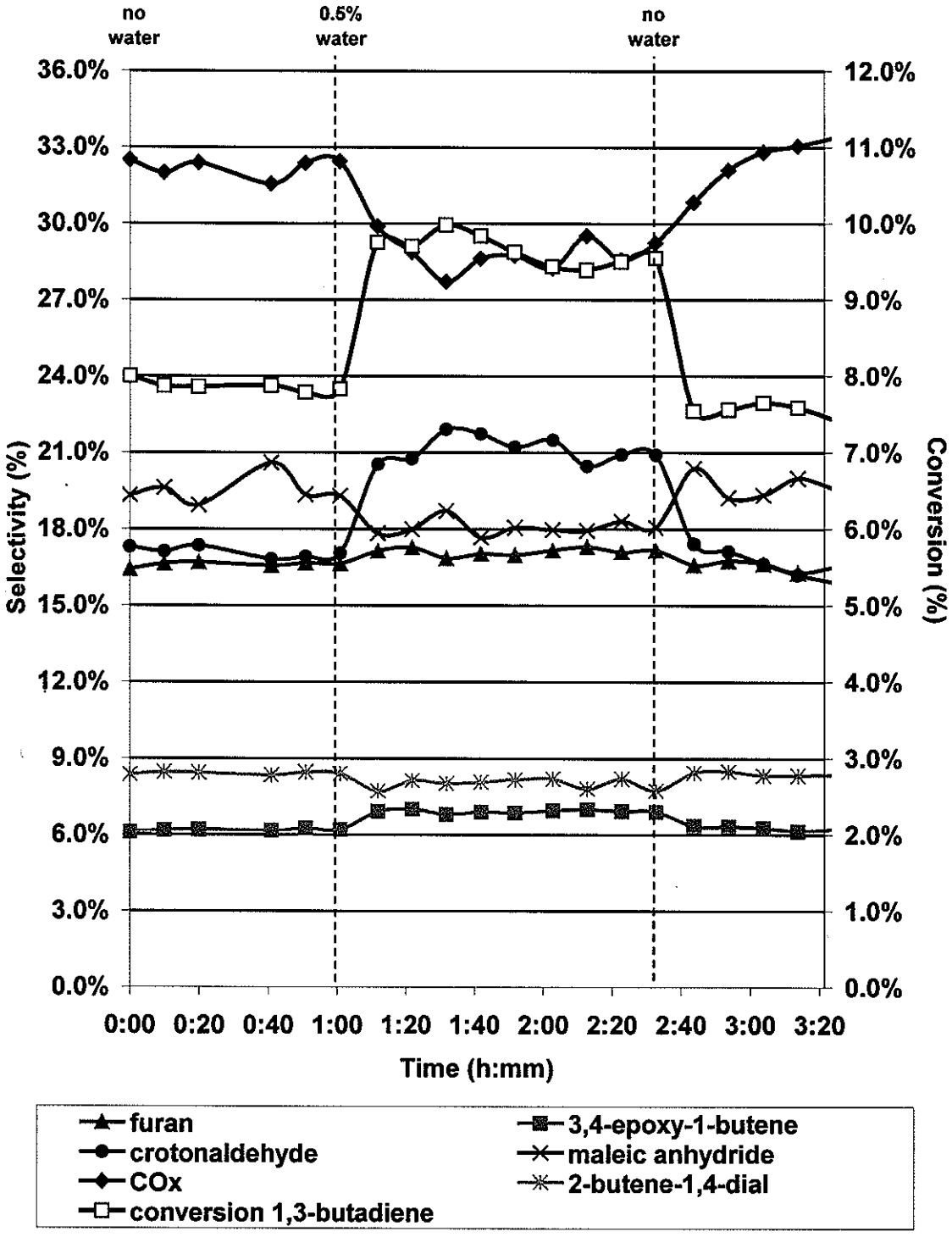
no water
0.5% water
no water
36.0%
33.0%
30.0%
27.0%
24.0%
21.0%
18.0%
15.0%
12.0%
9.0%
6.0%
3.0%
0.0%
Selectivity (%)
12.0%
11.0%
10.0%
9.0%
8.0%
7.0%
6.0%
5.0%
4.0%
3.0%
2.0%
1.0%
0.0%
Conversion (%)
0:00 0:20 0:40 1:00 1:20 1:40 2:00 2:20 2:40 3:00 3:20
Time (h:mm)
furan
crotonaldehyde
COx
conversion 1,3-butadiene
3,4-epoxy-1-butene
maleic anhydride
2-butene-1,4-dial

Figure 5

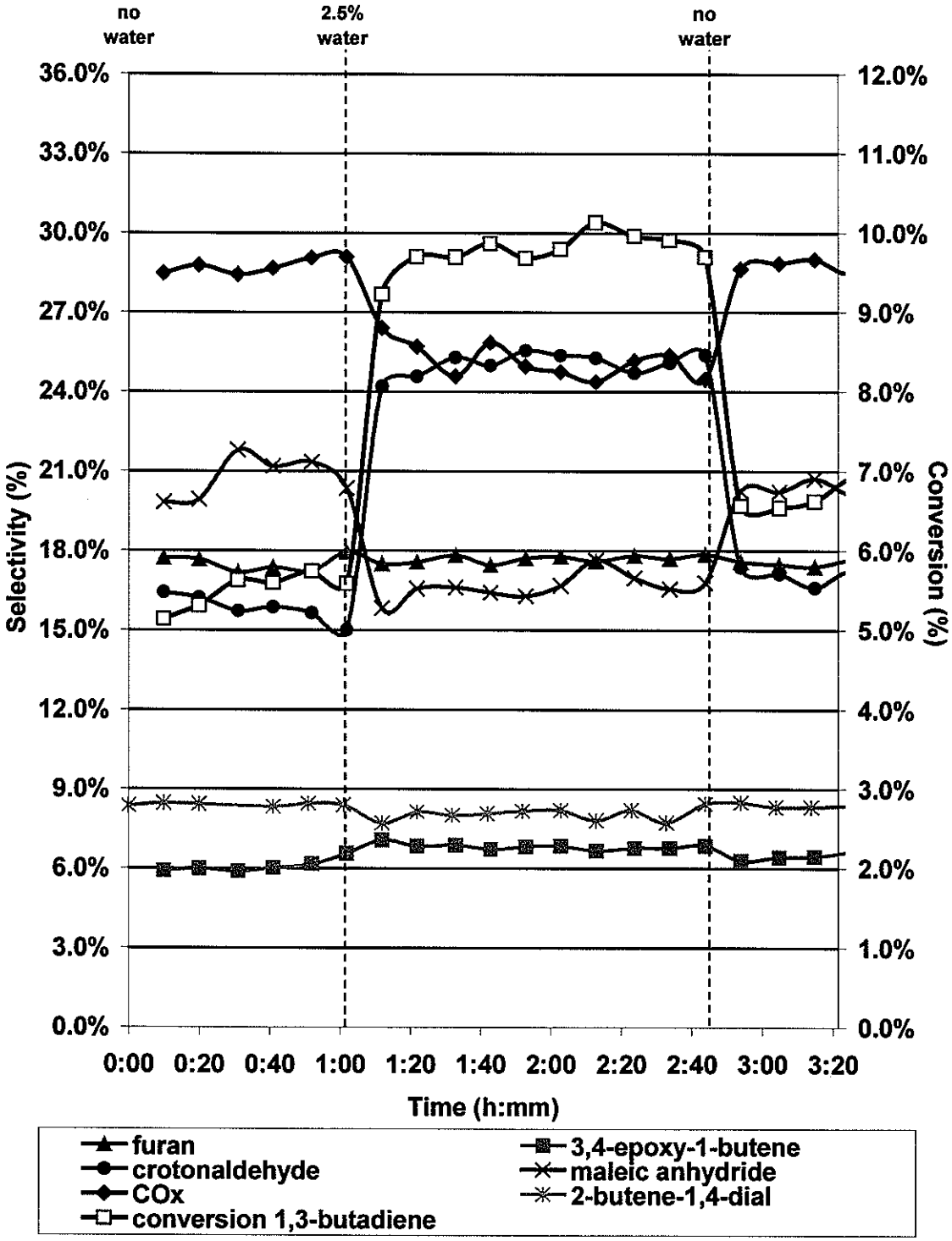
no water
2.5% water
no water
36.0%
33.0%
30.0%
27.0%
24.0%
21.0%
18.0%
15.0%
12.0%
9.0%
6.0%
3.0%
0.0%
Selectivity (%)
12.0%
11.0%
10.0%
9.0%
8.0%
7.0%
6.0%
5.0%
4.0%
3.0%
2.0%
1.0%
0.0%
Conversion (%)
0:00 0:20 0:40 1:00 1:20 1:40 2:00 2:20 2:40 3:00 3:20
Time (h:mm)
furan
crotonaldehyde
COx
conversion 1,3-butadiene
3,4-epoxy-1-butene
maleic anhydride
2-butene-1,4-dial

Figure 6

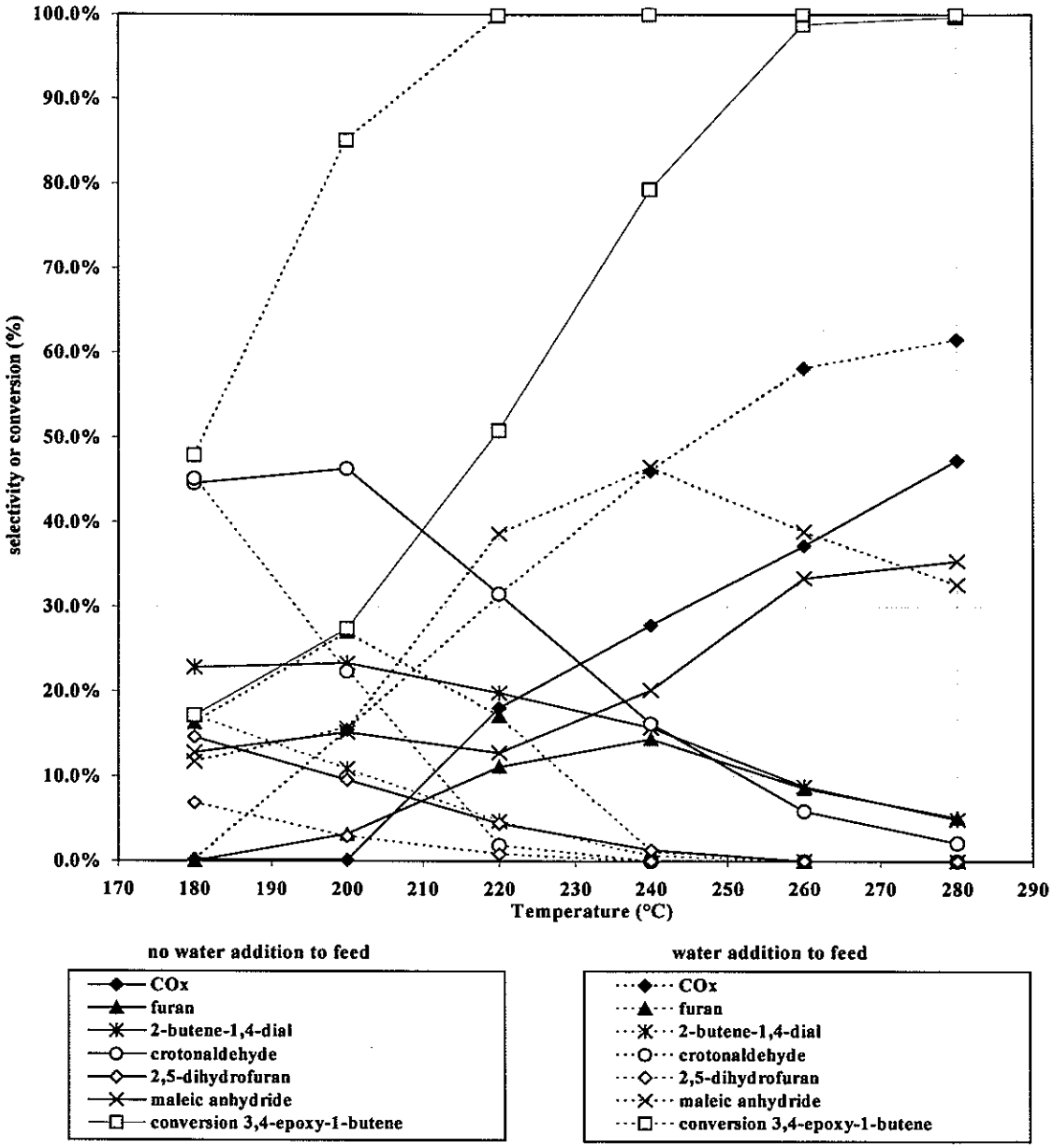
100.0%
90.0%
80.0%
70.0%
60.0%
50.0%
40.0%
30.0%
20.0%
10.0%
0.0%
selectivity or conversion (%)
170
180
190
200
210
220
230
240
250
260
270
280
290
Temperature (°C)
no water addition to feed
COx
furan
2-butene-1,4-dial
crotonaldehyde
2,5-dihydrofuran
maleic anhydride
conversion 3,4-epoxy-1-butene
water addition to feed
COx
furan
2-butene-1,4-dial
crotonaldehyde
2,5-dihydrofuran
maleic anhydride
conversion 3,4-epoxy-1-butene

Figure 7

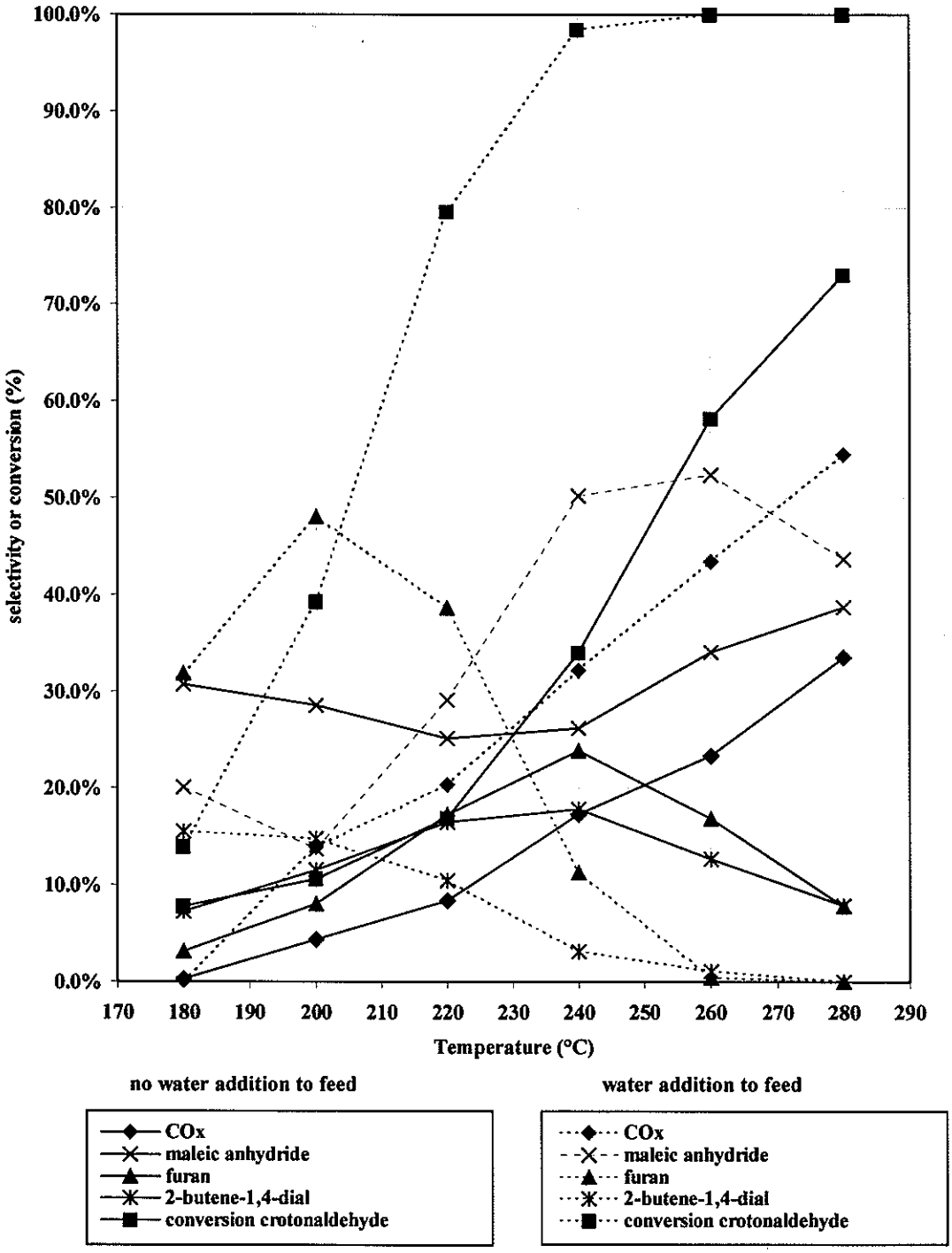
100.0%
90.0%
80.0%
70.0%
60.0%
50.0%
40.0%
30.0%
20.0%
10.0%
0.0%
selectivity or conversion (%)
170
180
190
200
210
220
230
240
250
260
270
280
290
Temperature (°C)
no water addition to feed
COx
maleic anhydride
furan
2-butene-1,4-dial
conversion crotonaldehyde
water addition to feed
COx
maleic anhydride
furan
2-butene-1,4-dial
conversion crotonaldehyde

Figure 8

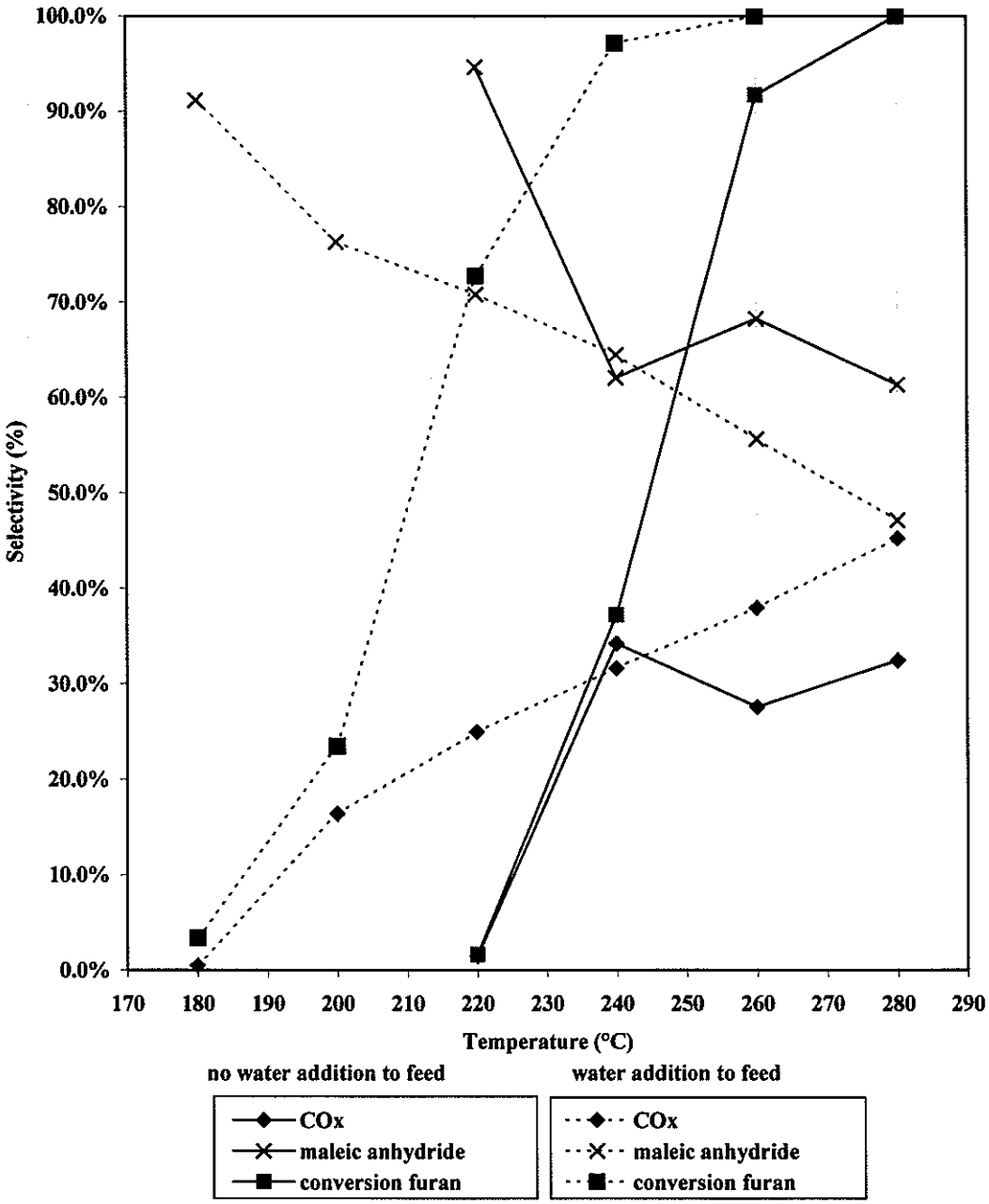
100.0%
90.0%
80.0%
70.0%
60.0%
50.0%
40.0%
30.0%
20.0%
10.0%
0.0%
Selectivity (%)
170
180
190
200
210
220
230
240
250
260
270
280
290
Temperature (°C)
no water addition to feed
COx
maleic anhydride
conversion furan
water addition to feed
COx
maleic anhydride
conversion furan

Figure 9

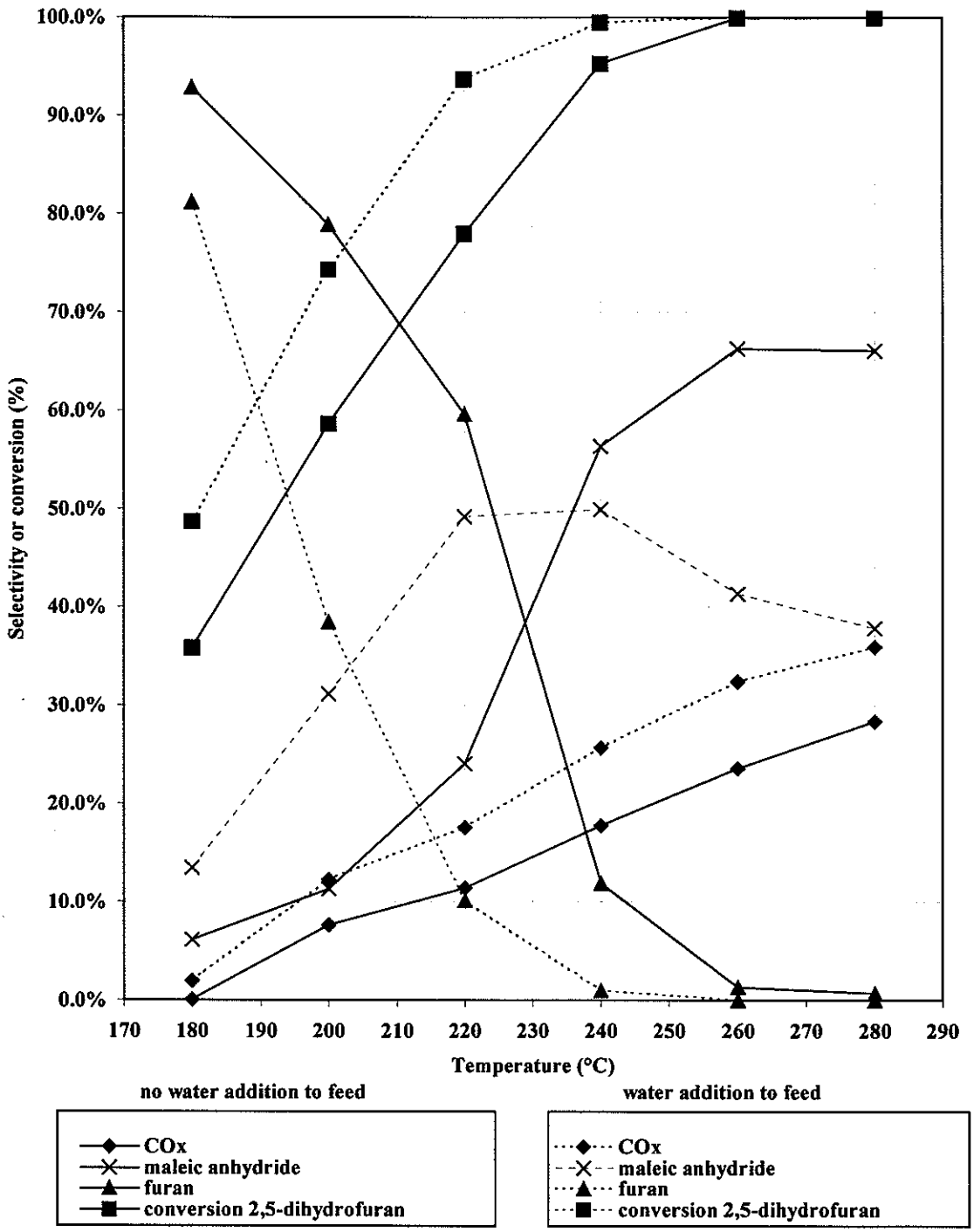
100.0%
90.0%
80.0%
70.0%
60.0%
50.0%
40.0%
30.0%
20.0%
10.0%
0.0%
Selectivity or conversion (%)
170
180
190
200
210
220
230
240
250
260
270
280
290
Temperature (°C)
no water addition to feed
COx
maleic anhydride
furan
conversion 2,5-dihydrofuran
water addition to feed
COx
maleic anhydride
furan
conversion 2,5-dihydrofuran

Figure 10

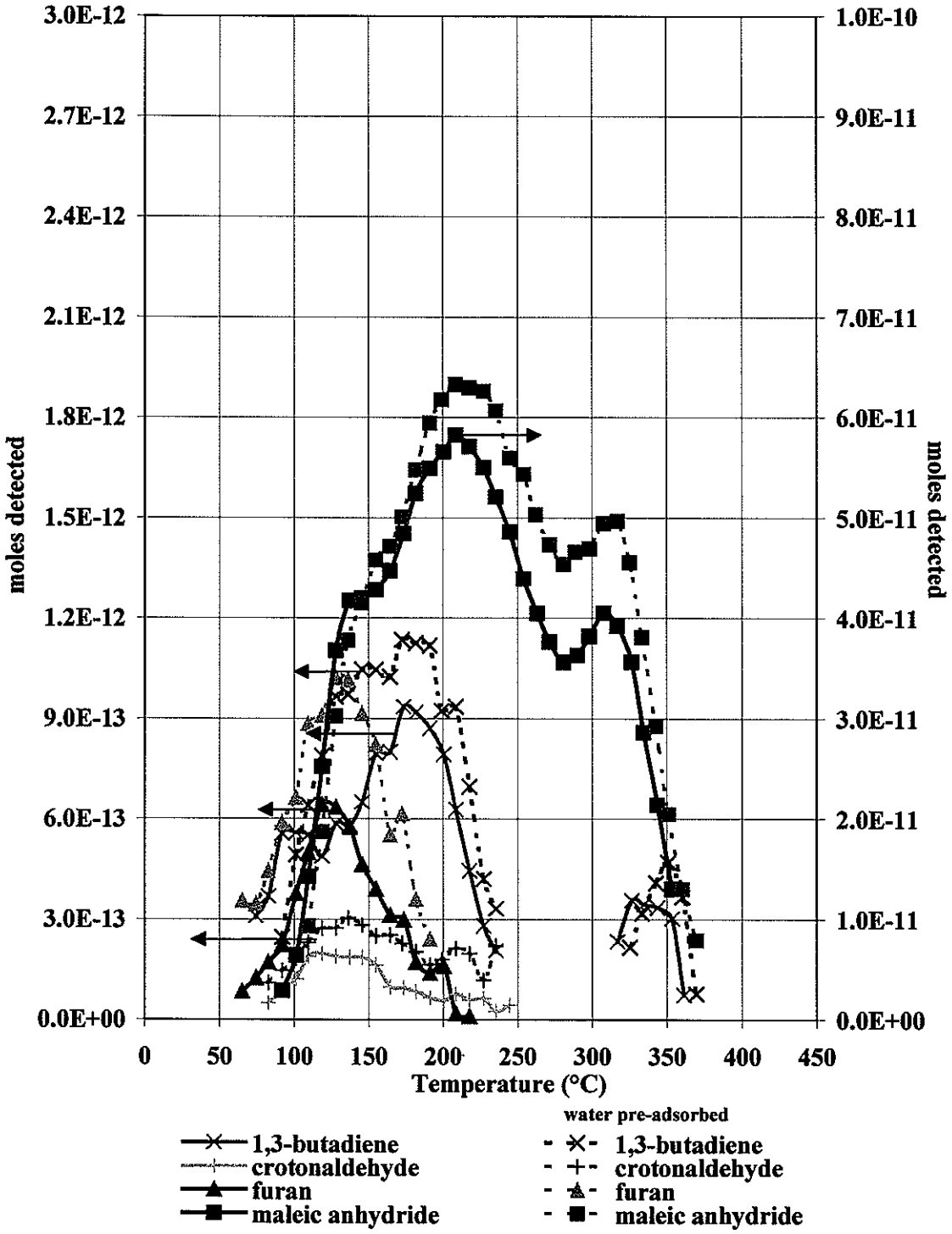
3.0E-12
2.7E-12
2.4E-12
2.1E-12
1.8E-12
1.5E-12
1.2E-12
9.0E-13
6.0E-13
3.0E-13
0.0E+00
moles detected
1.0E-10
9.0E-11
8.0E-11
7.0E-11
6.0E-11
5.0E-11
4.0E-11
3.0E-11
2.0E-11
1.0E-11
0.0E+00
moles detected
0
50
100
150
200
250
300
350
400
450
Temperature (°C)
water pre-adsorbed
1,3-butadiene
crotonaldehyde
furan
maleic anhydride
1,3-butadiene
crotonaldehyde
furan
maleic anhydride

Figure 11

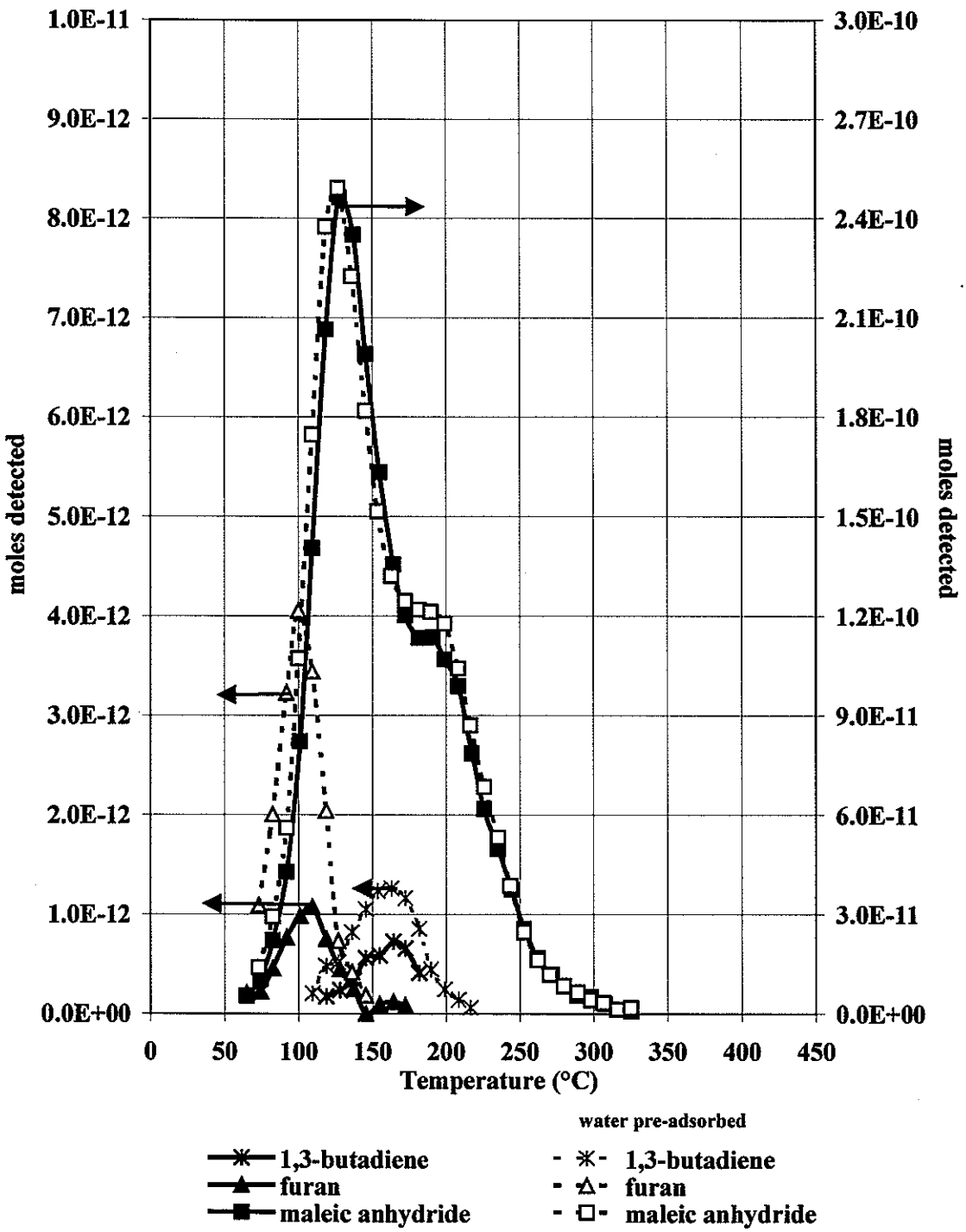
1.0E-11
9.0E-12
8.0E-12
7.0E-12
6.0E-12
5.0E-12
4.0E-12
3.0E-12
2.0E-12
1.0E-12
0.0E+00
moles detected
3.0E-10
2.7E-10
2.4E-10
2.1E-10
1.8E-10
1.5E-10
1.2E-10
9.0E-11
6.0E-11
3.0E-11
0.0E+00
moles detected
0
50
100
150
200
250
300
350
400
450
Temperature (°C)
water pre-adsorbed
1,3-butadiene
furan
maleic anhydride
1,3-butadiene
furan
maleic anhydride

Figure 12

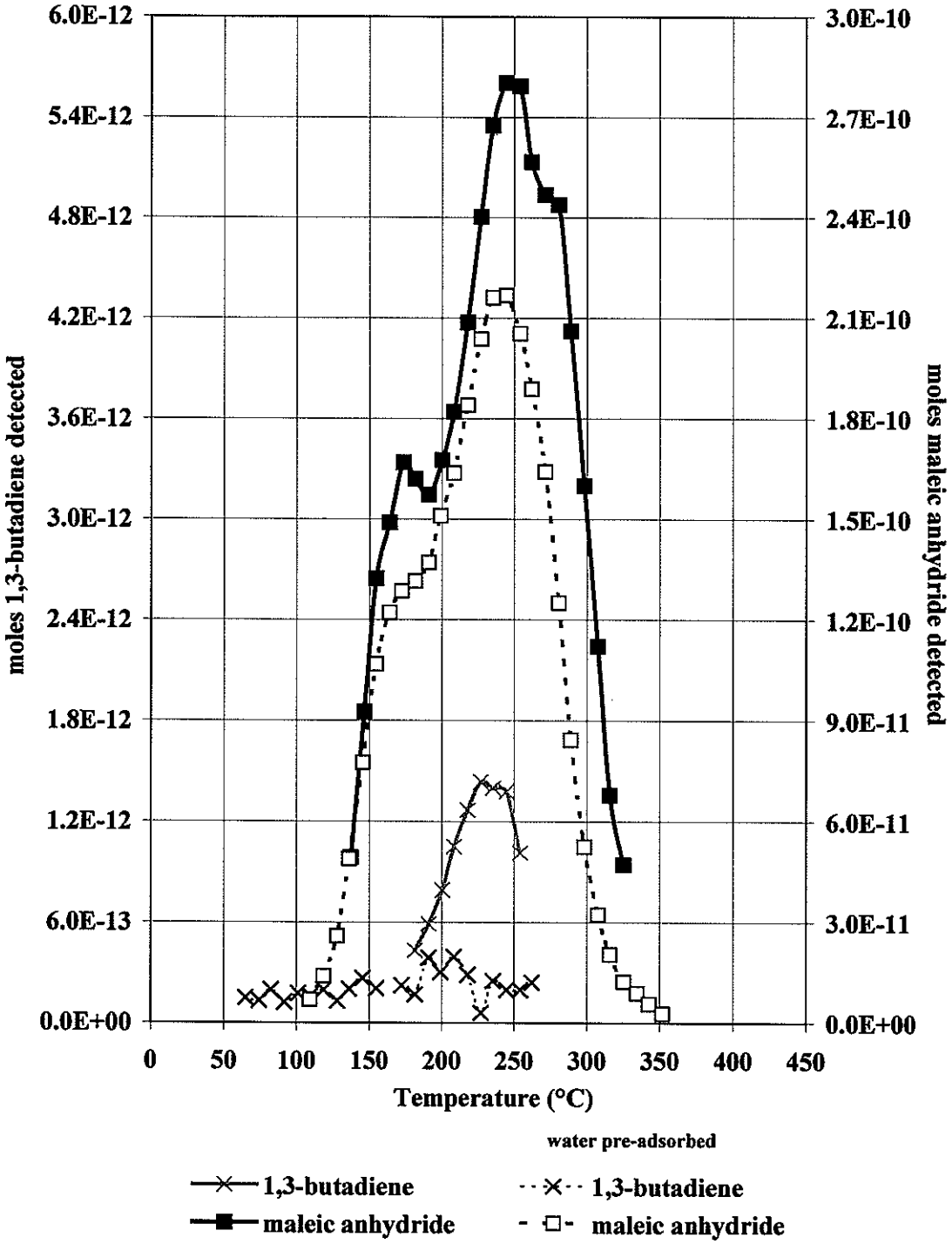
6.0E-12
5.4E-12
4.8E-12
4.2E-12
3.6E-12
3.0E-12
2.4E-12
1.8E-12
1.2E-12
6.0E-13
0.0E+00
moles 1,3-butadiene detected
3.0E-10
2.7E-10
2.4E-10
2.1E-10
1.8E-10
1.5E-10
1.2E-10
9.0E-11
6.0E-11
3.0E-11
0.0E+00
moles maleic anhydride detected
0
50
100
150
200
250
300
350
400
450
Temperature (°C)
water pre-adsorbed
1,3-butadiene
maleic anhydride
1,3-butadiene
maleic anhydride

Figure 13

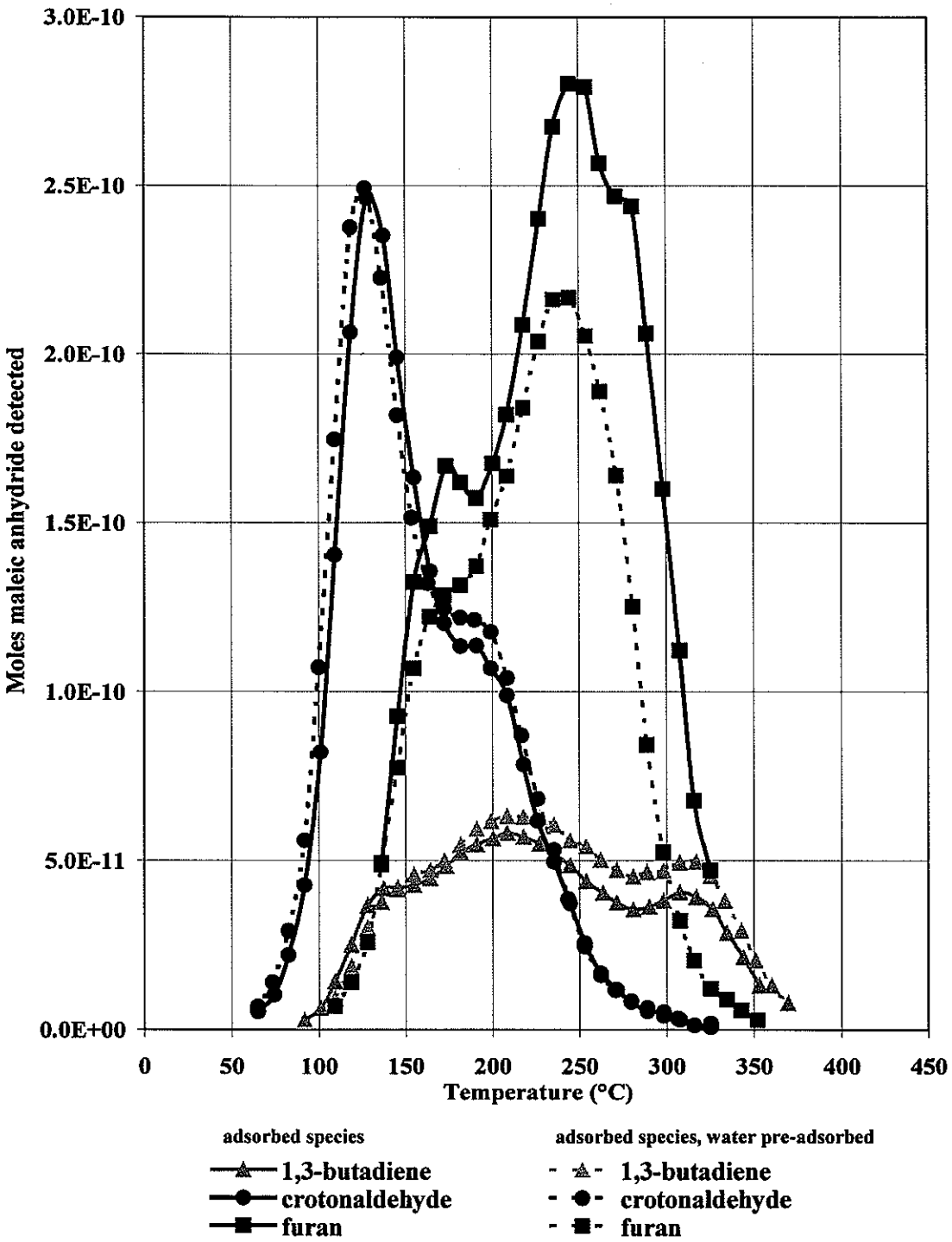
3.0E-10
2.5E-10
2.0E-10
1.5E-10
1.0E-10
5.0E-11
0.0E+00
Moles maleic anhydride detected
0
50
100
150
200
250
300
350
400
450
Temperature (°C)
adsorbed species
1,3-butadiene
crotonaldehyde
furan
adsorbed species, water pre-adsorbed
1,3-butadiene
crotonaldehyde
furan

Figure 14

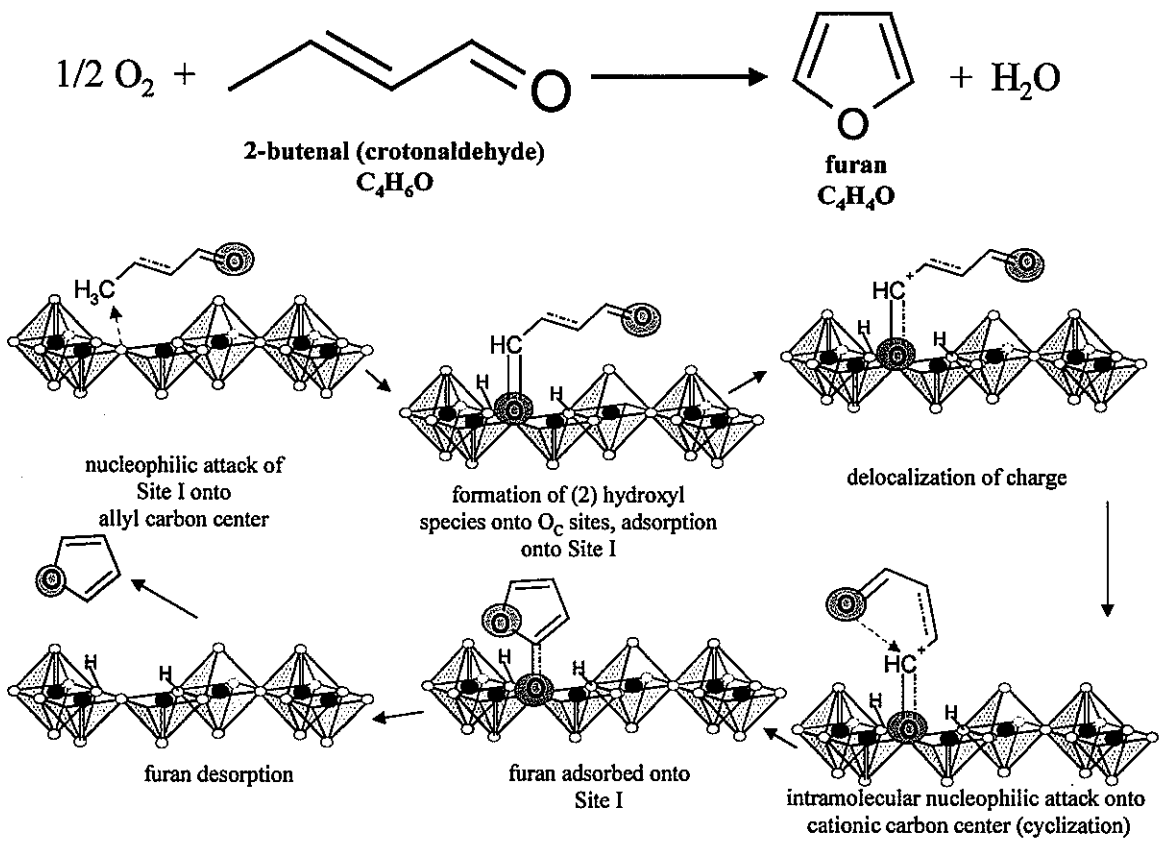
1/2 O2 +
O
+ H2O
2-butenal (crotonaldehyde)
C4H6O
furan
C4H4O
H3C
HC
H
H
HC+
H
H
nucleophilic attack of
Site I onto
allyl carbon center
formation of (2) hydroxyl
species onto Oc sites, adsorption
onto Site I
delocalization of charge
H
H
HC+
H
H
H
H
furan desorption
furan adsorbed onto
Site I
intramolecular nucleophilic attack onto
cationic carbon center (cyclization)

Figure 15

Table 1

FEED			% change	Temp. shift for max selectivity
3,4-epoxy-1-butene				
	selectivity to:	furan	**+ 87.5%**	**240 °C to 200 °C**
		2-butene-1,4-dial	**-26.5%**	**200 °C to 180 °C**
		maleic anhydride	**+ 31.4%**	**280 °C to 240 °C**
crotonaldehyde				
	selectivity to:	furan	**+ 104.2%**	**240 °C to 200 °C**
		2-butene-1,4-dial	**-13.9%**	**240 °C to 180 °C**
		maleic anhydride	**+ 30.0%**	**290 °C to 250 °C**

Table 2

Adsorbed Species	Pre-Treatment	SITE I 125°C	SITE II 175°C	SITE III 225-250°C	SITE IV 275-300°C	SITE V 350°C
	no pre-adsorption	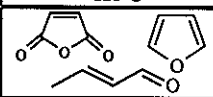	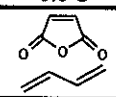	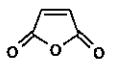	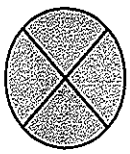	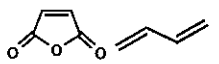
	H_2O pre-adsorption	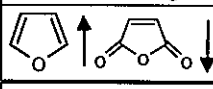	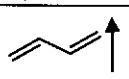	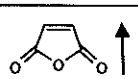		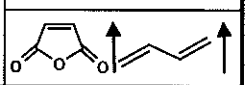
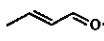	no pre-adsorption	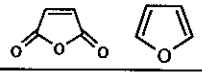	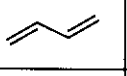	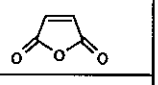	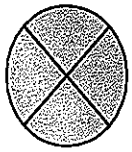	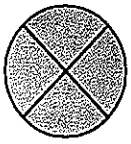
	H_2O pre-adsorption	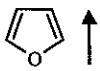	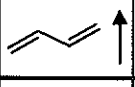	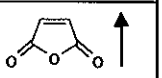		
	no pre-adsorption	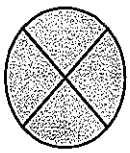	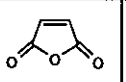	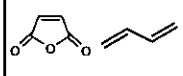	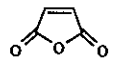	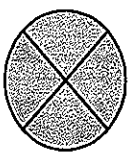
	H_2O pre-adsorption		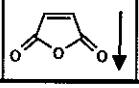	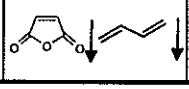	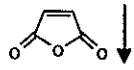	

CHAPTER 5

COMBINATORIAL SYNTHESIS OF VMoO THIN FILM MATERIALS USING SPUTTER DEPOSITION.

A manuscript prepared for submission to *Thin Solid Films*

William D. Schroeder and G.L. Schrader

Department of Chemical Engineering and Ames Laboratory – USDOE

Iowa State University Ames, IA 50011

5.1. Abstract

Binary metal oxide thin film arrays composed of vanadium, molybdenum and oxygen were synthesized using sputter deposition. The existing geometry in the sputtering chamber allowed these combinatorial arrays to be created without the use of multiple masks or sequential depositions per substrate. Thin film arrays of 225 individual squares were produced that ranged in composition and structure across the VMoO phase diagram, including V_2O_5, $V_9Mo_6O_{40}$, solid solutions of Mo in V_2O_5, and MoO_3. In addition to these phases, several reduced vanadium oxide phases were also detected, including VO_2, V_6O_{13}, and possibly others. There was no evidence of reduced molybdenum oxides. X-ray analysis (EDS) confirmed compositional gradients across the substrate and were related to composition with phases identified with LRS.

key words: Combinatorial; sputtering; mixed metal oxides; thin films; vanadium oxides

5.2. Introduction

Recently, thin film vanadium oxides have been gaining interest for several different applications, including host materials for lithium microbatteries and electrochromic devices (1, 2, 3). Within this V-O system is a subset of interesting reduced vanadium oxide phases, including VO_2, V_6O_{13}, V_4O_7, andV_3O_5. These reduced materials undergo metal-to-insulator transitions with temperature. In addition, V^{+4} present in solid solution materials has shown some degree of magnetic properties, directly related to paramagnetism of the reduced V^{+4} cation.

The use of combinatorial synthesis and characterization techniques has become useful in several industrial regimes, including drug discovery, magnetic materials, catalysis, zeolites and several others (C & EN, March 8, 1999, pp. 33-60). Catalysis screening for combinatorial arrays becomes difficult at times due to inefficient characterization techniques. At times, IR scanning of an entire catalyst array can be used to identify active "hot spots", although specific products typically are not detected. Other methods have been able to use physical or chemical properties of the reaction products themselves, such as laser fluorescence or resonance-enhanced multiphonon ionization. Yeung et al. used laser-induced fluorescence as a method to monitor the reaction of naphthalene to naphthaquinone over a V_2O_5-based catalyst. At 488 nm laser excitation, naphthaquinone fluoresced, while the reactant feed and other major product, phthalic anhydride did not. It was shown that small differences in catalytic activity directly associated with surface area changes were detectable with this screening method,

showing a relatively high level of sensitivity. This method would prove to be useful as long as some interesting aspect of the reaction can undergo laser-induced fluorescence 4.

In the 1930's, the oxidation of benzene was commercialized using promoted V_2O_5-MoO_3 catalysts. In the near 50 years when this catalyst was used to produce maleic anhydride, a vast amount of research was done on the V_2O_5-MoO_3 catalytic system (5). The catalytic behavior of these catalysts generally follows Mars van Krevelen redox kinetics, in which lattice oxygen is the active oxygen species (6). A general phase diagram of the V_2O_5-MoO_3 system is presented in Figure 1. As shown in the phase diagram, at the eutectic temperature (611°C) the solubility limit of MoO_3 in V_2O_5 is about 30 mol %. This solid solution is a substitutional type, with the same metal to oxygen ratio as V_2O_5. Formation of the solid solution involves either the reduction Mo^{+6} to Mo^{+5} or V^{+5} to V^{+4} must take place, but Bielanski et al. have used EPR measurements to confirm the existence of the V^{+4} cations (and absence of Mo^{+5}) (7). Below 10-15 mol % MoO_3 incorporation, the structure is orthorhombic (denoted phase α), and at higher solid solution concentrations (approaching 15 mol % MoO_3) the crystal structure begins to transform from orthorhombic to monoclinic (8, 5).

Previous studies of the reaction pathway for the oxidation of 1,3-butadiene has indicated a dependence of maleic anhydride selectivity on V^{+4} cations in the VMoO catalysts. The existence of V^{+4} in the catalyst was related to two different phenomena; 1) direct replacement of Mo^{+6} for V^{+5} in the catalyst structure in solid solutions of Mo in V_2O_5 caused a V^{+5} to V^{+4} transformation in order to retain overall charge neutrality, and 2) reduction of the catalyst surface V^{+5} to V^{+4} during reaction (9).

The objective of this research was to develop a sputter deposition technique to synthesize multicomponent metal oxide materials. In this work combinatorial thin film arrays of vanadium, molybdenum and oxygen were synthesized on silicon wafer substrates. The inherent orientation of the sputter guns to the substrate was used to impose a material gradient across the wafer. Substrates were masked to isolate 225 square spots, each consisting of a varying V and Mo composition. Laser Raman spectroscopy (LRS) and energy dispersive spectroscopy (EDS) were used to characterize the arrays in terms of phase and composition.

5.3. Materials and Methods

5.3.1. Sputtering system

Figure 1 shows the planar magnetron reactive sputtering system (Plasmatron Coating & Systems, Inc.) that was used to deposit thin film arrays of vanadium and molybdenum (10, 11, 12). Two direct current (DC) and one radio-frequency (RF) power supplies were available. The two DC power supplies had independent current (1.5 A max) and voltage (600 V max) controls and the RF power supply operated at 13.56 MHz with 500 W maximum power. Thin film arrays were deposited on single crystal (111) silicon wafers (3" x 0.018",n/p-type, International Wafer Service.) No attempt was made to remove the native SiO_2 layer (approximately 50 Å thick) and subsequently epitaxial growth was not expected. Base pressure was evacuated below 8 x 10^{-7} Torr using a mechanical pump and a cryopump. Independent mass flow controllers (MKS) were used to regulate the Ar (ultrahigh purity, Matheson) and O_2 (zero grade, Air Products) flows between 4-50 sccm. Overall chamber pressure was regulated between 4 and 50 mTorr

using a bypass throttle valve (MKS.) Metal targets of V (2" x 0.125", 99.7%, Alfa Aesar), Mo (2" x 0.25", 99.995%, International Advanced Materials) were mounted on separate sputtering guns (US, Inc.) 40° normal to the substrates and 8.5 cm from the substrate surface.

5.3.2. Deposition of VMoO thin film arrays

The following deposition conditions were used: RF power was 200 W, DC current was 25 mA. Sputtering guns half-shuttered to impose a more severe composition gradient. No additional heating was applied to the substrates, making temperatures less than 100°C. Ar flow rate was held at 20 sccm, and deposition times were between 30 and 60 minutes.

Figure 2 illustrates the procedure used to prepare the array. A stainless steel mask with 225 2.0 x 2.0 mm square holes was positioned directly on top of the silicon substrate. In order to organize the prepared arrays, a Cartesian coordinate system was implemented. This system was useful also to specify the "point sources" for V and Mo, defined as the point of highest material deposition on the wafer. Point sources for V and Mo were at coordinated (0,2) and (16,2), respectively. These coordinates of highest material deposition were determined using SEM analysis of V and Mo thin film standards. Post-deposition samples were heated in a furnace to 400°C for 8 hours under air. Increased heating times were investigated, however little change in Raman spectra or composition was observed. Heating at 500°C caused complete phase separation to occur, and possibly resulted in some sublimation of MoO_3.

5.3.3. Characterization

Laser Raman spectroscopy (LRS) was performed in a backscattering mode using a fiber-optic probe head coupled to a Kaiser Holospec f/1.8 spectrometer. A Coherent 532-50 diode-pumped solid state laser was the excitation source (532 nm, 50 mW at the source), and a Princeton Instruments CCD (1100x330) detector system was used with Winspec acquisition and processing software. In most Raman spectra taken of thin films, characteristic bands from the Si substrate were detected, consisting of a strong band at 521 cm^{-1} and a broad band from approximately 950 to 1000 cm^{-1}. These bands were characteristic with other reported results (12, 13).

A JEOL JSM-840A scanning electron microscope was used to determine deposition profiles and verify thickness of thin film materials. Using the same instrument, EDS scans were performed using a Kevex Quantum model thin-window, Si(Li) x-ray detector. The thin window allowed detection of boron or heavier elements. Quantitation was done with ZAF correction routine. Concentrations were expressed in terms of MoO_3 concentration, so that they could be related to the MoO_3-V_2O_5 phase diagram.

5.4. Results and Discussion

5.4.1. V-O thin films

A thin film array using a vanadium target was deposited onto a silicon wafer using the RF power source at 200W for 60 minutes. The point source coordinate for V was (0,2) and the sputtering gun was half-shielded using V-coated aluminum foil. The 2mm x 2mm thin film squares were golden in color. After heating in air, deposited thin

films were various shades of red, blüe and yellow. This color change is a well-explained behavior, resulting from destructive interference of light reflected from the metal oxide film. Thickness of the metal oxide change the light path length and therefore produce different colors at different thicknesses (14. Laser Raman spectra of several array spots have been presented in Figure 5. Near the target source (Figures 5a-g), LRS spectra had bands at 224, 258, 286, 306, 403, 428, 483, 529, 612, 703, 845, 880, 913, 935, 995, and 1034 cm^{-1}. Bands near 286, 306, 403, 529, 703 and 995 were characteristic of V_2O_5 (15). Bands at 224, 258, and 612 cm^{-1} were assigned to VO_2 (16). The 845, 880, 913, 945, and 1034 cm^{-1} bands were not assignable to any well-defined V-O phase. Gorenstein et al. observed broad Raman bands in the 830 to 920 cm^{-1} range for V_6O_{13} flash-evaporated films, however in the same studies crystalline V_6O_{13} exhibited no such bands. Considering the existence of both V_2O_5 and VO_2 bands in the Raman spectra, it was likely that these remaining bands are an additional reduced phase such as V_3O_7 or V_6O_{13}. These bands did not correspond to known V-Si or V-Si-O compounds. Further away from the V source, bands characteristic of the Si substrate began to appear, identified by a strong 521 cm^{-1} signal and broad band between 950-1000 cm^{-1}. This would indicate our spot thickness decreasing, as Si substrate was under the deposited thin films. In addition to stronger Si bands, the remaining peaks were characteristic of only V_2O_5, located at 286, 305, 406, 485, 706, and 995 cm^{-1}. Normally there is also a peak near 529 cm^{-1} for V_2O_5, however it was hidden next to the strong Si band at 521 cm^{-1}. It is possible that thinner films were not able to accomodate reduced structures, forming only V_2O_5.

5.4.2. Mo-O thin films

Thin films of Mo were deposited onto a silicon wafer using the DC power source at 25mA for 60 minutes. The sputtering gun was half-shielded using Mo-coated aluminum foil. As-deposited thin film squares were all golden in color, similar to the V samples. After calcination at 400°C for 8 hours, Raman spectra were collected for several spots on the thin film, presented in Figure 6. The region closest to the Mo source (Figures 6f, I, l and k) produced Raman bands at 247, 292, 337, 379, 521, 667, 820 and 995 cm^{-1}, as well as a broad band between 950 and 1000 cm^{-1}. As with the V-O samples, Raman signal at 521 cm^{-1} and the broad band between 950 and 1000 cm-1 were characteristic of the Si substrate. All of the other bands detected were assigned to α-MoO_3. Raman spectra indicated no evidence of reduced Mo-O compounds. Spectra further away from the Mo source also contained bands for α-MoO_3 and Si, except those associated with α-MoO_3 become much weaker. At the furthest point from the Mo source (Figure 6c), only the strongest band (820 cm^{-1}) was barely detectable for α-MoO_3, indicating a very thin film.

5.4.3. VMoO thin films

The binary metal system V-Mo was deposited using deposition parameters 200 W RF for V and 25 mA DC for Mo. Similar to the individual metals, sputtering guns were half-shielded, and located at coordinates (0,2) and (16,2) for V and Mo targets, respectively. After 60 minute deposition, materials were calcined at 400°C for 8 hours. Results from EDS measurements have been provided in Table 1 and illustrated in Figure 8. Composition in terms of MoO_3 ranged from 7.3% to 42.4% across the substrate. LRS

results for select spots are presented in Figure 7. In regions closest to the V source (Figures 7a,d and b), Raman bands were located at 284, 295, 398, 526, 606, 704, 847, 875, 932, 988, and 1030 cm^{-1}. The Raman bands were broader compared to pure V-O samples, but peak positions were similar. Bands at 526, 704 and 988 cm^{-1} could be attributed to solid solution formation of Mo in V_2O_5, in which direct Mo substitution for V in the V_2O_5 structure causes a downward shift the stretching vibrations 529 cm^{-1} (corner-sharing V-O-V), 706 cm^{-1} (edge-sharing V-O) and 995 cm^{-1} (V=O). EDS measurements showed the region near the V source contained approximately 7-15% MoO_3. This corresponds to the solid-solution regime of the V_2O_5-MoO_3 phase diagram. As with pure V-O samples, peaks at 606, 847, 875 and 932 cm^{-1} were assigned to reduced vanadium oxides, possibly in this case reduced solid-solution vanadium oxides. The 606cm^{-1} band associated with VO_2 could have exhibited the same downward shift with the incorporation of Mo as V_2O_5 materials. None of the bands observed could be associated with known reduced Mo oxides (17).At the point closest to the Mo source (Figure 7k), Raman spectra had bands near 398, 712, 860, and 978 cm^{-1}. Further away from the Mo source (Figures 7f, g, i, j, l and m), bands near 284, 315, 406, 470, 526, 701, 854, and 983 cm^{-1} were detected. Some of these bands were similar to those of V_2O_5 solid solution, however saturated solid solutions synthesized using conventional techniques exhibited shifts for V=O to a minimum of 985 cm^{-1}(18). Concentrations of MoO_3 were in the 30-40% range, corresponding to the dual-phase region in which small amounts of solid solution and large amounts of V_2MoO_8 would exist. Raman spectrum in Figure 7e most resembled solid solution of Mo in V_2O_5, with bands at 284, 306, 404, 480,

526, 701, and 991 cm^{-1}. Weak bands at 852, 874 and 932 cm^{-1} were also present. Composition corresponding to the Raman spectra in Figure 7e was 12.8% MoO_3.

Comparing EDS studies with the phase diagram in Figure 1, solid state synthesis techniques have been shown to produce solid solution and/or intermediate phase V_2MoO_8.in the range of compositions studied (8). Raman studies indicated the thin films produced partially conformed to the phase diagram, as LRS of solid solution VMoO materials were detected. Unfortunately, Raman bands for V_2MoO_8 have not been well defined. Structurally, V_2MoO_8 has been proposed to be similar to V_2O_5, however instead of two-fold corner-sharing rows of VO_6-octahedra in the (010) and (001) directions, they are separated by an additional corner-sharing row of MoO_6-octahedra, shown in Figures 8 and 9 (19, 20). With this similar structure, it would be expected that some similar bands to V_2O_5 would be detected. At spots with MoO_3 concentrations above 25%, predominant peaks were 284, 315, 406, 526, 701, 855, and 980 cm^{-1}. Most of these could be attributed to V_2O_5, however the strong broad bands at 712, 860 and 978 cm^{-1} could represent the new Mo-O linkages in the V_2MoO_8 structure. Additionally, reduced vanadium oxides were shown to be produced in pure V deposition and post-calcination studies, particularly VO_2 and possibly V_6O_{13} or V_3O_5.

5.5. Conclusions

The orientation and target power was used to sputter deposit compositional gradients of vanadium and molybdenum across a Si wafer. Combinatorial VMoO produced that contained compositions that ranged from 7–42 mol % MoO_3. Using Raman spectroscopy, certain phases corresponding to the V_2O_5-MoO_3 phase diagram

were identified. Additionally, stable reduced vanadium oxide thin films were also produced, possibly forming substitutional solid solutions with Mo.

5.6. Acknowledgements

This research was performed under funding from Ames Laboratory – USDOE contract No. W-7405-Eng-82.

5.7. List of Figures

1. $V_2O_5 - MoO_3$ phase diagram.
2. Magnetron sputtering system.
3. Sputter gun and mask arrangement for mixed-metal oxide array. Coordinate system was applied to 15 x 15 array.
4. Appearance of VMoO sputtered sample.
5. Raman spectra of select coordinates of thin film V-O array, sputtered at 200W RF for 60 minutes, followed by 8-hour calcination at 400°C.
6. Raman spectra of select coordinates of thin film Mo-O array, sputtered at 25 mA DC for 60 minutes, followed by 8-hour calcination at 400°C.
7. Raman spectra of select coordinates of thin film V-Mo-O array, sputtered at 200W RF (V) and 25 mA DC (Mo) for 60 minutes, followed by 8 hour calcination at 400°C.
8. Composition of VMoO array from EDS x-ray analysis.
9. Idealized crystal structure of V_2O_5.
10. Idealized crystal structure of V_2MoO_8.

5.8. List of Tables

1. Compositions of select coordinates in the VMoO array using EDS analysis.

5.9. References

1 Julien, C., A. Gorenstein, A. Khelfa, J. P. Guesdon, I. Ivanov, *Mater. Res. Soc. Symp. Proc.* **369**, 639 (1995).

2 Julien, C., A. Gorenstein, A. Khelfa, J. P. Guesdon, I. Ivanov, *Mater. Res. Soc. Symp. Proc.* **369**, 649 (1995).

3 Ask, M., U. Rolander, J. Lausmaa, B. Kasemo, *J. Mater. Res.* **5(8)**, 1662 (1990).

4 Yeung, E. and H. Su, *J. Am. Chem. Soc.* **122**, 7422 (2000).

5 Bielanski, A. and M. Najbar, *Applied Catalysis A: General* **157**, 254 (1997).

6 Mars, P. and D.W.v. Krevelen, *Chem. Eng. Sci. Suppl.* **3**, 41 (1954).

7 Bielanski, A., K. Dyrek, I. Kracik and E. Wenda, *Bull. Pol. Ac. Chem.* **19**, 512 (1971).

8 Kihlborg, L., *Acta Chim. Scand.* **21**, 2495 (1967).

9 Schroeder, W.D., C.J. Fontenot and G.L. Schrader, *Journal of Catalysis,* submitted 2001.

10 Koo, K. F. and G. L. Schrader, *U.S. Pat. App.* 1994, 8 pp. CODEN: USXXAM US 5370778 A 19941206.

11 Obeng, J. A. and G. L. Schrader, *Suface Coatings and Technology* **68/69**, 422 (1994).

12 Zou, J. and G.L. Schrader, *Thin Solid Films* **324**, 52-62 (1998).

13 Zou, J. and G.L. Schrader, *Journal of Catalysis* **161**, 667-686 (1996).

14 Colclaser, R. A., Microelectronics – Processing and Device Design, New York : Wiley, 1980, pp. 96-97.

15 Abello, L., Husson, E., Repelin, Y., and Lucazeau, G., *Spectrochimica Acta* **39A/7**, 641 (1983).

16 Srivastava, R. and L. L. Chase, *Physical Review Letters* **27 (11)**, 727 (1971).

17 Olson, K.A., PhD. Dissertation, p. 82 (1989), Iowa State University

18 Hirata, T. and H-Y Zhu, *J. Phys.: Condens. Matter* **4**, 7377 (1992).

19 Haber, J., M. Witko and R. Tokarz, *Applied Catalysis A: General* **157,** 3-22 (1997).

20 Eick, H.A. and L. Kihlborg, *Acta Chemica Scandinavica* **20,** 1658-1666 (1966).

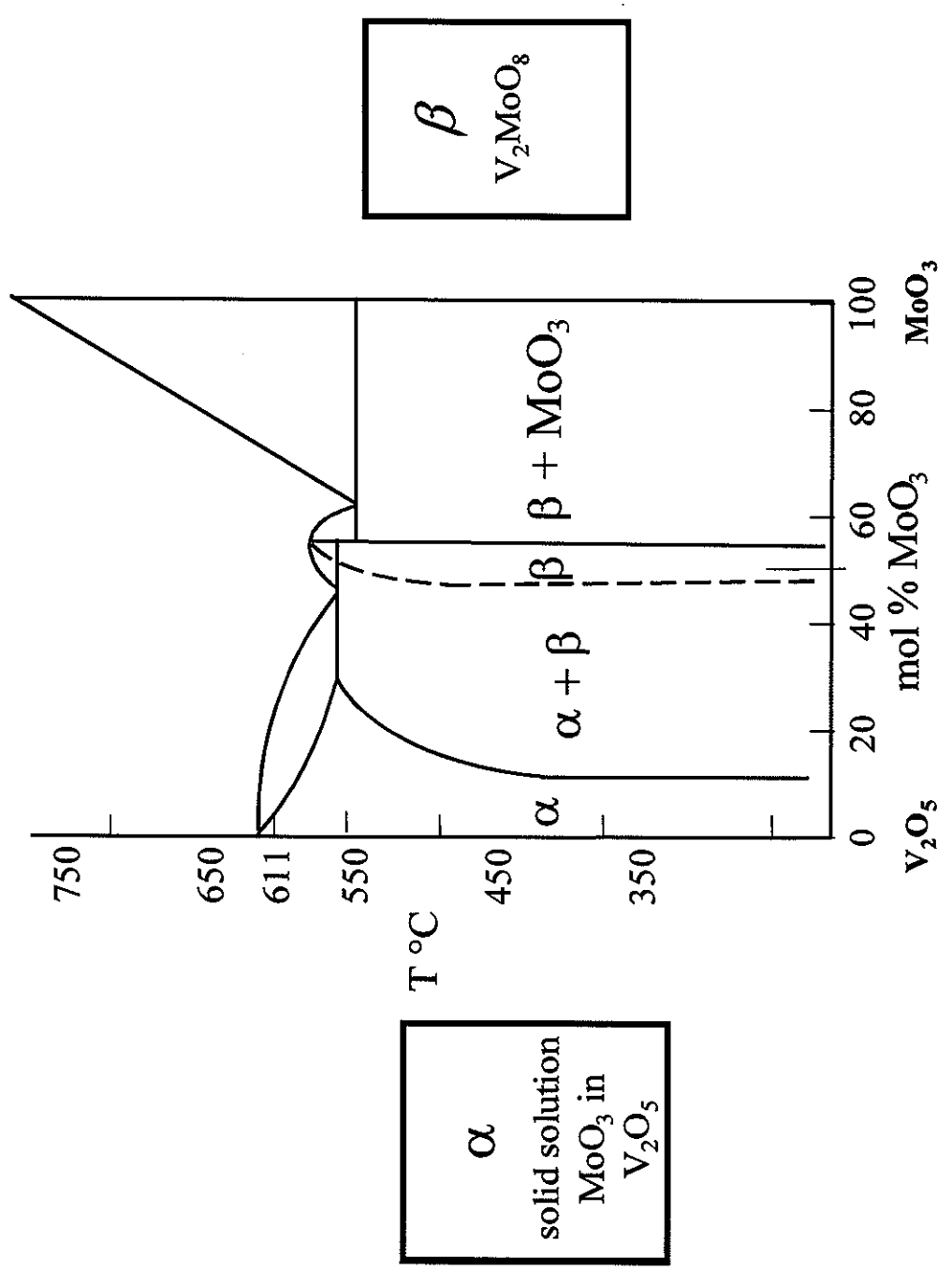
β
V_2MoO_8
α
solid solution
MoO_3 in
V_2O_5
T °C
750
650
611
550
450
350
α
α + β
β
β + MoO_3
0
20
40
60
80
100
V_2O_5
mol % MoO_3
MoO_3

Figure 1

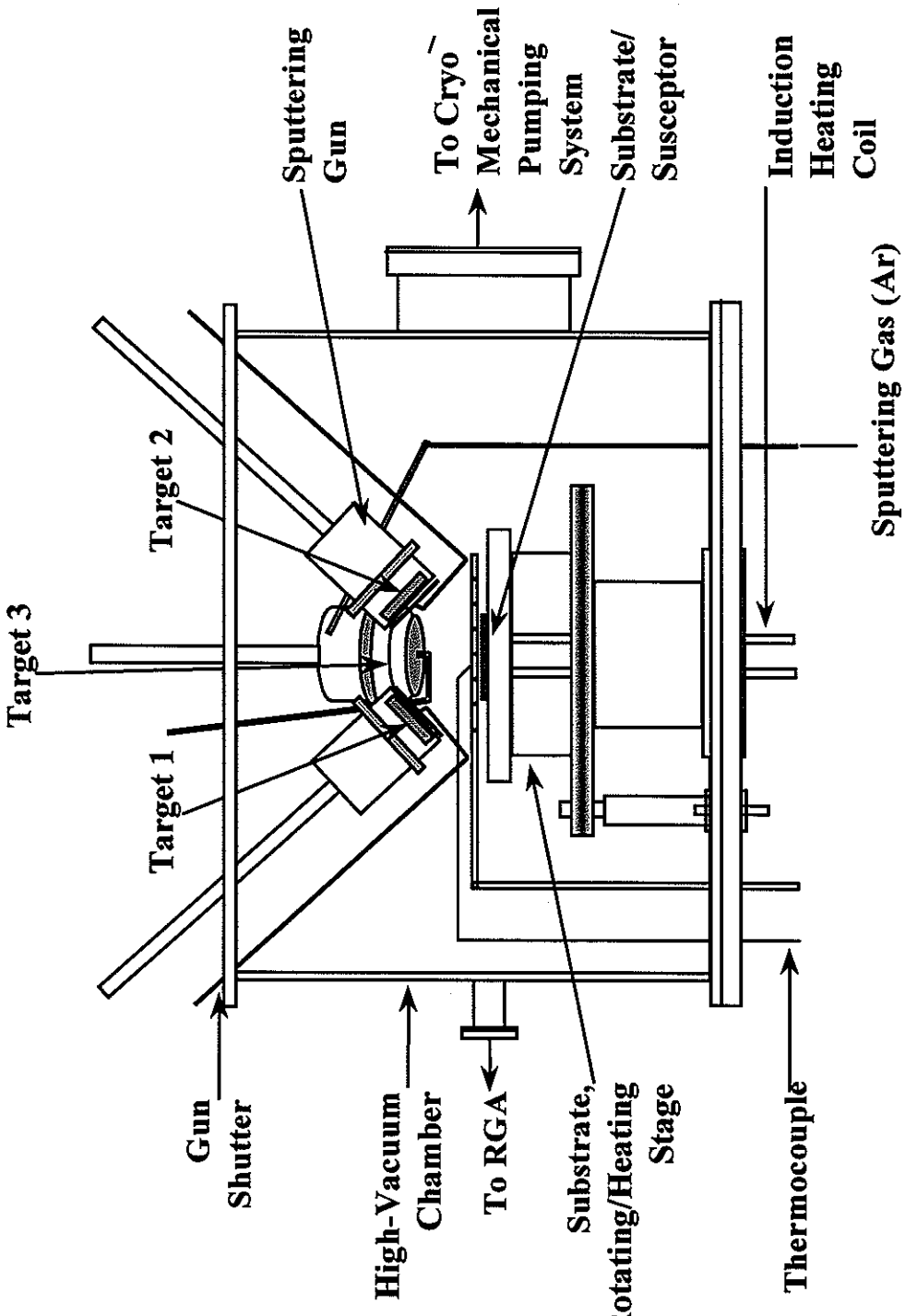
Sputtering Gun
To Cryo-Mechanical Pumping System
Substrate/ Susceptor
Induction Heating Coil
Sputtering Gas (Ar)
Target 2
Target 3
Target 1
Gun Shutter
High-Vacuum Chamber
To RGA
Substrate, Rotating/Heating Stage
Thermocouple

Figure 2

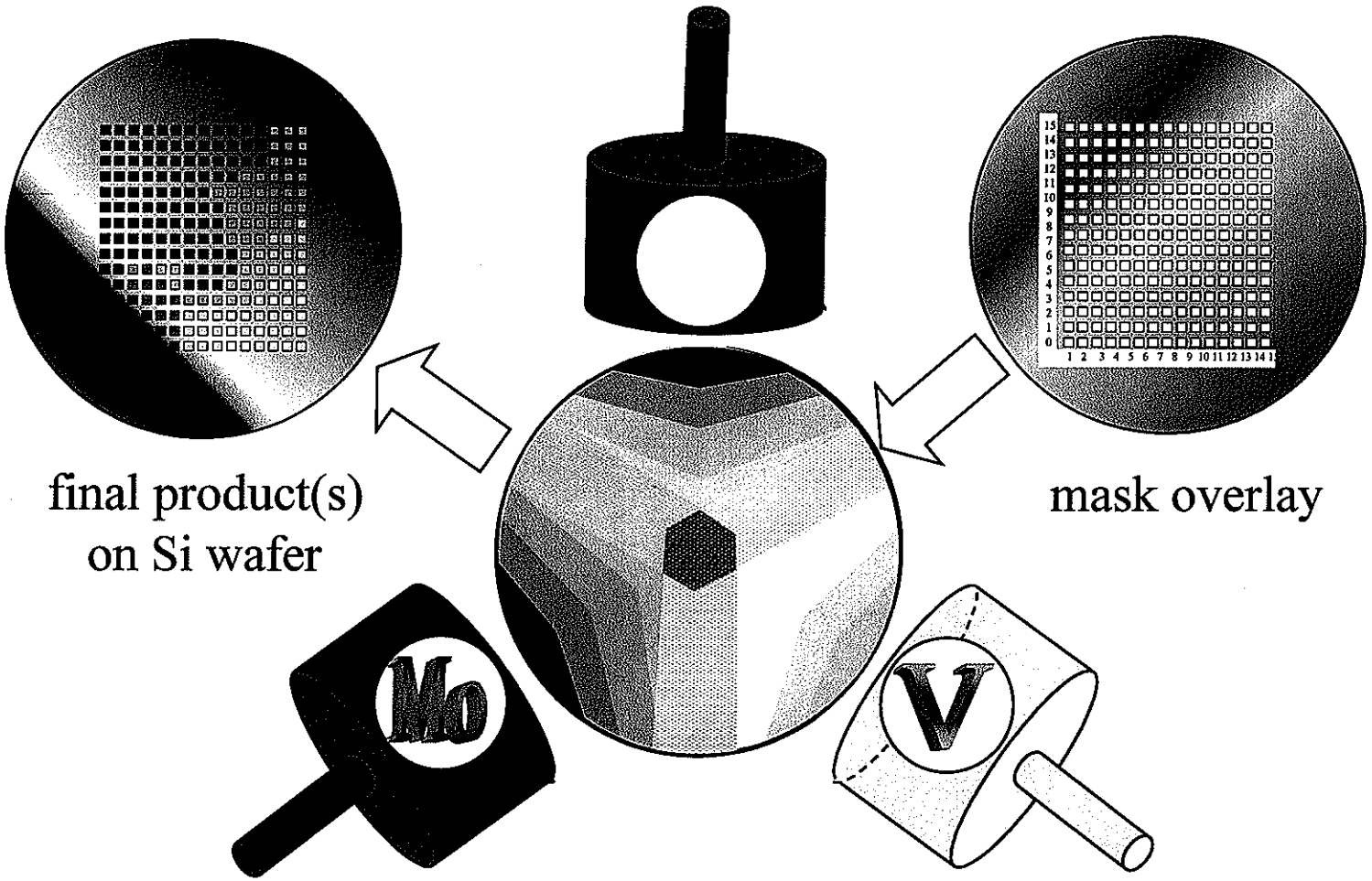

Figure 3

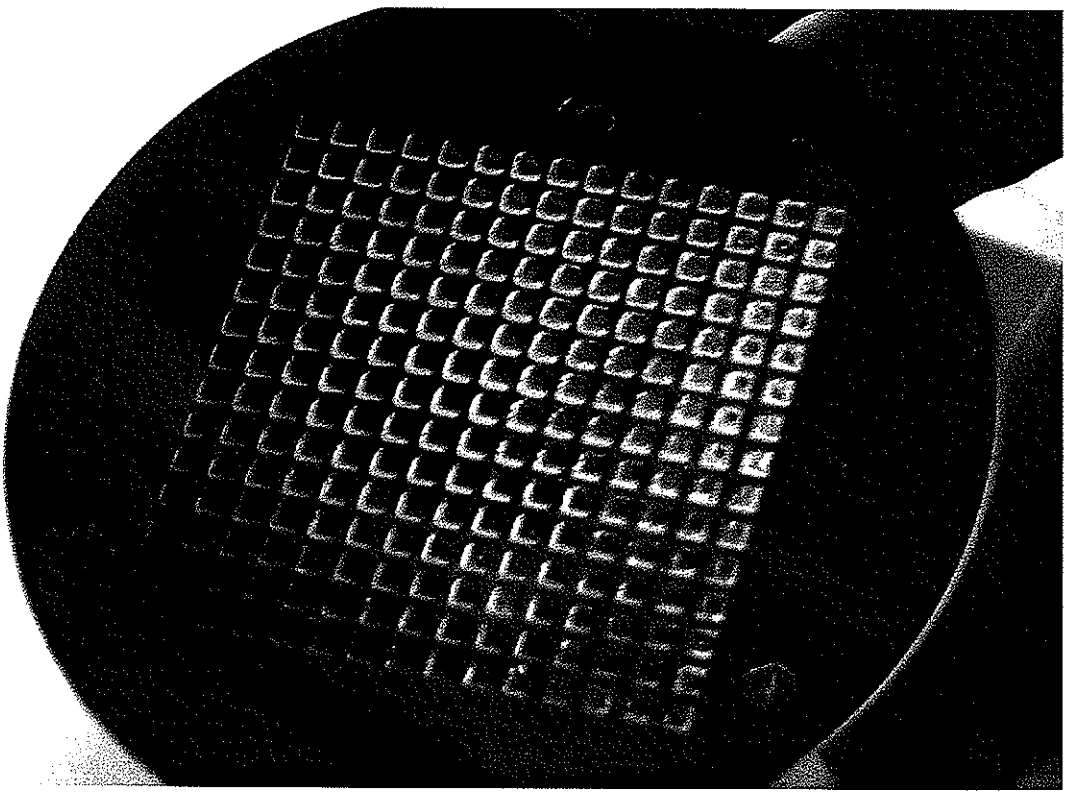

Figure 4

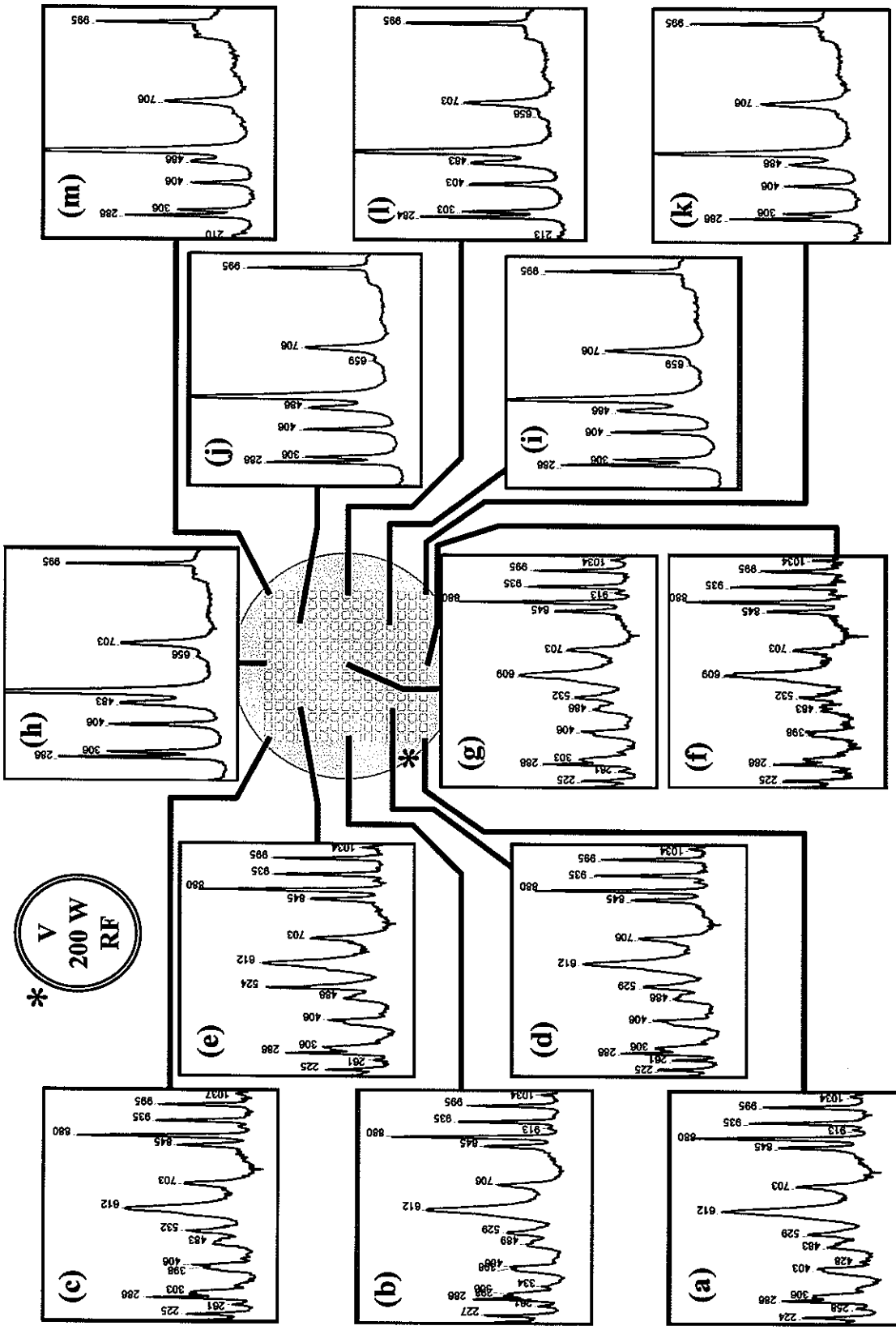

Figure 5

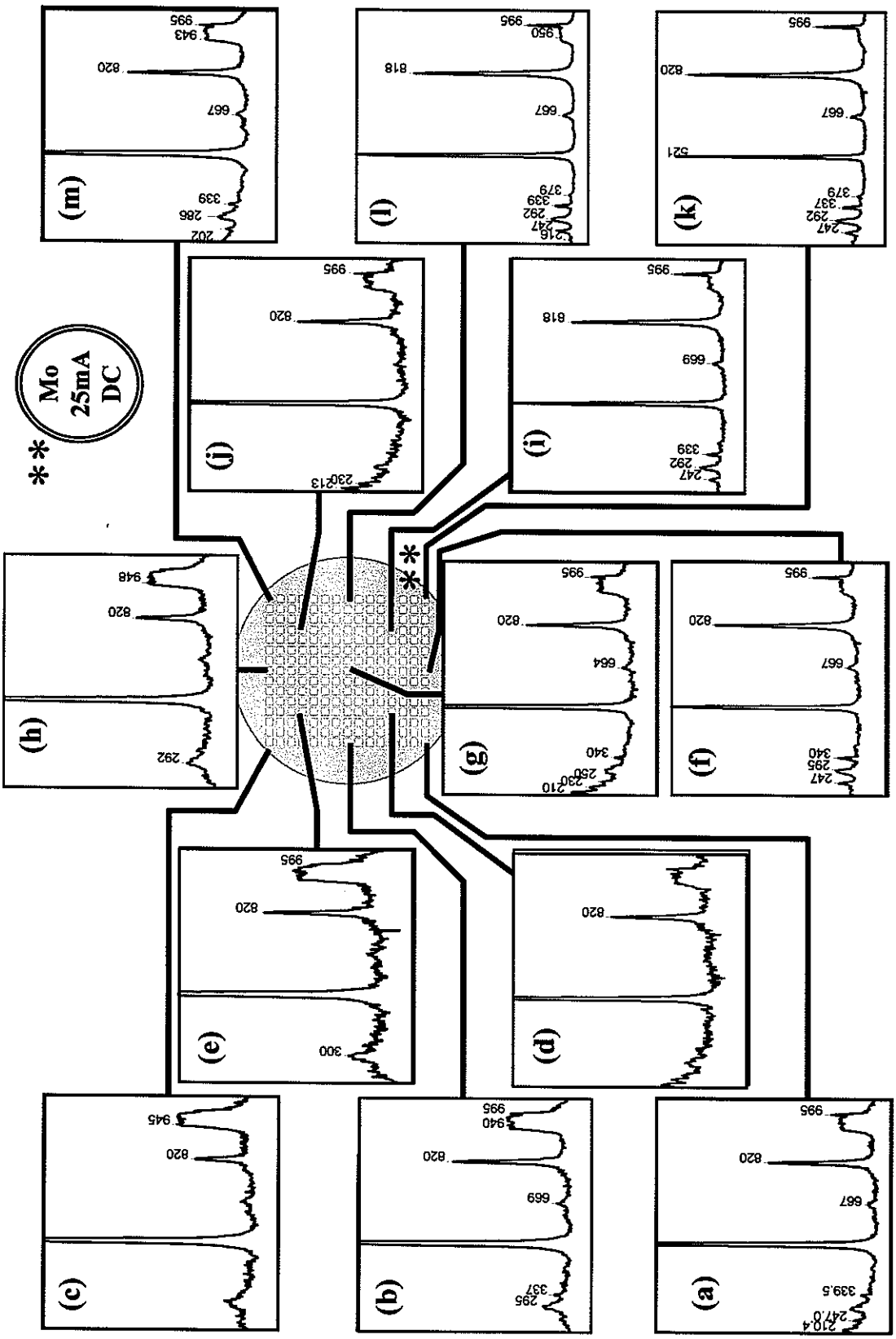

Figure 6

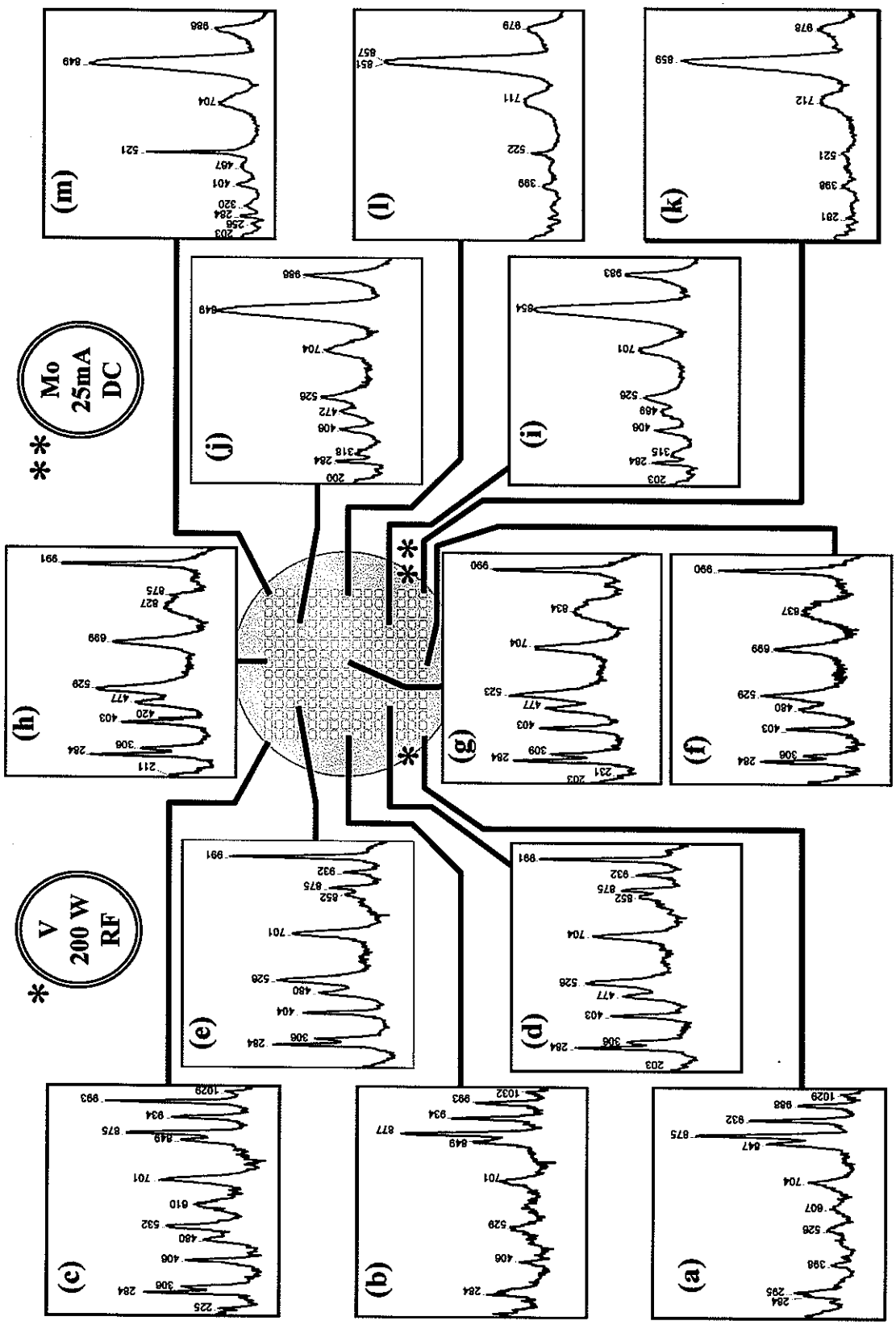

Figure 7

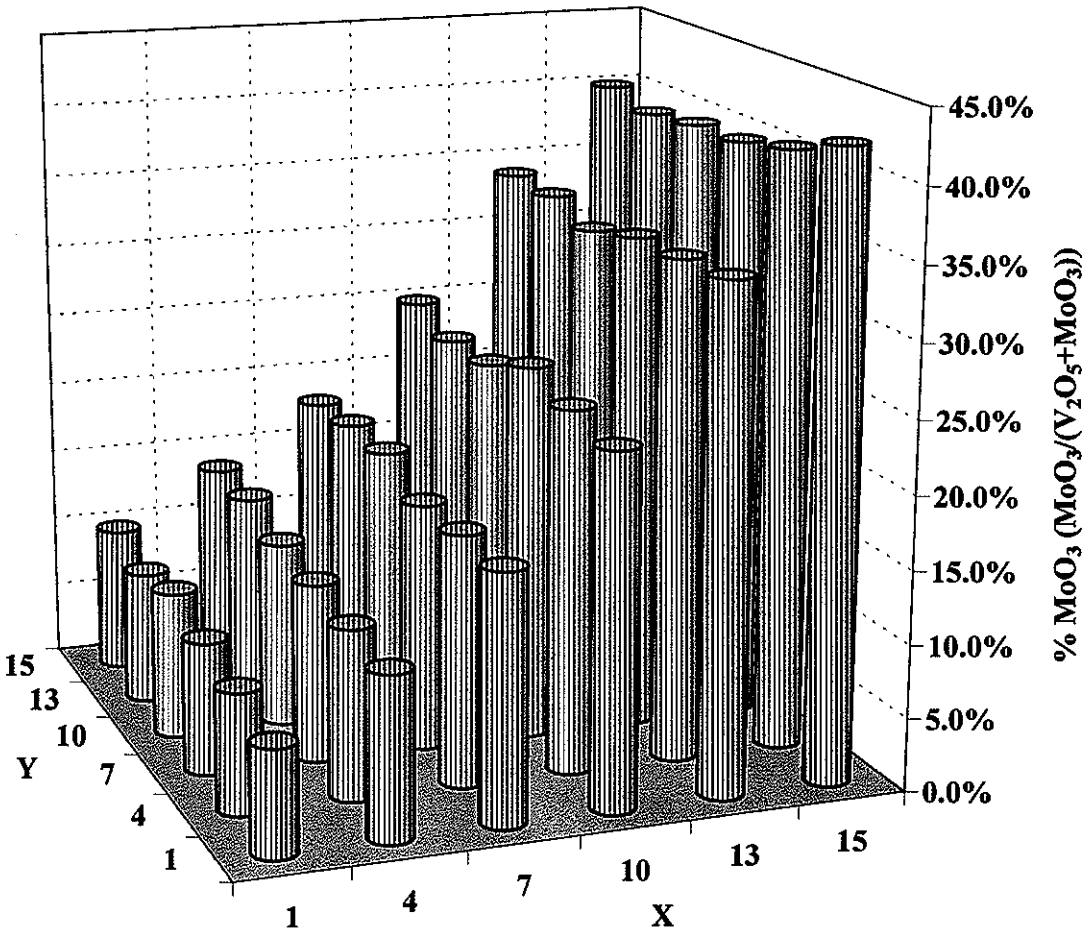
45.0%
40.0%
35.0%
30.0%
25.0%
20.0%
15.0%
10.0%
5.0%
0.0%
% MoO3 (MoO3/(V2O5+MoO3))
15
13
10
7
4
1
Y
1
4
7
10
13
15
X

Figure 8

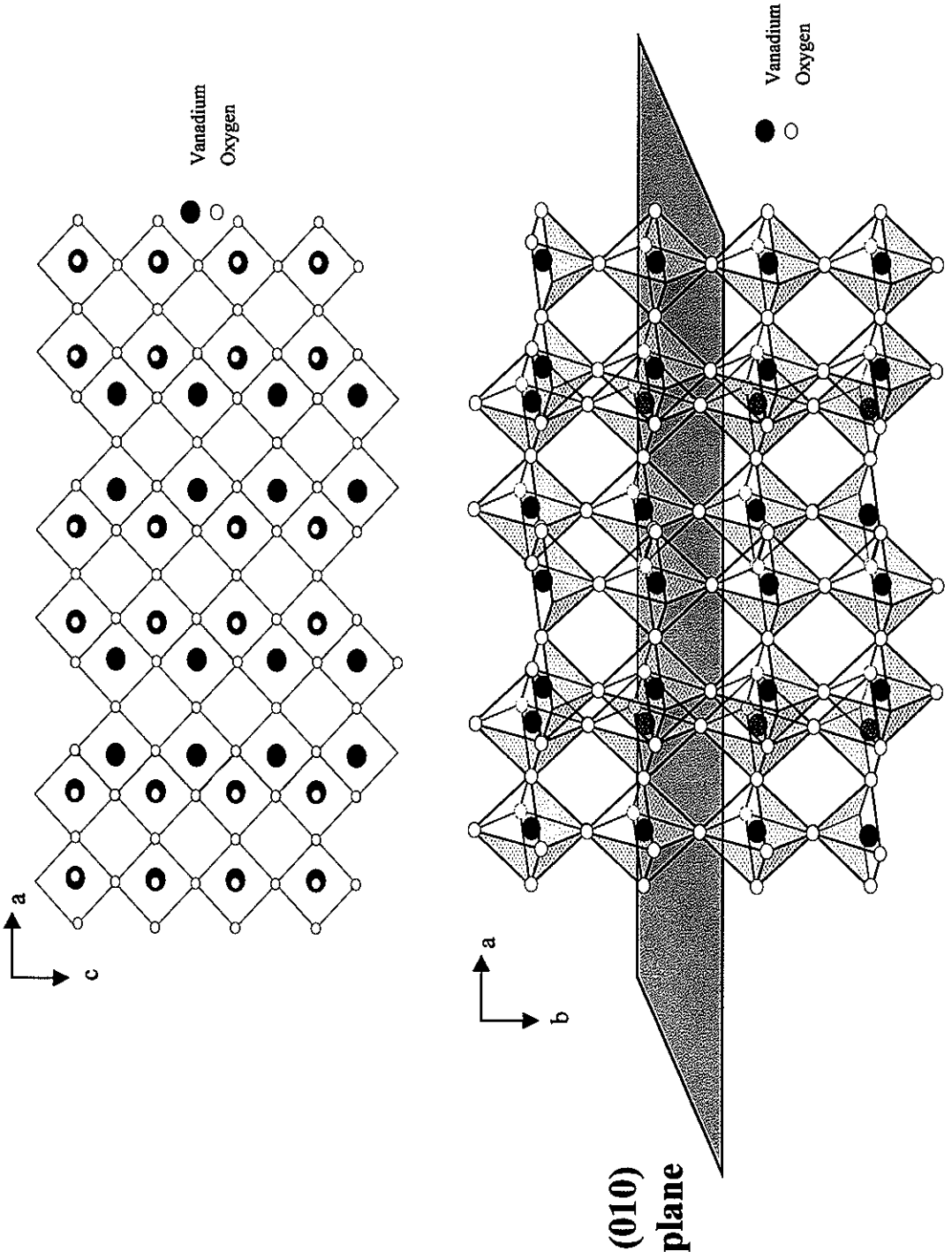

Figure 9

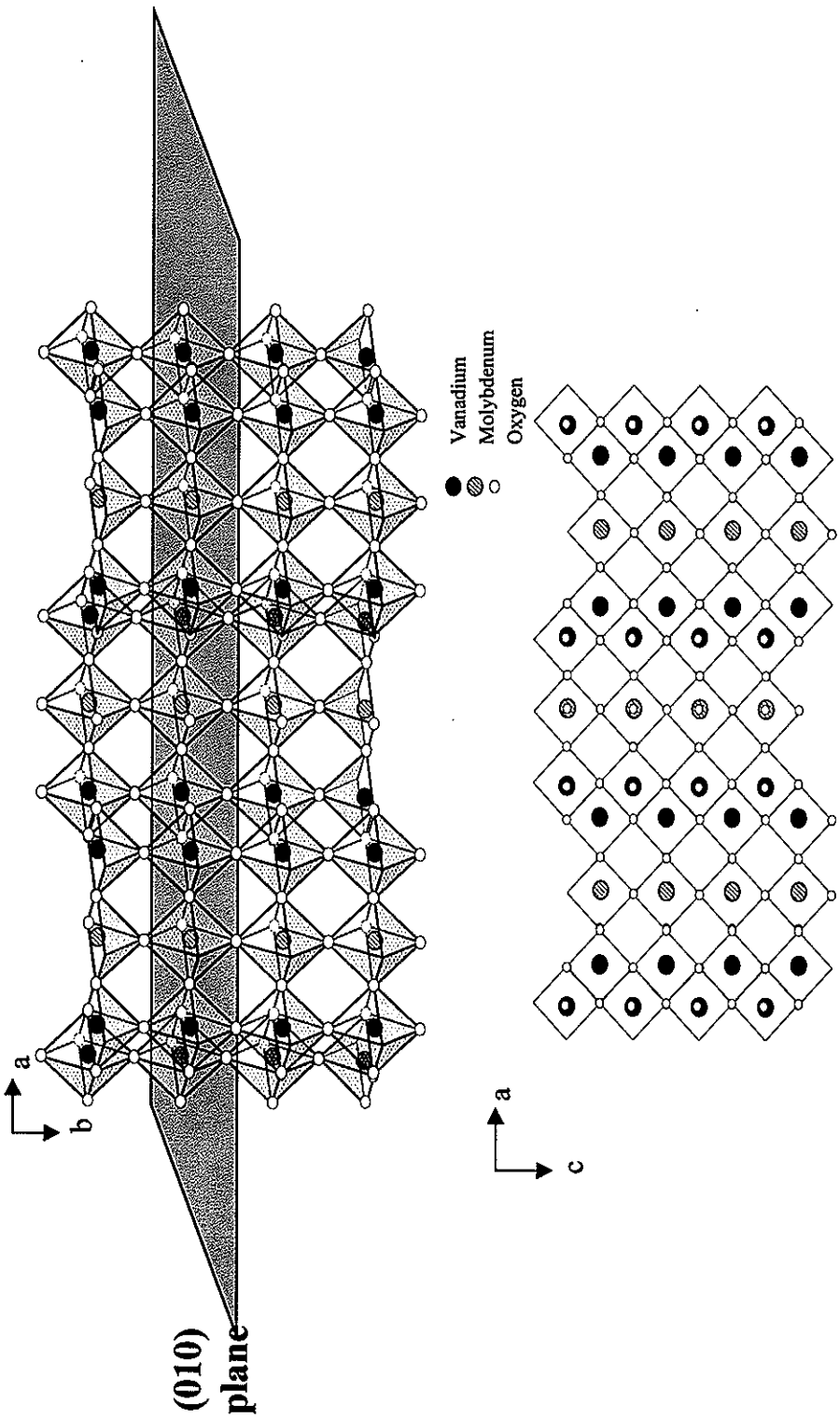

Figure 10

Table 1

Percent $MoO_3/(V_2O_5 + MoO_3)$ in WDS-1-165-4 V-Mo-O Mask Array
V: 200W RF 1/2 shutter Mo:25 mA DC, 1/2 mask 30 minute deposition
Post-Anneal in air for 8 hours at 400°C

15	10.0%	13.8%	18.1%	25.0%	34.0%	40.1%
13	9.1%	13.8%	18.5%	24.0%	33.9%	39.3%
10	10.1%	12.8%	18.5%	24.1%	32.9%	39.8%
7	9.1%	12.3%	17.0%	25.8%	34.0%	40.0%
4	8.3%	11.7%	17.2%	24.8%	34.1%	40.8%
1	7.3%	11.2%	17.0%	24.1%	34.4%	42.4%
	1	4	7	10	13	15

CHAPTER 6

CONCLUSION AND RECOMMENDATIONS

6.1. General Discussion

The selective oxidation of 1,3-butadiene over solid-solution VMoO catalysts is quite complex, involving a multi-step reaction pathway including both electrophilic and nucleophilic oxidations. My current research provided valuable information on the reaction pathway, effects of water addition to the reactant stream and combinatorial techniques for synthesizing VMoO thin films.

Using reactor studies of not only 1,3-butadiene but also selective oxidation products thereof, a reaction pathway was proposed that suggested an epoxidation of 1,3-butadiene to 3,4-epoxy-1-butene as a first step in the reaction. 3,4-Epoxy-1-butene isomerized to crotonaldehyde, which appeared to have two possible pathways in further oxidation, either cyclization to form furan or allylic hydrogen abstraction followed by oxygen insertion to form 2-butene-1,4-dial.

Water addition to the reactant feed resulted in beneficial effects for overall catalytic performance, increasing conversion while selectivity to some intermediate products also increased. This effect was contributed to a combination of both competitive adsorption and surface acid site formation from dissociative water adsorption. Structural effects did not appear to occur with 0-12% water addition. Five distinct surface sites were proposed, involving each of the three oxygen species in the V_2O_5 structure as well as vacancy sites. Combined with theoretical studies of the V_2O_5

surface, water addition and an understanding of the chemistry involved in the partial oxidation of 1,3-butadiene, reasonable site assignments were made.

In order to further investigate the solid solution behavior and VMoO system, 15 x 15 combinatorial arrays were synthesized in which sputter deposition was used to create composition gradients across a Si substrate. EDS measurements revealed that the VMoO array had compositions corresponding to solid solution Mo in V_2O_5 and V_2MoO_8 phases in V_2O_5-MoO_3 phase diagram. LRS characterization, however, revealed that in addition to these two phases there was also at least one reduced vanadium oxide present, probably more than one.

The information obtained in these studies has provided valuable information in the reaction pathway of 1,3-butadiene over VMoO catalysts. Shown to possess both electrophilic and nucleophilic characteristics, the solid solution VMoO catalysts have been shown transform 1,3-butadiene to 3,4-epoxy-1-butene through a 1,2 epoxidation, contrary to the often cited 1,4-cycloaddition to 2,5-dihydrofuran over metal oxide catalysts. The role of Mo incorporation in the catalyst should provide better understanding in designing a V_2O_5-based catalytic system. For example, a solid solution of ReVO could prove interesting, as Re^{+7} could cause a reduction of V^{+5} to V^{+3} or V^{+2}.

6.2. Recommendations for Future Research

There are several directions that could be pursued from this research. Expanding from binary metal oxide VMoO to a ternary metal oxide could prove interesting both from a catalytic and synthesis standpoint. An exploration of the oxygen exchange potential of the VMoO catalyst with labeled $H_2{}^{18}O$ and or ^{18}O could provide additional

useful information about the interaction of water with the catalyst surface, as well as possibly confirm oxidation steps involved with different surface sites. [1, 2] This would be particularly useful in further elucidating the effects of water on crotonaldehyde vs. furan production.

The combinatorial sputter deposition method has a third material source available, meaning that ternary systems could be synthesized and characterized for composition and phase. There is definitely exploration potential in the areas of high volume catalytic screening methods for these thin film catalysts.

Further reactor studies using vanadium oxide based catalysts would help to solidify the role of the V^{+4} cation in the structure for 1,3-butadiene oxidation – possibly using a different metal to form a solid solution. Lastly, deviation from 1,3-butadiene to another species such as n-pentane or pentadiene may provide some interesting information of both the catalyst and reaction pathway to citroconic, phthalic, and maleic anhydrides[3, 4]

6.3. References

[1] Moro-oka, Y, Takita, Y., and Ozaki, A., *Journal of Catalysis* **27**, 177 (1972).

[2] Ono, T. and H. Numata, *Journal of Molecular Catalysis A: Chemical* **116,** 421 (1997).

[3] Zazhigalov, V. A., J. Haber, J. Stoch, B. D. Mikhajluk, A. I. Pyatnitskaya, G. A. Komasko, and I. V. Bacherikova, *Catalysis Letters* **37**, 95 (1996).

[4] Cavani, F., A. Colombo, F. Giuntoli, E. Gobbi, F. Trifiro, P. Vazquez, *Catalysis Today* **32**, 125 (1996).

ACKNOWLEDGEMENTS

This work was performed at Ames Laboratory under Contract No. W-7405-Eng-82 with the U.S. Department of Energy. The United States government has assigned the DOE Report number IS-T 1965 to this thesis.

I would like to give special thanks to Professor Glenn Schrader for his guidance and providing funding for my research. I appreciate Prof. Schrader taking a chance on a chemistry major from Augsburg College - I hope I contributed in my work at least some of what I gained at Iowa State. I would also extend thanks to my fellow graduate students, including Kirk Thompson, Allen Xue, T. J. Paskach and Craig Fontenot. Your discussions and insight helped me view my research results from a new perspective when I needed one. To Linda Edson, you will be sorely missed – you were my Chemical Engineering adopted mother, and I am grateful for the times we shared.

To my extended family and friends, your support is very appreciated through this journey that started five years ago – without you I would not be who I am today. My mother, Betsy Schroeder, who helped me keep everything in perspective (she still thinks I do "spackling" for research). My father Jim Schroeder and his wife, Linda, who provided support and often found a reason to come to Ames and give me much needed relief from the lab. And finally, to my loving wife Shannon, who provided unwavering support and love throughout what at times was a continuous uphill battle. The things I have accomplished could not have been done without her support.